

**SURVEY AND ANALYSIS OF CHANNEL MORPHOLOGY OF THE BRAZOS
RIVER ALONG A SELECTED STUDY SITE FOR RIVER ASSESSMENT**

TWDB Contract 0904830966

Final Report

İnci Güneralp¹

Billy Hales²

¹ Assistant Professor, Department of Geography, 3147 TAMU, Texas A&M University,
College Station, TX 77843-3147

² Graduate Research Assistant, Department of Geography, 3147 TAMU, Texas A&M
University, College Station, TX 77843-3147

2014 NOV - 7 AM 8:15
CONTRACT ADMINISTRATION

**SURVEY AND ANALYSIS OF CHANNEL MORPHOLOGY OF THE BRAZOS
RIVER ALONG A SELECTED STUDY SITE FOR RIVER ASSESSMENT**

TWDB Contract 0904830966

İnci Güneralp¹

Billy Hales²

¹ Assistant Professor, Department of Geography, 3147 TAMU, Texas A&M University,
College Station, TX 77843-3147

² Graduate Research Assistant, Department of Geography, 3147 TAMU, Texas A&M
University, College Station, TX 77843-3147

<u>CONTENT</u>	<u>Pg.</u>
1. BACKGROUND	8
1.1. Purpose of the Study	8
1.2. River Morphology, Hydrology, and Aquatic Habitat Interaction	9
2. OBJECTIVES OF THE STUDY	23
3. STUDY REACH	23
3.1. Selection of the Study Reach	23
3.2. The Lower Brazos River, Texas	24
3.3. Study Reach Characteristics	26
4. DATA COLLECTION AND PROCESSING	30
4.1. Field Data Collection	30
4.2. Field Data Processing	32
4.3. Generation of Digital Terrain Model (DTM) of the Study Reach	33
5. CHARACTERIZATION OF CHANNEL MORPHOMETRY	38
5.1. Characterization of Planform Morphology	38
5.2. Characterization of Terrain Morphology	38
6. CHARACTERIZATION OF FLOW HYDRAULICS AT DIFFERENT FLOW CONDITIONS	39
6.1. Hydraulic Modeling	40
6.2. Delineation of the Physical Boundaries of Habitat Types	47
7. RESULTS	49
7.1. Morphometric Characteristics of the Study Reach	49
7.2. Physical Boundaries of Habitat Types	54
7.3. Substrate Sediment Characteristics of the Study Reach	56
7.4. Hydraulic Characteristics of the Study Reach	63
7.5. Distribution of Hydraulic Characteristics of Study Reach in Relation to the Physical Boundaries of Habitat Types	72
7.6. Relations Between Channel Morphology and Flow Hydraulics	84
7.7. Limitations of the Study	86
8. SUMMARY AND CONCLUSIONS	87
9. REFERENCES	89

FIGURE CAPTIONS

Pg.

Figure 1. Three types of stream disturbance: (a) Pulse, (b) Press, and (c) Ramp (after *Lake* (2000): pp. 575, Figure 1)..... 15

Figure 2. Scale of habitat classification (after Thomson et al. 2001: pp. 380, Figure 3)..... 17

Figure 3. Hierarchical approach to habitat classification, RiverStyles framework (after *Thomson et al.* (2001): pp. 377, Figure 1)..... 19

Figure 4. Geomorphic unit and hydraulic unit map for an example of the meandering gravel bed RiverStyles for the Cobark River (31°57 S, 151°42 30 E) (after Thompson et al. 2001: Plate 1C)..... 21

Figure 5. Study reach and its access point south of FM 60 (Raymond Stotzer Pkwy) on the lower Brazos River, Texas, shown on an aerial photograph obtained in August 2008 (i.e., a true-color digital orthophoto quarter quadrangle (DOQQ))..... 24

Figure 6. Floodplain boundary (marked with the elevation range of 43–113 m) of the study reach (Figures 5, 7) located within meandering incised valley fill zone on the lower Brazos River, Texas. The river is characterized by a single-thread channel with tributary avulsive channels. Elevation data shown are from the U.S. Geological Survey (USGS) National Elevation Dataset (NED) (cell size = 10 m)..... 25

Figure 7. Study reach (reach entrance X,Y coordinates, 751,122.2251, 3,381,298.5804; reach exit coordinates, 751,415.3741, 3,381,365.4222, based on NAD 83 UTM Zone 14 (units = meters)). The flow direction is from left to right. The numbers 1–3 mark the location of the features shown on Figure 8. Background aerial photo was acquired on August 17, 2010 (source: Japan Aerospace Exploration Agency (JAXA)/Alaska Satellite Facility)..... 26

Figure 8. Panoramic views of the incised river section along the study reach, which is located on the lower Brazos River, Texas. The photos were taken on August 19, 2010, looking (a) downstream (arrow A on Figure 7) and (b) upstream (arrow B on Figure 7)..... 27-28

Figure 9. Study reach photographs taken during the field campaign of August 18–19, 2010: (a) Exposed mid-channel bar (looking upstream) marked as (1) on Figure 7; (b) the region on the left side of the mid-channel bar looking toward the left bank, marked as (2) on Figure 7; the beginning of the point bar is seen on the right; and (c) Slightly downstream of the region in (b) looking upstream, marked as (3) on Figure 7, showing the beginning of the point bar..... 28

Figure 10. Daily mean discharge at the Brazos River at Bryan, TX, USGS gaging station (08108700), over a period from 7/15/1993 to 3/19/2013. The horizontal (blue) dashed line represents the average discharge ($Q_{ave} = 134.51 \text{ m}^3/\text{s}$); the vertical (red) dashed line marks the discharge on August 18, 2010..... 29

Figure 11. Monthly discharge (m^3/s) statistics over a period from October 1993 to September 2011..... 29

Figure 12. ADCP data collection points along the study reach during the field campaigns on August 18–19, 2010. Background aerial photo was acquired on August 17, 2010 (source: JAXA/Alaska Satellite Facility)..... 30

<u>FIGURE CAPTIONS (cont'd)</u>	<u>Pg.</u>
Figure 13. Locations of transects T1–T11 at which the sediment sampling was performed. The flow direction is from T1 to T11. Background aerial photo was acquired on August 17, 2010 (source: JAXA/Alaska Satellite Facility).....	31
Figure 14. Intermap Technologies® NEXMap® interferometric synthetic aperture radar (InSAR)-derived Digital Terrain Model (DTM) (in vertical and horizontal units of meters) used in the terrain generation for the study reach (cell size = 4.396 m).....	34
Figure 15. Point Kriging-interpolated Digital Terrain Model (DTM) of the study reach (cell size = 5 m) including the terrain information (from Intermap Technologies® NEXMap® InSAR-derived DTM) and bathymetric information (from field survey)-visualized bilinear interpolation with a cell size of 1 m.....	36
Figure 16. Elevation model representing the river channel clipped for the boundary defined by high discharge (Q3). Mid-channel bar represents a macro roughness structure (Figure 9a). Background aerial photo was acquired on August 17, 2010 (source: JAXA/Alaska Satellite Facility).....	46
Figure 17. Water surface elevations predicted using the hydrodynamic model FaSTMECH and based on low-discharge scenario, Q1. Background aerial photo was acquired on August 17, 2010 (source: JAXA/Alaska Satellite Facility).....	46
Figure 18. Difference between the measured and modeled water surface elevations. Background aerial photo was acquired on August 17, 2010 (source: JAXA/Alaska Satellite Facility).....	47
Figure 19. Water surface centerline and the location of the inflection points (large green full circles) and the curvature maxima (small orange full circles). Background aerial photo was acquired on August 17, 2010 (source: JAXA/Alaska Satellite Facility).....	49
Figure 20. Planform curvature spatial series along the water surface centerline obtained from the edge-of-water data collected during the field campaign of August 18–19, 2010. CW denotes the dimensionless curvature (i.e., curvature scaled with average channel width). The numbers 1–6 show the location of the inflection points (Figure 19). The curvature maxima marked as small dots (in the color orange) in Figure 19; (b) spatial variations in the channel width computed for the same WSE condition along the streamwise axis.....	50
Figure 21. Terrain slope (in degrees) computed from the generated DTM of the study reach.....	51
Figure 22. Morphological units along the study reach determined using terrain morphometrics and hydraulic modeling, which is discussed in detail below in <i>Section 7.1</i> . The purpose of the modeling was to determine the spatial characteristics of the flow hydraulics and the influence of channel morphology on the hydraulics. The mid-channel bar and the bank-protection structure can be seen in Figure 23. Background aerial photo was acquired on August 17, 2010 (source: JAXA/Alaska Satellite Facility).....	52
Figure 23. (a) Aerial photograph (acquired on February 26, 2013; true color, <i>source</i> : Google Earth) of the region containing the bank-protection structure, mid-channel bar, and the deep pool at a discharge lower than Q1 (see Figure 22); (b) Enlarged aerial photograph subset of the bank-protection structure bounded by the box seen in (a); and (c) its ground-level photo (looking downstream) taken during the field campaign of August 18–19, 2010.....	53

<u>FIGURE CAPTIONS (cont'd)</u>	<u>Pg.</u>
Figure 24. Detrended topographic surface of the terrain (Figure 25) characterizing the study reach. The positive residuals correspond to the topographic highs, and the negative residuals correspond to the topographic lows. Background aerial photo was acquired on August 17, 2010 (source: JAXA/Alaska Satellite Facility).....	54
Figure 25. Topographic residual classes (presented in Table 10) obtained from the detrended elevations (Figure 24). Note that topography is defined as positive (bars) and negative (pools) residuals of the bed topography about the channel centerline level. Background aerial photo was acquired on August 17, 2010 (source: JAXA/Alaska Satellite Facility).....	55
Figure 26. Histogram of habitat unit classes determined using the detrended elevation data (Figures 24–25).....	56
Figure 27. Sediment size distribution (%) along the study reach at the transects from T1–T 11 (Figure 13, Table 11), along the left bank (LB). Legend: TCOARSE: sediment >2 mm percent total; TFINE: sediment < 2 mm; TCLAY: clay percent total; TSILT: silt percent total; TSAND: sand percent total; VFSAND: very fine sand percent; FSAND: fine sand percent; MSAND: medium sand percent; CSAND: coarse sand percent; and VCSAND: very coarse sand percent.....	57
Figure 28. Sediment size distribution (%) along the study reach at the transects from T1–T 11 (Figure 13, Table 11), along the centerline (C). Legend: TCOARSE: sediment >2 mm percent total; TFINE: sediment < 2 mm; TCLAY: clay percent total; TSILT: silt percent total; TSAND: sand percent total; VFSAND: very fine sand percent; FSAND: fine sand percent; MSAND: medium sand percent; CSAND: coarse sand percent; and VCSAND: very coarse sand percent.....	58
Figure 29. Sediment size distribution (%) along the study reach at transects from T1–T 11 (Figure 13, Table 11), along the right bank (RB). Legend: TCOARSE: sediment >2 mm percent total; TFINE: sediment < 2 mm; TCLAY: clay percent total; TSILT: silt percent total; TSAND: sand percent total; VFSAND: very fine sand percent; FSAND: fine sand percent; MSAND: medium sand percent; CSAND: coarse sand percent; and VCSAND: very coarse sand percent.....	59
Figure 30. Sediment size distribution (%) along the study reach at each transect (T1–T 11) (Figure 13, Table 11) at the left bank (LB), right bank (RB), and centerline (C). Legend: TCLAY: clay percent total, TSILT: silt percent total, VFSAND: very fine sand percent, FSAND: fine sand percent, MSAND: medium sand percent, CSAND: coarse sand percent, VCSAND: very coarse sand percent, and TCOARSE: sediment >2 mm percent total.....	60
Figure 31. Elevation distribution above datum of river channel.....	64
Figure 32. Water depth distribution along the reach.....	65–66
Figure 33. Streamwise velocity distribution along the reach.....	66–67
Figure 34. Normal velocity distribution along the reach.....	68–69
Figure 35. Froude number distribution along the reach.....	69–70
Figure 36. Helix strength distribution along the reach.....	71–72

FIGURE CAPTIONS (cont'd)

Pg.

Figure 37. Histograms of water depth values at (a) low (Q1), (b) medium (Q2), and (c) high (Q3) discharge conditions. Min depth and Max depth denote the minimum and maximum values of water depths associated with given discharge conditions. The classes used in the spatial distribution directly correspond to the classes used in the histogram.... 73-74

Figure 38. Histograms of streamwise velocity at (a) low (Q1), (b) medium (Q2), and (c) high (Q3) discharge conditions. Min SVel and Max SVel denote the minimum and maximum values of velocities associated with given discharge conditions. The classes used in the spatial distribution directly correspond to the classes used in the histogram. For the definition of streamwise velocity, refer to Table 8..... 75-76

Figure 39. Histograms of normal velocity at (a) low (Q1), (b) medium (Q2), and (c) high (Q3) discharge conditions. Min Vel and Max Vel denote the minimum and maximum values of velocities associated with given discharge conditions. The classes used in the spatial distribution directly correspond to the classes used in the histogram. For the definition of normal velocity, refer to Table 8..... 78-79

Figure 40. Histograms of Froude number at (a) low (Q1), (b) medium (Q2), and (c) high (Q3) discharge conditions. Min Froude and Max Froude denote the minimum and maximum values of Froude number associated with given discharge conditions. The classes used in the spatial distribution directly correspond to the classes used in the histogram. For the definition of Froude number, refer to Table 8..... 80-81

Figure 41. Spatial distribution and histogram of helix strength at (a) low (Q1), (b) medium (Q2), and (c) high (Q3) discharge conditions. The classes used in the spatial distribution directly correspond to the classes used in the histogram. For the definition of the helix strength, refer to Table 8..... 82-83

<u>TABLE CAPTIONS</u>	<u>Pg.</u>
Table 1. Scale-based classification of relations between geomorphological and ecological structure of a stream system (<i>after Frothingam et al. 2002:pp. 19, Table 1</i>).....	22
Table 2. Key characteristics of the study reach on the lower Brazos River, Texas.....	27
Table 3. Key properties of the Kriging performed to interpolate the DTM point cloud data to a continuous surface.....	35
Table 4. Cross-validation results for the interpolated DTM point data using Kriging (Table 3).....	37
Table 5. Select discharges and corresponding hydrologic conditions.....	40
Table 6. Details of Model Boundary Conditions and Calibration Parameters for Q1, Q2, and Q3 flow discharge conditions.....	41
Table 7. Curvilinear grid parameters for Q1, Q2, and Q3 discharge conditions.....	42
Table 8. Hydrodynamic Model Output Parameters**.....	44
Table 9. FaSTMECH model error characteristics of each scenario.....	45
Table 10. Topographic residual classes determined using the detrended elevation data of the study reach.....	55
Table 11. Sediment size distribution along the study reach at transects from T1–T 11 (Figure 13).....	61
Table 12. D_{50} (<i>i.e.</i> , sediment size characterizing the 50% finer sediment than the rest of the sediment) type, size, and corresponding geomorphic units and water depths along transects T1–T11 (Figure 13).....	62-63
Table 13. The model output parameters and their values for the field-based low flow (Q1), and exploratory medium (Q2), and exploratory high flow (Q3) discharge conditions. For the definition of these parameters, refer to Table 8.....	64

1. BACKGROUND

1.1. Purpose of the Study

Geomorphic assessment is an important part of the Texas Instream Flow Program (TIFP). TIFP, created in response to Senate Bill 2 passed by the 77th Texas Legislature in 2001, is jointly administered by Texas Commission on Environmental Quality, Texas Parks and Wildlife Department, and Texas Water Development Board. “The purpose of the program is to perform scientific and engineering studies to determine flow conditions necessary for supporting a sound ecological environment in the river basins of Texas” (TPWD et al., 2008). The physical processes of a river, activated by and operating in conjunction with the flow regime, play an important part in supporting a sound ecological environment. As recommended by NRC (2005), TIFP has pursued the development and application of a geomorphic river classification scheme to enable greater understanding of individual river segments and assist with completion of instream flow studies.

After investigation of several alternatives (Phillips, 2006), TIFP has moved forward with a river classification scheme based on the River Styles framework described in (Brierley and Fryirs, 2005). This framework was developed to address land management impacts on river channels in Australia and some adjustments have been necessary in order to focus on instream flow related issues in Texas. The River Styles framework has been adapted to classify segments of rivers in Texas (Phillips, 2007a-b, 2008a, 2011). At a finer scale, in-channel and out-of-channel geomorphic units relevant to Texas rivers have been identified (Phillips, 2008b; Coffman et al., 2011). It was recognized, however, that additional work was necessary to develop descriptions of finer-scale physical units of relevance as habitat to fish and other biota.

Thus, this study aims to outline a methodology to (1) characterize channel morphology and flow conditions, with the purpose of mapping/assessing/monitoring fish habitat characteristics; and (2) determine the hydraulic parameters valuable in monitoring and assuring an ecologically sound river-channel environment on a reach of the Lower Brazos River, Texas. For this purpose, the study involves field data collection and hydraulic modeling to determine the major relationships between channel morphology and flow hydraulics. It also performs an exploratory analysis of how these relationships change under different flow conditions.

1.2. River Morphology, Hydrology, and Aquatic Habitat Interaction

The spatiotemporal distribution of fish habitats is largely dependent upon the coupled dynamics between stream geomorphology and hydrology (Frissell et al., 1986; Gregory et al., 1991; Braaten and Berry Jr, 1997; Moir and Pasternack, 2008; Schmitt et al., 2011). The distribution of fish habitats is a function of the interaction between hydrologic flow regimes shaping channel morphology, and the resistant geomorphic features in the channel driving flow hydraulics. This process-form relationship between flow hydraulics and geomorphic resistance generates features, or geomorphic units, such as pools, riffles, waterfalls, cascades, gravel bars, runs and large woody debris, that serve as habitats for aquatic species to progressively use for daily needs (*i.e.*, feeding, resting and refugia from predation), during specific life cycles (*i.e.*, spawning, acquiring juvenile and adult resources) and as refugia during periods of disturbance (*i.e.*, extreme low or high flows, significant temperature change, human modification) (Hart and Finelli, 1999; Thomson et al., 2001; Schwartz, 2002; Moir et al., 2004; Moir and Pasternack, 2008; Schneider and Winemiller, 2008).

A healthy aquatic community within a habitat is largely dependent upon the ability of species to fulfill their niche and to acquire the necessary resources to cultivate to an aquatic community. Accordingly, fish habitats are dependent upon the geomorphology and hydrology of a reach to distribute the necessary resources, refugia and suitable environmental factors in order to nurture a healthy aquatic community (Frissell et al., 1986; Gorecki et al., 2006).

It has become of utmost concern to federal and state agencies to maintain a sustainable quality of life for fish amidst the ever-increasing effects of human modification to fluvial environments and related stress added to fish populations. The physical structure of fish habitats change in space and time, and their form is dependent upon flow conditions, sediment transport and channel stability (Frothingham et al., 2001). Yet, in order to define the boundaries of a particular habitat, investigators must know ecological parameters along with geomorphology and hydrology dynamics. These attributes need to be adequately classified in order to measure the state and health of individual habitats and to subsequently quantify the effects of human modification on river ecosystems.

Recently, collaborative efforts among the fields of geomorphology, hydrology and ecology have been recognized. Frothingham et al. (2001: pp. 106) proposes:

“The potential linkage between geomorphology and ecology centers on a common interest in the physical properties of streams where geomorphological

conditions define the amount, diversity and structure of the physical habitat. Ecologists recognize that spatial variability of physical properties, such as mean velocity, flow depth and substrate characteristics, has a strong influence on relationships between habitat and community structure and function...Fluvial geomorphologists, on the other hand, have developed theories and techniques related to the dynamic interaction between fluvial forms and processes. The theories provide a foundation for an improved understanding of physical habitat and time-related changes in habitat conditions.”

In accordance with the purpose of the study, this review synthesizes existing literature concerning stream geomorphology and flow hydraulics relative to fish habitats in fluvial systems. It provides a general overview of the research conducted and theories developed to identify the physical interactions between stream geomorphology, hydrology and ecology.

Geomorphology

There are a number of physical properties of river systems that have been used to define habitat boundaries and conditions relative to fish habitats. The physical characteristics of water depth, channel and flow widths, flow-current velocity, substrate size and type, channel slope, bed morphological stability, sediment transport, and vegetation cover determine the suitability of certain species for habitat utilization (Dent et al., 2001). The type of habitats fish occupy is largely controlled by the life cycle stage of particular species including larval, juvenile, and adult.

Hesse et al. (1937) used channel slope and bed stability to define a “longitudinal zonation” of benthic invertebrates. Statzner and Higler (1986) found the highest number of fish to be located in bank vegetation transition zones where coniferous forest was replaced by hardwood forest, and the floodplain transitioned to debris cone zone. Additionally, they suggest that changes in the substrate of a stream segment induce changes in macroinvertebrate assemblage whereas stony substrates tend to have more stable populations of species.

In large sand-bed rivers, Statzner and Higler (1986) suggest that habitats have a greater “richness” as hydro-morphodynamics create more biologically diverse habitats. Frothingham et al. (2001) found that an increase in the spatial variability of channel morphology resulted in higher richness in individual habitats. They also found that a more diverse collection of fish habitats within a stream provides higher abundance and biomass of fish communities. Findings of Fischer et al. (2003) illustrated that sediment turnover (sediment transport and active work on

substrate within a habitat) positively effects the health of fish habitats; it is a major mechanism in the supply of oxygen and nitrogen to sediment bacteria. Thus, in habitats where the sediment turnover and transport are high, there are more resources to support community structure. In addition, substrate supply distributes particulate organic carbon deeper into the sediment with faster flows, which begins a positive feedback between stream hydraulics and microbial activity.

Meander bends tend to feature great spatial and temporal variability of habitats, which produces a higher abundance and biomass concentration due to erosion-deposition dynamics, or sediment turnover, within bends. Frothingham et al. (2001) reported that fish in meander bends were twice as large as those in a channelized stream. Marchese et al. (2005) also found a higher turnover of species and higher landscape diversity in meander bends.

Fish habitats serve as temporary refugia from predation for smaller fish or temporary habitation: gravel bars serve as spawning grounds or nurseries for fish (Baras et al., 1996); pools and riffles provide necessary food resources and community structure (Brown and Brussock, 1991). In addition, waterfalls, cascades and bedrock steps form discrete habitats for particular species (Thomson et al., 2001). Pools, riffles, floodplains, gravel bars, runs, and secondary channels form discrete habitats for transient or resident aquatic organisms and are a function of basin substrate characteristics, hydrology, valley configuration, and catchment processes.

Pools often serve as refuge from high flows, turbulent conditions, and predation, while providing an adequate food source without significant energy expenditure (Saffel and Scarnecchia, 1995). On a smaller geomorphic scale, substrate and bedform type become increasingly important for habitat preference based on hydraulic conditions, substrate material, and resource distribution. Bedform type creates zones of similar hydraulic conditions, or hydraulic biotypes that can serve as areas where particular species thrive and others do not. Amsler et al. (2009) investigated these hydraulic biotypes within dunes, finding troughs of dunes provide refuge and specific food resources for benthic invertebrates whereas reattachment zones were not preferred as there was a significant amount of sediment movement. Additionally, large-scale dunes migrate very slowly, allowing benthic organisms to migrate as well (Amsler et al., 2009), yet migration rate is dependent upon the substrate material and grain size.

At the bedform/grain scale, substrate particles arrange themselves to make-up bedforms such as ripples, dunes, plane beds, or antidunes. As sediment transport is largely a function of grain size, the migration and sustainability of these bedforms is dependent on their substrate. Coarse grains and gravel can act as armor and be sustained during high shear-stress conditions,

supplying an area for fish spawning to occur that enhances the population of macroinvertebrates within channel reaches (Frothingham et al., 2002). Marchese et al. (2005) note that patches with silt and clay have more biodiversity than sandy sediments, and habitat patchiness developed is dependent on grain size and substrate characteristics. In sand-bed rivers, Marchese et al. (2005) suggest logs and snags contribute significantly to benthic productivity due to the absence of silt and clay substratum. Substrate gradation enhances the distribution of microhabitats within a reach and provides a positive feedback with spatial biodiversity within a channel reach.

However, the physical characteristics of fish habitats are protean and difficult to classify as stages or structures change with flow conditions, and consequently, alter microhabitat development. For instance, pools do not serve as a specific habitat-type throughout a river system, but rather, pool microhabitats are determined based on flow conditions in conjunction with substrate characteristics as these properties support different aquatic organisms. Therefore, understanding these geomorphic characteristics and their related hydraulic flow conditions is vital for adequately quantifying the spatial and temporal evolution of fish habitats.

Hydrology

Hydrodynamic conditions within a stream or river are major determinants for habitat selection by fish, and consequently, a number of conceptual studies to relate flow conditions and channel morphology relative to benthic invertebrate habitat use have been conducted (Statzner and Higler, 1986; Statzner et al., 1988; Lancaster and Hildrew, 1993; Wadeson and Rowntree, 1998; Rhoads et al., 2003; Brooks et al., 2005; Schwartz and Herricks, 2005; Moir and Pasternack, 2008). Early formulations describing the physical structure of fish habitats based on hydraulic parameters within a stream were identified by the zonation concept (Hesse et al., 1937; Huet, 1949). Huet (1949) used the slope and width of a stream segment to calculate drag coefficients to describe the physical hydraulic conditions of zonation. Statzner and Higler (1986) found distinct changes in stream hydraulics produced a distinct change in species assemblage. Hart and Finelli (1999) relate the local boundary layer conditions of the water column to the spatial and temporal zonation of benthic invertebrates.

By comparing the frequency distributions of local hydraulics, bed elevations over channels with different morphologies and bank vegetation characteristics, Rhoads et al. (2003) show the relationship between fish habitat, bank vegetation and stream hydraulics. They found that large wood debris (LWD) and bank vegetation (dense grass) produced flow separation along

the banks and a decrease in flow velocities and adult fish typically inhabited deep pools, but the distribution of fish was also found to coincide with secondary flows within pools.

Wadson and Rowntree (1998) classify hydraulic conditions in a stream into “hydraulic biotopes” based on flow measurements of mean velocity, depth and bed roughness. From these measurements a series of flow parameters based on the aforementioned flow measurements can be used to characterize the hydraulic conditions, including Reynolds number (Re) and Froude number (Fr), shear velocity (V^*), and ‘roughness’ Reynolds number (Re^*). Re and Fr numbers are commonly used to characterize the stream hydraulics of fish habitats (Wadson and Rowntree, 1998; Kemp et al., 1999; Brooks et al., 2005).

In an attempt to relate the complexity of hydraulic parameters at a particular location to fish habitats, the Froude number (Fr) is used to determine the flow type. The Fr is the ratio of the inertial forces to gravitational forces. $Fr < 1$, classifies the flow as subcritical, $Fr = 1$ critical, and $Fr > 1$ supercritical. The Fr is scale independent, and therefore can be used as an indicator of hydraulic biotype. In backwater and pool units, the Fr is relatively low in comparison to run, riffle and rapid units where the Fr number is larger (Wadson and Rowntree, 1998).

Hydraulic complexity in a stream has also been used to characterize flow conditions (*i.e.*, whether the flow is laminar, transitional or turbulent). The Reynolds number (Re) is the ratio of the inertial forces to viscous forces within the stream and is dependent on scale. The Re is a measure of forces acting on the stream bed and therefore, experienced by the organisms within a habitat or biotype (Wadson and Rowntree, 1998). Wadson and Rowntree (1998) warn that the use of just the Re and/or Fr numbers is impractical in shallow/rocky or boulder streams. The Re is also lower in backwaters and pools, while progressively higher from runs, riffles, cascades, glides and chutes to rapids.

Shear stress is exerted on the channel bed surface from the boundary-layer conditions and bed roughness. This is ultimately the mechanism which moves sediment and affects the flow conditions which are experienced by benthic invertebrates. However, shear stress cannot be directly measured in the field, and shear velocity, proportional to shear stress, is used as a surrogate to describe the conditions at the surface. Shear velocity (V^*) is defined as (Wadson and Rowntree, 1998)

$$V^* = \nu / [5.75 + \log (12.3d/k)]$$

where v denotes mean velocity; d denotes depth, and k denotes bed roughness.

The ‘roughness’ Reynolds number (Re^*) determines whether the boundary layer is hydraulically smooth or hydraulically rough (Wadson and Rowntree, 1998) and incorporates the shear velocity (V^*) and bed roughness (k):

$$Re^* = V^*k / \nu$$

Davis and Barmuta (1989) found that Re^* is an excellent habitat indicator which uses both velocity and substrate characteristics. Wadson and Rowntree (1998) found Fr , V^* , and Re^* to be the most useful in classifying habitat biotypes. In studying riffle habitats specifically, Brooks et al. (2005) successfully demonstrates how invertebrates prefer particular types of hydraulic conditions.

Species abundance and community composition has negative correlation with Re^* , (Brooks et al., 2005). This suggests that species are less likely to be found where there are rough flow conditions. In areas of high roughness, organisms have higher metabolic needs as they are exposed to increased drag, and therefore, increased movement and attachment. This concept is incredibly significant, as only particular species will inhabit areas where hydraulic roughness is large at the surface, creating a species delineation of habitat preference. This implies that the areas of low Re^* are hotspots for species that have a lower metabolic processing rate. With this basic understanding, we can begin to elucidate between particular environments based on species type, and health.

Brooks et al. (2005) found velocity to be the best explanatory variable for the *spatial* distribution and patterns of invertebrates within riffle habitats, while Re^* best explained macroinvertebrate abundance, taxonomic richness, and community composition. Amsler et al. (2009) found shear stresses associated with dune morphology to be a significant factor in the distribution of fish. Troughs of the dunes had lower shear velocity values, and therefore decreased suspended sediment concentrations than at the crests and reattachment zones. Troughs served as refuge from high suspended sediment concentrations located at the reattachment zones and crests of dunes (Amsler et al., 2009).

Natural and Human Disturbance

A disturbance is a disruption in an aquatic habitat that alters the state of the system and can be natural or human induced. Natural disturbances include floods, droughts, climatic changes, or wildfires, whereas human-induced disturbances include the construction of dams, channelization of streams, installation of reservoirs, divergence of water from river and its redistribution to cities or agricultural fields, or land use land cover change.

In differentiating between perturbation, disturbance, and response, Lake (2000) proposes that a disturbance is the *cause of a perturbation* and the response of a system is the *effect of the disturbance*. Lake (2000) delineates three types of disturbances in river systems based on temporal patterns: (1) pulses, (2) presses, and (3) ramps (Figure 1). A pulse disturbance is a short-lived deviation from normal conditions but ultimately river system returns to normal conditions (Figure 1a), such as floods. Floods changes channel morphology, thus and can alter fish habitats, by causing the scour of substrate material and depositing suspended material. Floods do not constitute an entirely negative impact on fish habitats, as habitats can migrate downstream or new habitats can be developed in response to floods. During floods, fish utilize floodplain habitats as refugia (Schwartz and Herricks, 2005). A press is a disturbance that is marked by an abrupt change in stream conditions, and the altered conditions are sustained (Figure 1b). For example, increased heavy metal concentration, dam construction and channelization are forms of press disturbance (Lake, 2000). On the other hand, a ramp disturbance gradually stresses the environment to a point of negatively impacting the river system (Figure 1c). Droughts and sedimentation are examples of ramp disturbances. Droughts provide an added complexity to river systems and increase stress on fish habitats. With droughts, the water level of a river is dropped, which consequently reduces space for habitats (Lake, 2000; Rivers-Moore and Jewitt, 2007).

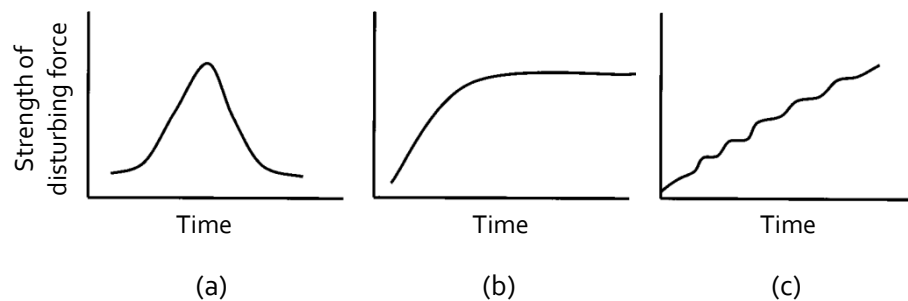


Figure 1. Three types of stream disturbance: (a) Pulse, (b) Press, and (c) Ramp (after Lake (2000): pp. 575, Figure 1).

Flow conditions are dependent upon local synoptic conditions, and the prediction of the temporal distribution of flood or drought events becomes difficult. Richter et al. (2003) suggest using baseflows during these periods for reference to the most severe conditions the river should experience. In each of these severe conditions, the first process to be affected is the hydraulic condition, which ultimately changes the morphology of a river and subsequently alters habitat development, migration, and distribution. Lancaster and Hildrew (1993), for example, relate macroinvertebrate response and habitat selection to hydraulic conditions, as the hydraulic conditions distribute the litter mass and resources needed by the invertebrates. Lancaster and Hildrew (1993) found that after periods of high and fluctuating flows, a higher abundance of invertebrates were found in flow refugia. In addition, Frothingham et al., 2002 show that shallow-pool habitats diminish during high flows as deeper pool-riffle units are more pronounced during low flows. Furthermore, habitat preference along with temperature changes as the hydraulic properties within a channel change. For instance, with decrease in flow velocities and sustained increase in temperatures during summer months, the potential for variability from reference conditions is high (Rivers-Moore and Jewitt, 2007). This introduces another aspect of disturbance as invertebrates have to sustain their population under biological limits. For juvenile Bull Trout, Saffel and Scarnecchia (1995) reported that higher temperatures constrain productivity and seasonal temperatures control the growth rate.

Not all disturbances to a system are negative. Moir et al. (2004) demonstrate geomorphic and hydraulic controls on spawning activity of Atlantic salmon (*Salmo salar* L.). Specifically, they showed that fish spawning that occurred during high flows in an upland Scottish stream. Schneider and Winemiller (2008) found large woody debris patches in the Brazos River served as both refuge from predation, an area of high food resource for macroinvertebrates, and protection from high-velocity flows.

Classification Schemes

Processes governing geomorphic and hydraulic properties of habitats operate on different spatial and temporal scales; thus, it is difficult to adequately classify and characterize the state of habitats. Several methodologies have been developed that combine the multi-scalar dynamics of geomorphic, hydrological and ecological functioning of habitats (Frissell et al., 1986; Rosgen, 1994, 1996; Wadson and Rowntree, 1998; Kemp et al., 1999; Brierley and Fryirs, 2000; Thomson et al., 2001; Frothingham et al., 2002; Thomson et al., 2004; Brierley and Fryirs, 2005).

One way to place assessments into context is to characterize habitats based on a hierarchical scheme. Fish habitats are influenced by factors that operate over a number of temporal and space scales, ranging from watershed scale to localized geomorphic units, hydraulic units, and microhabitats (Figure 2) (Thomson et al., 2001). Scale is important as the processes influencing habitats differ depending upon the time that is required to affect the habitat. The physical structure of habitats is continually changing through time, on the scale of days, events, decades, or millennia. For instance, watersheds operate on geologic time scales that primarily influence habitats based on the geometry of valley, such as valley slope and stream channel slope, or infiltration rates associated with climate conditions and vegetation. For example, habitat preference and utilization by the juvenile Bull Trout (*Salvelinus confluentus*) population in northern Idaho changed spatially within a watershed, and periodically as climate changed from cooler to warmer (Saffel and Scarnecchia, 1995). The juvenile Bull Trout prefers cooler waters and migrates to areas more suitable for their biologic needs, and these needs arise from the resources operating at a watershed scale.

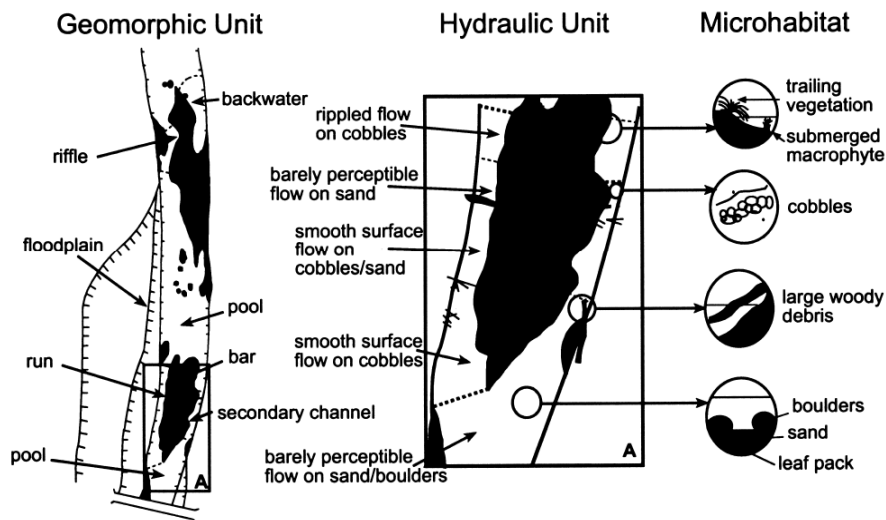


Figure 2. Scale of habitat classification (after Thomson et al. 2001: pp. 380, Figure 3).

On the other hand, smaller-scale individual hydrologic units operate on daily, weekly, or event-based time scales and are constrained by larger-scale processes. For example, pool and riffle development is a function of the larger-scale watershed drainage processes (Frissell et al., 1986). Pool and riffle morphology affect the distribution of resources needed for fish species and healthy aquatic habitats. In this sense, habitats can be viewed as the product of a continuum

of processes operating across numerous time scales. Because of this, the physical structure of habitats must be placed into context based on their distribution and migration through space and time. Frissell et al. (1986) advocated for the use of a hierarchical framework to capture the influence of watershed characteristics, reach-scale processes, and local community structures on fish habitats. This hierarchical framework places fish habitats into context, and more importantly, provides a universal classification scheme accounting for the dynamic nature of physical habitat structure. Frissell et al. (1986) classified the physical structure of habitats according to their sensitivity, with microhabitats being the most sensitive to natural disturbances because microhabitats are directly affected by local disturbances along with larger-scale disturbances felt by the reach, segment, stream, and watershed. Based on this hierarchical scheme, sensitivity to disturbances decreases with increasing spatial scale (*i.e.*, the watershed scale being the least sensitive to disturbances).

The River Continuum Concept (RCC) developed by Vannote et al. (1980) is another approach for conceptualizing the hierarchical framework produced by the interaction of stream geomorphology, hydrology and ecology. RCC bases organic matter loading, sediment transport, habitat utilization, and organism function with the physical habitat change along a river continuum. This concept was widely used as it incorporated climate, geology, stream geomorphology, and human modifications at the network scale of the continuum (Frothingham et al., 2002).

Another approach is RiverStyles developed by Brierly and Fryris (2000). RiverStyles bases the classification of specific units on a hierarchical scheme that places smaller-scale features into a larger context: hydraulic and geomorphic units to RiverStyles delineation to landscape units to catchment units (Figure 3).

Yet, a number of federal and state agencies use classification systems that have been scientifically validated as being insufficient in characterizing the health of river systems. Texas Parks and Wildlife Department (TPWD), for example, uses the Index for Biotic Integrity (IBI), a score-based assessment to measure the health of biotic habitats in the rivers in Texas (Linam et al., 2002). One key issue with IBI assessments is that the scoring criteria, based on 13 biotic characteristics, completely exclude the physical components of the habitats. The TPWD reported that an unmistakable geographical trend was evident in the fish habitats from west to east, *i.e.*, lower IBI values were found in the east, and was most likely due to “the [use] of a single index over a large land area comprised of a diversity of land forms, soil types, vegetation,

climatic conditions, and zoogeographic factors” (pp. v, Linam et al. (2002)). Also, southeastern Texas Rivers have been affected by anthropogenic influences, and consequently, have directly shaped the physical characteristics along with water quality and chemistry of the southeastern fish habitats.

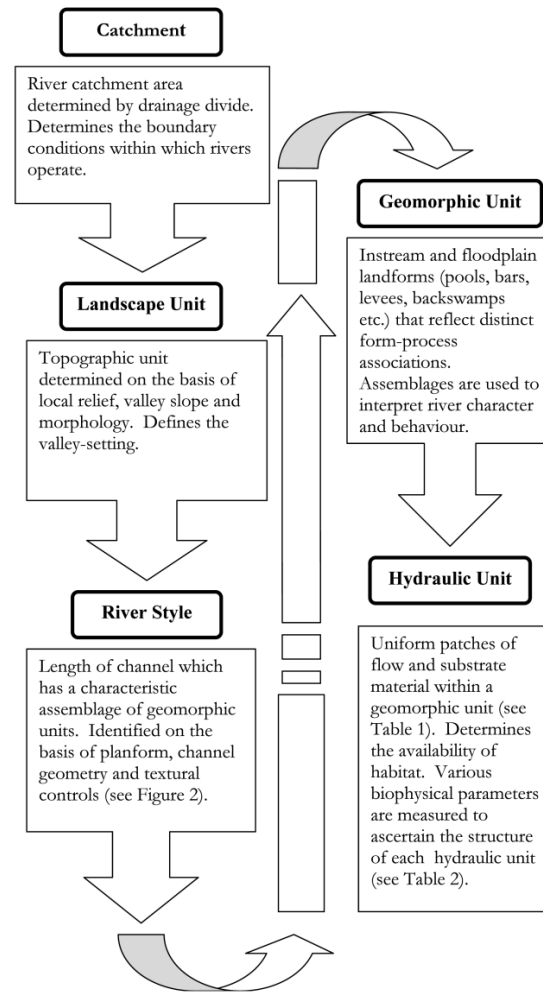


Figure 3. Hierarchical approach to habitat classification, RiverStyles framework (after Thomson et al. (2001): pp. 377, Figure 1).

USDA Forest Service, Environmental Protection Agency, and the U.S. Army Corp of Engineers (Phillips, 2006), for example, have utilized the Rosgen Classification System (RCS) (Rosgen, 1994, 1996), despite negative reviews on its ability to adequately assess the state of river systems (Miller and Ritter, 1996; Naiman, 1998; Kondolf et al., 2003; Caratti et al., 2004; Niezgodna and Johnson, 2005). The RCS is a four-level hierarchy classification system, which scales down from landscape relief, landform and valley morphology at Level I to channel form

and substrate characteristics at Level II to “stream condition and stability” at Level III, with Level IV for validation through in-field measurements (Phillips, 2006). Problems found with RCS include “unsupported assumptions about the relationship between stream types and geomorphic equilibrium, lack of linkages to hydrologic and climatic regimes, and the assumption of a one-to-one relationship between forms and processes” (Phillips, 2006). The hierarchy of this classification also assumes that if rivers exhibit similar morphologic patterns, they will behave in similar ways (Niezgoda and Johnson, 2005). Rosgen (1994, 1996) does not use process-form relationships inherent in channel morphology as an indicator of change or behavior. Phillips (2006) also notes that RCS does not conform to the dynamic or time-dependent nature of river systems constituting the classification scheme, only a “static” one (Miller and Ritter, 1996).

Thomson et al. (2001) characterizes varying river typologies based on geomorphic and hydraulic characteristics, including a gorge, a partially-confined valley with bedrock-controlled discontinuous floodplain, and a meandering gravel bed. A gorge has a particular spatial distribution of cascades, pools, and runs with more bedrock steps. A partially-confined valley reach can exhibit these geomorphic features, too, but with a different spatial distribution of the units. Also, in partially-confined beds and meandering gravel beds, it will be less likely to find certain units, such as cascades. The meandering gravel bed has a far different geomorphology than a gorge. Meandering gravel beds present different types of habitats (Figure 4). For instance, the presence of gravel bars is conducive to spawning activities, and these features are found in larger numbers in meandering river beds. Nevertheless, the approach presented in Thomson et al. (2001) addresses the analysis of small meandering rivers with gravel beds, typically with channel widths of 4–11 meters and depths of 0.20–0.66 meters.

Various hydraulic parameters characterizing flow types, such as velocity, substrate, Reynolds number (Re), Froude number (Fr) and ‘roughness’ Reynolds number (Re^*), are useful to characterize individual habitats. Varying combinations of these parameters along with channel morphology, presence/absence of bank vegetation, large woody debris, flow stratification and accumulations of organic matter create microhabitats within hydraulic units and hydraulic units within geomorphic units (*e.g.*, backwater, pool, riffle, floodplain, bar, and run). As these stream characteristics operate at different spatial and temporal scales, a number of classification schemes have been developed to better represent preferred habitat types and provide context for habitat selection.

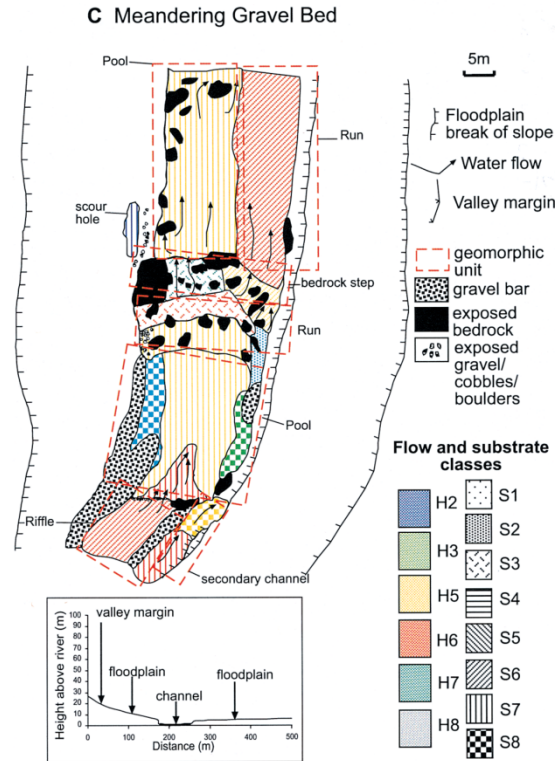


Figure 4. Geomorphic unit and hydraulic unit map for an example of the meandering gravel bed RiverStyle for the Cobark River (31°57 S, 151°42 30 E) (after Thompson et al. 2001: Plate 1C).

Frothingham et al. (2002) provides a very useful hierarchical approach to identify the ecological functioning of habitats (Table 1). They reiterate the necessity of incorporating the spatial variability in channel morphology as an indicator of the state of aquatic communities as the lack of spatial diversity is potentially the most critical habitat attribute limiting biodiversity within a channel. This implies that reduced flow rates and variability in rivers will result in reduced spatial biodiversity, and, therefore, different orders of flow are needed to sustain complex interactions between geomorphology, hydrology, and ecological functioning of habitats.

In brief, new innovative research conducted to classify the state of fish habitats that incorporates the geomorphology and hydrology of fish habitats has recently refocused direction to habitat classification. Because fish habitat types are spatially and temporally dynamic, the most useful approaches for classifying habitats are multi-scalar, hierarchical approaches. Methodologies, which include measurements at each scale, provide the most holistic and inclusive datasets to appropriately delineate habitat state and structures within channel reaches and their context in space and time.

Table 1. Scale-based classification of relations between geomorphological and ecological structure of a stream system (*after* Frothingam et al., 2002:pp. 19, Table 1).

Scale	Geomorphological view	Ecological view
Network	Links and nodes Influence of network structure on hydrological response Hydraulic geometry relations Downstream trends in sediment characteristics Downstream trends in stream power along discrete sediment-transport pathways	Species composition of network/watershed River Continuum Concept Influence of network structure on spatial variation in community composition
Link	Uniform hydrology, sedimentology, and average channel size, but planform may vary	Functional and structural uniformity of internodal physical habitat or assemblage of planform habitat patches
Planform	Reaches with uniform planform characteristics	Planform habitat patches
Bar unit	Discrete bedform that scales with channel width; fundamental bed unit of planform development	Characteristic mosaic of bar element habitat patches; pool-riffle sequences, stream confluences
Bar element	Discrete sedimentological elements of bar units, e.g., pools, riffles, point bars	Bar element habitat patches or mosaic of microhabitat patches
Grain	Individual large grains, grain clusters, or bedforms	Microhabitat patches

2. OBJECTIVES OF THE STUDY

The purpose of this study is to characterize the channel morphology and flow hydraulics of a select river reach on the lower Brazos River, Texas to inform fish habitat mapping and assessment. The study reach is a large sand-bed reach, with a high meandering planform. For this purpose, we asked four specific questions:

- 1) What are the spatial characteristics of the channel morphology (*i.e.*, geomorphic units)?
- 2) What are the spatial characteristics of flow hydraulics at different discharge conditions, including low, medium, and high discharges?
- 3) How does channel morphology influence the spatial characteristics of flow hydraulics within the study meander bend and how does this morphological influence change with changing discharge?

3. STUDY REACH

3.1. Selection of the Study Reach

To select the study reach, we evaluated the lower Brazos River between the bridge on the State Highway (SH) 79 near Hearne [30°49'38.06"N, 96°39'3.48"W] and the SH 105 near Navasota [30°21'41.17"N, 96° 9'20.35"W]. We used the following criteria for the selection of potential study reaches included:

- 1) Presence of complex planform geometry (*e.g.*, compound meander loop);
- 2) Presence of spatially (and potentially temporally) diverse river morphology observable from remote-sensing images (*e.g.*, multiple point bars and pools in one meander bend);
- 3) Characteristics of historical evolution of the channel pattern (*i.e.*, differential migration rates and patterns along the planform);
- 4) Accessibility to the river (through the bridge ramps and/or roads); and
- 5) Proximity to College Station (*i.e.*, preferable due to fish study field work logistics)

Selection of potential study sites based on *criteria 1–3* listed above involved visual examination of current and historical aerial photographs, starting from the 1940s to 2008. Once the candidate sites were selected, we discussed them with the aquatic habitat group PI, Dr. F.I. Gelwick (Department of Wildlife and Fisheries Sciences, Texas A&M University), and reevaluated the candidate sites based on their appropriateness for the fish sampling and analysis. Based on these discussions, we selected a couple of sites to further explore whether they could

fulfill the rest of the criteria (*i.e.*, *criteria 4–5*). For this purpose, we contacted property owners (*e.g.*, via phone calls, visits to properties, inquiry letters, etc.) in order to obtain permission to use their properties to access the river. Finally, we selected the site presented in Figure 5 as our study reach.



Figure 5. Study reach and its access point south of FM 60 (Raymond Stotzer Pkwy) on the lower Brazos River, Texas, shown on an aerial photograph (a true-color digital orthophoto quarter quadrangle (DOQQ)) obtained in August 2008.

3.2. The Lower Brazos River

The Brazos River is the largest river in Texas with a length of >1900 km, extending from its headwaters in New Mexico to the Gulf of Mexico at Freeport, and with a drainage area of ~118,000 km². The lower Brazos River is located in the coastal plains of Texas, characterized by a humid subtropical climate. The mean annual precipitation ranges from 750 to 1300 mm/yr. Watersheds are dominated by agricultural land uses, mainly grazing (Phillips, 2006). The lower Brazos River experienced several episodes of cutting, filling, channel migration, extension, and contraction related to Quaternary sea level and climate changes (Alford and Holmes, 1985; Blum et al., 1995; Waters and Nordt, 1995; Morton and White, 1996).

The dominant planform pattern of the lower Brazos River is meandering, characterized by both historical and recent channel migration on relatively wide floodplains with moderate to high connectivity between the river channel and its floodplain. Floodplains contain landforms typical of dynamic meandering channels including oxbow lakes resulting from neck and chute cutoffs, meander scars, and scrolls, as well as a set of avulsive channels (Figure 6). The channel substrate ranges from sandy to muddy (Phillips, 2006). The bed material is highly mobile; however, in certain areas bedrock, which is typically composed of cohesive clayey pre-Quaternary sediments, it is exposed or covered by a thin (<1 m) alluvial sediment layer (Phillips, 2006).

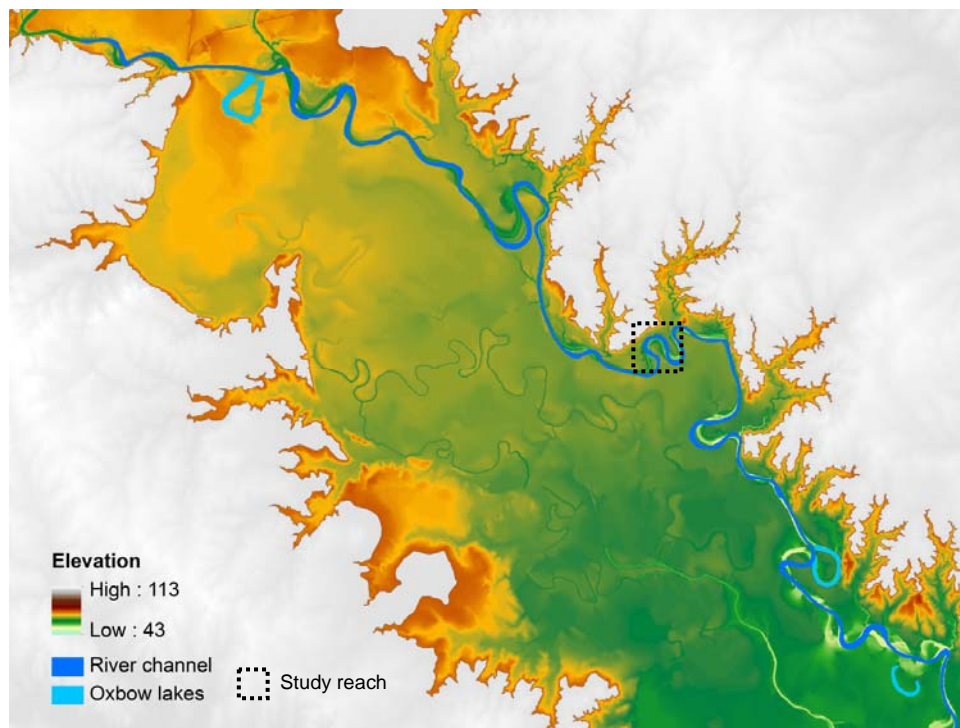


Figure 6. Floodplain boundary (marked with the elevation range of 43–113 m) of the study reach (Figures 5 and 7) located within meandering incised valley fill zone on the lower Brazos River, Texas (Phillips, 2006). The river is characterized by a single-thread channel with tributary avulsive channels. Elevation data shown are obtained from the U.S. Geological Survey (USGS) National Elevation Dataset (NED) (cell size = 10 m).

3.3. Study Reach Characteristics

Geomorphology

The study reach is located on a section of the lower Brazos River incised into Pleistocene alluvial terraces (Phillips, 2006) (Figures 6–7, Table 2). The topographic and morphological characteristics of these alluvial terraces influence modern river dynamics (Blum et al., 1995; Waters and Nordt, 1995). The lower Brazos River in this area is characterized by a single-thread meandering channel with tributary avulsive channels (Figure 6). The average floodplain width ($W_{floodplain}$) is 8.57 km, and channel slope (S) is 0.000164 m/m.

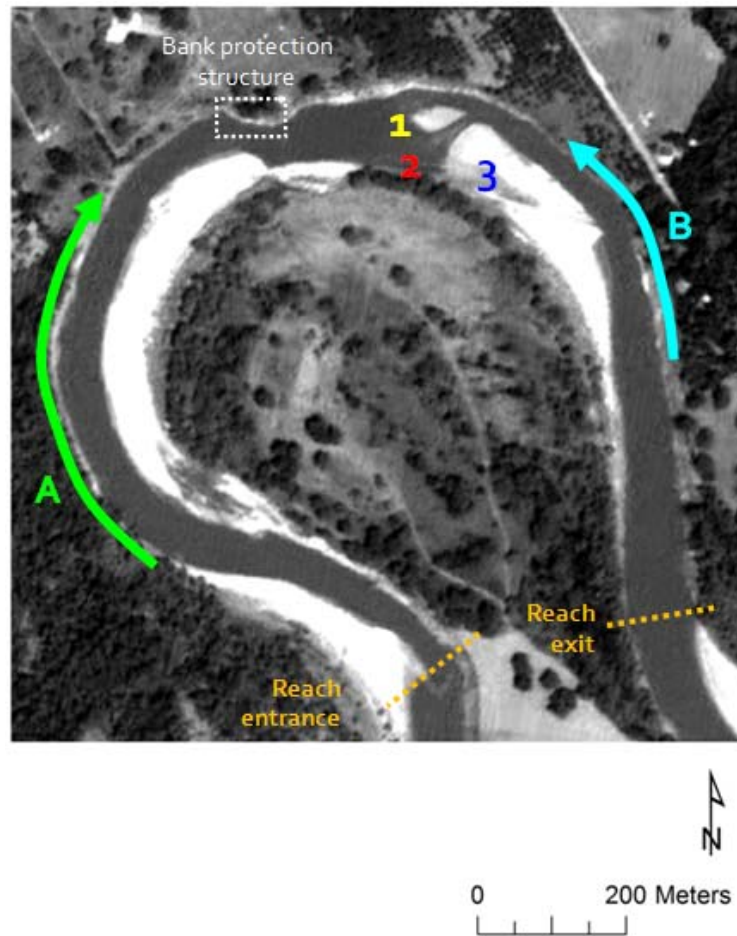


Figure 7. Study reach (reach entrance X,Y coordinates, 751,122.2251, 3,381,298.5804; reach exit X,Y coordinates, 751,415.3741, 3,381,365.4222, based on NAD 83 UTM Zone 14 (units = meters)). The flow direction is from left to right. The arrows A–B mark the location of the views of the river sections shown on Figure 8. The numbers 1–3 mark the location of the features shown on Figure 9. Background aerial photo was acquired on August 17, 2010 (source: Japan Aerospace Exploration Agency (JAXA)/Alaska Satellite Facility).

Table 2. Key characteristics of the study reach on the lower Brazos River, Texas.

Location	Entrance coord. (NAD 83 UTM Zone 14)	751,122.2251; 3,381,298.5804
	Exit coord. (NAD 83 UTM Zone 14)	751,415.3741, 3,381,365.4222
Valley characteristics	Valley type	Meandering incised valley fill
	Average valley width, $W_{floodplain}$ (km)	8.57
	Channel type	Single-thread meandering with avulsive tributaries
Hydrology	Average discharge (m^3/s)	
	Average annual peak	1291.917
	Average daily	134.51
	Min–max	3.54–2389.96
Reach characteristics	Reach type	Meandering, incised
	Reach length (km)	2.27
	Channel width, W (m)	
	Reach averaged	61.4
	Min–max	33.7–110
	Reach averaged bed slope, S (m/m)	0.000164
	Reach sinuosity	3.59
	Average reach bed material	Sand (very fine to medium sand)
	Direct human impact	Via a localized bank-protection structure located along the cutbank on the left side of the channel immediately upstream of the deep pool (Figures 7 and 22).

The river banks exhibit marked spatial variability, resulting from in-channel morphological complexity and varied land-cover types (e.g., soil, grass, and trees) occupying the river banks (Figure 8).



Figure 8. Panoramic views of the incised river section along the study reach, which is located on the lower Brazos River, Texas. The photos were taken on August 19, 2010, looking (a) downstream (arrow A on Figure 7) and (b) upstream (arrow B on Figure 7).



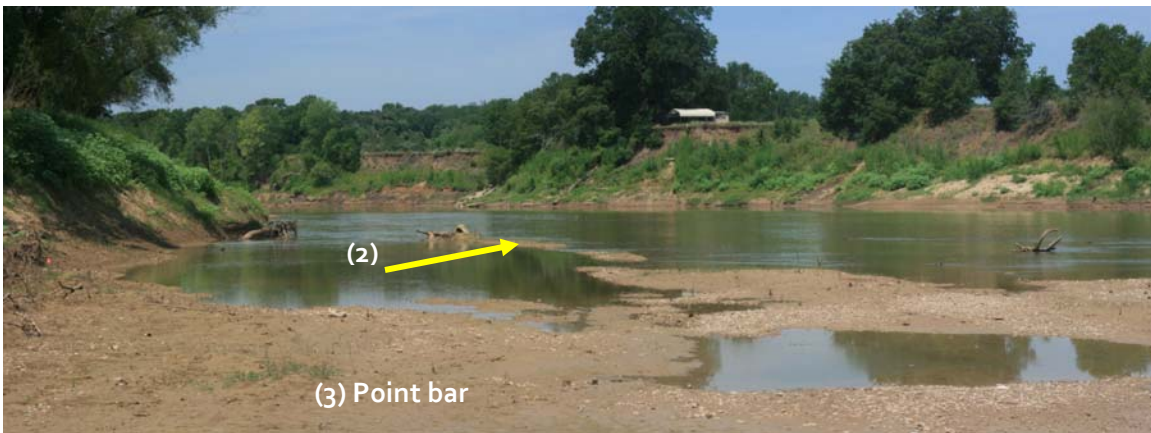
Figure 8 (cont'd). Panoramic views of the incised river section along the study reach, which is located on the lower Brazos River, Texas. The photos were taken on August 19, 2010, looking (a) downstream (arrow A on Figure 7) and (b) upstream (arrow B on Figure 7).



(a)



(b)



(c)

Figure 9. Study reach photographs taken during the field campaign of August 18–19, 2010: (a) Exposed mid-channel bar (looking upstream) marked as (1) on Figure 7; (b) the region on the left side of the mid-channel bar looking toward the left bank, marked as (2) on Figure 7; the beginning of the point bar is seen on the right; and (c) Slightly downstream of the region in (b) looking upstream, marked as (3) on Figure 7, showing the beginning of the point bar.

Hydrology

At the USGS gaging station at the Brazos River at SH 21 near Bryan, TX (08108700), the daily mean discharge over the period of July 15, 1993–March 19, 2013 ranges between 3.54 and 2389.96 m³/s, with an average of 134.51 m³/s (Figures 10–11, Table 2). Figure 10 shows daily mean discharge and Figure 11 shows the monthly discharge (m³/s) between October 1993 and September 2011. Field surveys were performed during the August 18–19, 2010 field campaign (i.e., red dashed line on Figure 10). The field survey dates correspond to low-discharge conditions with an average daily discharge, $Q_{\text{Aug 18-19, 2010}} = 25.28 \text{ m}^3/\text{s}$, with a return interval of 1.5 days at the gaging station; thus, the discharge during the field campaign approximately corresponds to only 19% of the mean daily average discharge.

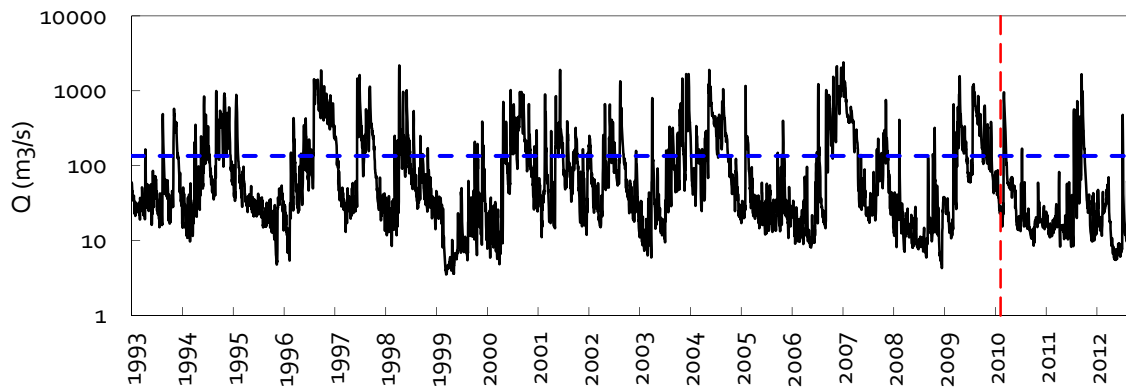


Figure 10. Daily mean discharge at the Brazos River at Bryan, TX, USGS gaging station (08108700), over a period from 7/15/1993 to 3/19/2013. The horizontal (blue) dashed line marks the average discharge ($Q_{\text{ave}} = 134.51 \text{ m}^3/\text{s}$); the vertical (red) dashed line marks the discharge on August 18, 2010.

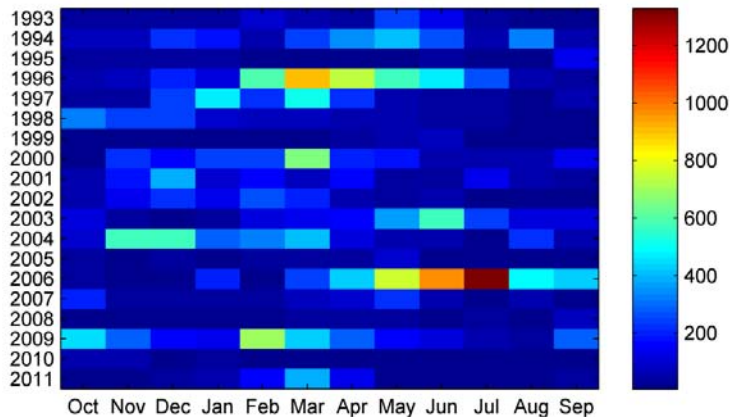


Figure 11. Monthly discharge (m³/s) statistics over the period of October 1993–September 2011.

4. DATA COLLECTION AND PROCESSING

4.1. Field Data Collection

Hydroacoustic data collection

The hydroacoustic data collection was conducted during the August 18–19, 2010 field campaign by the TWDB field crew led by David Flores, with support from the PI and a graduate student, Christy Swann (Department of Geography, Texas A&M University). During these surveys, the aquatic habitat group, led by Dr. Gelwick (Department of Wildlife and Fisheries Sciences, Texas A&M University), also conducted fish data collections in the study reach. The data collection was performed using an Acoustic Doppler Current Profiler (ADCP) River Surveyor M9 (SonTek, 2011). The data included water depth and water surface elevation (WSE) at the survey points (X,Y) and the edge-of-water (EOW) coordinates (X,Y) (Figure 12). The RiverSurveyor M9 presents two options for Depth Reference, including Vertical Beam (using the echo sounder) and Bottom Track, using the velocity transducers (SonTek, 2011).

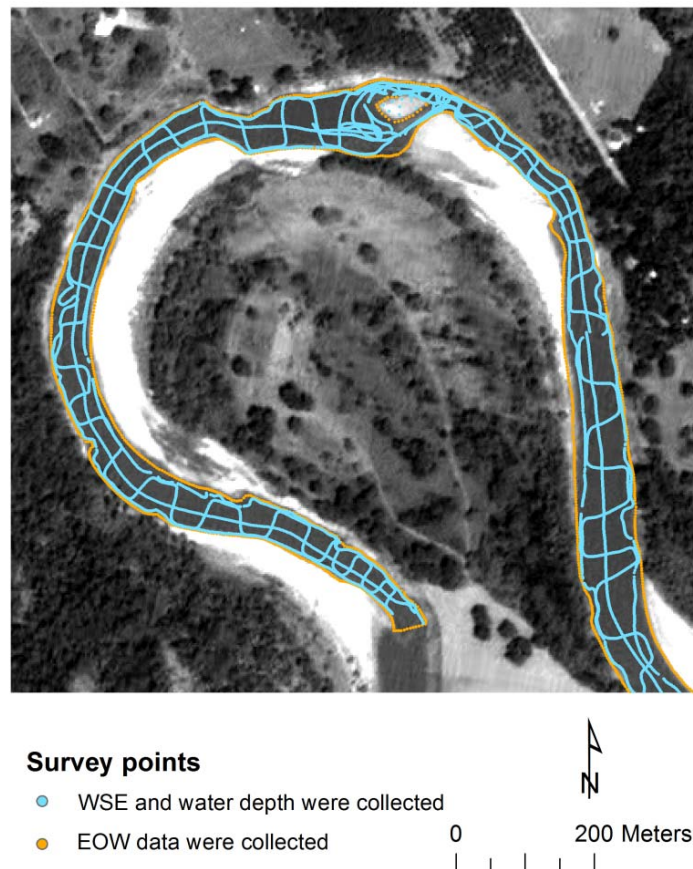


Figure 12. ADCP data points along the study reach during the field campaigns at August 18–19, 2010. Background aerial photo was acquired on August 17, 2010 (source: JAXA/Alaska Satellite Facility).

Sediment sampling

In addition to hydroacoustic data collection, we also sampled riverbed substrate material within the study reach. We performed particle size distribution analysis on the sediment samples collected to 1) determine sediment/substrate characteristics of point bars, cut banks, and channel bed; and 2) to inform the analysis for fish habitats within the study reach.

The substrate sediment samples were collected along 11 transects (T1–T11) during the field campaigns of August 18–19, 2010 (Figure 13). Using a hand-held GPS receiver, the transect coordinates were located and flagged on the left and right banks of the river. Along each transect, the sediment samples were taken at three locations: 1) the left bank, 2) the right bank, and 3) the centerline. The left and right banks denote the channel banks along the left and the right side of the channel, respectively, in the downstream direction (i.e., looking downstream).

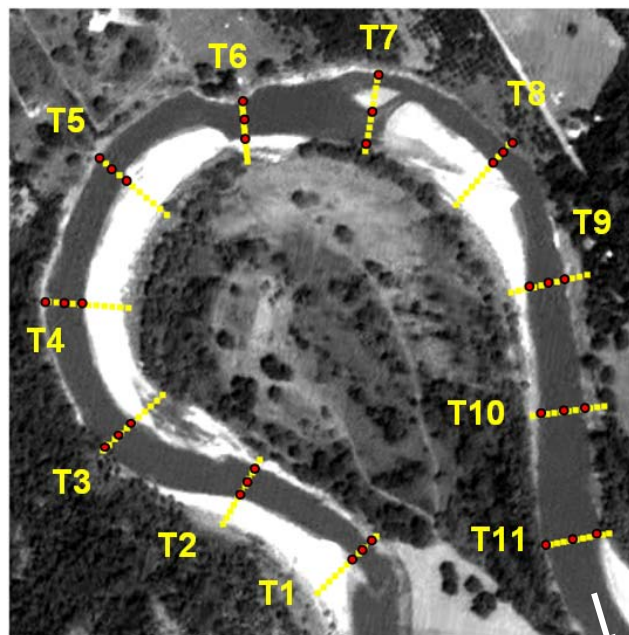


Figure 13. Locations of transects T1–T11 at which the sediment sampling was performed. The flow direction is from T1 to T11. Background aerial photo was acquired on August 17, 2010 (source: JAXA/Alaska Satellite Facility).

A motorized John boat was used to access each location for substrate sediment sampling. Sediment samples were collected using a mechanical, spring-loaded grab sampler that was lowered to the riverbed to retrieve sediment. Samples that were collected close to the point bar were taken from the riverbed one foot from the water line, and samples collected close to the cut banks were taken on the river bed at a distance of three feet from the bank. Due to

strong currents in mid-channel locations, centerline samples were taken as close to the channel centerline as possible (approximately within five feet of centerline). Transect T7 data was excluded from the analysis due to incomplete data. Additionally, transects T9 and T11 had no centerline data collected due to strong currents causing inability for accurate measurement.

4.2. Field Data Processing

Hydroacoustics data processing

We processed the hydroacoustics data following the procedure described below:

- 1) Obtain the ADCP raw data using the capabilities of MATLAB;
- 2) Extract the water depths associated with the survey points (Figure 12) measured by the Vertical Beam as well as Bottom Track (BT);
- 3) Evaluate the data to assure the Vertical Beam and Bottom Track depth scales are the same and check for any major discrepancies;
- 4) Delineate the edge-of-water (EOW);
- 5) Extract the water surface elevation (WSE) for all survey points (X,Y,Z) within the EOW boundary;
- 6) Calculate the water depths for each point (X,Y, Depth) within the EOW boundary from Bottom Track, by taking the average of four Bottom Track beam velocity transducers for each survey datasets;
- 7) Merge sub datasets to create complete water surface elevation and depth data sets;
- 8) Compute bathymetric elevation at each point (X,Y) by taking the difference between WSE and water depth; and
- 9) Merge the bathymetric elevations with the EOW elevations.

We performed the delineation of the EOW (i.e., (3)) by utilizing River Surveyor M9 ADCP data. The delineation of EOW boundaries was guided by use of an Advanced Land Observation Satellite (ALOS) Panchromatic Remote-sensing Instrument for Stereo Mapping (PRISM) image (ground sample distance (GSD) = 2.5 m, panchromatic; nadir view (0°); source: Japan Aerospace Exploration Agency (JAXA)/Alaska Satellite Facility), which was acquired on August 17, 2010. The elevation data set created in (7) was used to generate the digital terrain model (DTM) of the study site via interpolation as discussed in *Section 4.3*.

Sediment data processing

The substrate sediment samples, which were collected at transects T1–T11 (Figure 13), were labeled and brought back to the Sediment Lab at Texas A&M University. The sediment samples were prepared for further analysis (*i.e.*, pipette analysis), performed by the Soils Lab. This preparation included drying samples and carefully sieving for grains larger than 2 millimeters. Pipette analyses determine the fractions of sand, silt and clay within a sediment sample.

Each transect sample was labeled according to the transect number and location on the corresponding transect (*e.g.*, T1 Left Bank (T1 LB), T2 Right Bank (T2 LB), T3 Centerline (T3 C)). Grain size distribution analysis was performed, and the sediment distributions, as well as D_{50} along the left bank, right bank, and the centerline, were determined. The depth for each sample varied depending upon local bathymetry.

4.3. Generation of Digital Terrain Model (DTM) of the Study Reach

We generated the digital terrain model (DTM) of the study reach to be used for the morphometric analysis and hydraulic modeling. We performed the interpolation as follows. To obtain the terrain and bathymetric information for the elevations that were not covered during the field data acquisition (*i.e.*, beyond the EOW), we utilized an Intermap Technologies® NEXTMap® airborne interferometric synthetic aperture radar (InSAR)-derived DTM of the study reach (Figure 14).

This NEXTMap® radar-derived DTM (*i.e.*, DTM v1.5 5mP) was generated based on airborne InSAR data, acquired between July 05 and July 19, 2005, with a nominal 5-m ground sample distance. Horizontal positional accuracy for these data is 2 meters RMSE or better in areas of unobstructed flat terrain; vertical positional accuracy is 1 meter RMSE or better, also in areas of unobstructed flat terrain (as per Intermap Technologies® metadata). Data were acquired with a primary look direction to the West.

First, we converted the raster-based radar-derived DTM data to point-cloud data. Then, we removed the radar-derived DTM data points corresponding to the area overlapping with our field survey-based bathymetric data (*i.e.*, the data corresponding to the area defined by the boundary of the EOW). Next, we fused the radar-derived “outside the EOW boundary” point

data with the ADCP-derived “within the EOW boundary” point survey data to create a point cloud representing complete terrain including the bathymetry.

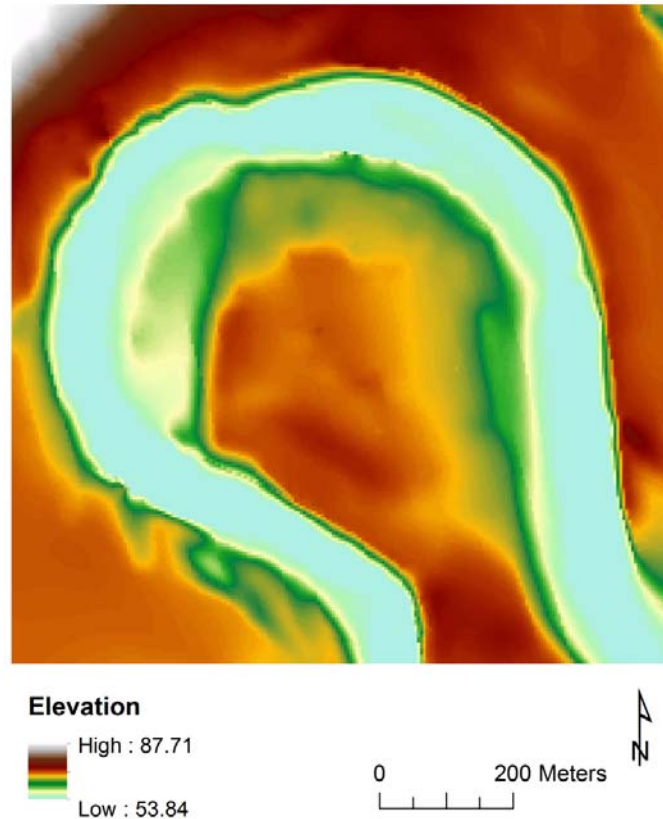


Figure 14. Intermap Technologies® NEXTMap® interferometric synthetic aperture radar (InSAR)-derived Digital Terrain Model (DTM) (in vertical and horizontal units of meters) used in the terrain generation for the study reach (cell size = 4.396 m).

Then, we interpolated the complete DTM point-cloud data to a continuous raster surface via Kriging. Kriging is a very flexible geostatistical gridding method that produces maps from irregularly spaced data. It attempts to express trends suggested in spatial data, so that, for example, high points might be connected along a ridge rather than isolated by bull's eye-type contours. Kriging can be either an exact or a smoothing interpolator depending on the user-specified parameters. It incorporates anisotropy and underlying trends in an efficient and natural manner (Goovaerts, 1997).

We performed the Kriging using Surfer® 10, which is a professional tool for geoscientists for contouring and surface mapping (Surfer, 2012). Specifically, we performed the interpolation of the point data with a spatial resolution of 5 meters – following the nominal resolution of the

original radar-derived DTM. We performed the interpolation using point Kriging with the parameter values given in Table 3 (Figure 15).

Table 3. Key properties of the Kriging performed to interpolate the DTM point cloud data to a continuous surface.

Kriging Type:	Point	Search Parameters	
Gridding spatial resolution (m):	5	Search Ellipse Radius #1:	1200
Polynomial Drift Order:	0	Search Ellipse Radius #2:	1200
Kriging std. deviation grid:	no	Search Ellipse Angle:	0
Semi-Variogram Model		Number of Search Sectors:	4
Component Type:	Linear	Maximum Data Per Sector:	16
Anisotropy Angle:	0	Maximum Empty Sectors:	3
Anisotropy Ratio:	1	Minimum Data:	8
Variogram Slope:	1	Maximum Data:	64

To assess the spatial variation in gridding quality and to guide data sampling, we performed a cross validation analysis. The cross-validation analysis involved three steps: 1) For each observation location, interpolation of the value using the neighboring data, but not the observation itself; 2) computation of the resulting interpolation errors; and 3) assessment of the quality of the selected gridding method, using various summary statistics of the errors.

We performed the cross validation for the interpolated zone within the EOW region and excluded data above the EOW region. The rationale behind this was that we are to determine the accuracy of the interpolation within the region of surveyed data. Radar-derived DTM point data were acquired in an already interpolated form with a spatial resolution of 5 meters. Under such circumstances, a standard cross validation approach may not generate useful results, as inclusion of the above “the EOW region” data obtained from the radar-derived DTM would artificially increase the accuracy of the interpolation. To counter this potential problem, we set elevation (Z) limits ($\min Z$, $\max Z$) on the to-be-interpolated data and selected validation points within these limits. This restricted the cross validation to the data extent of the surveyed region. Data falling outside of these limits were used during the interpolation, but they were not used as cross validation points.

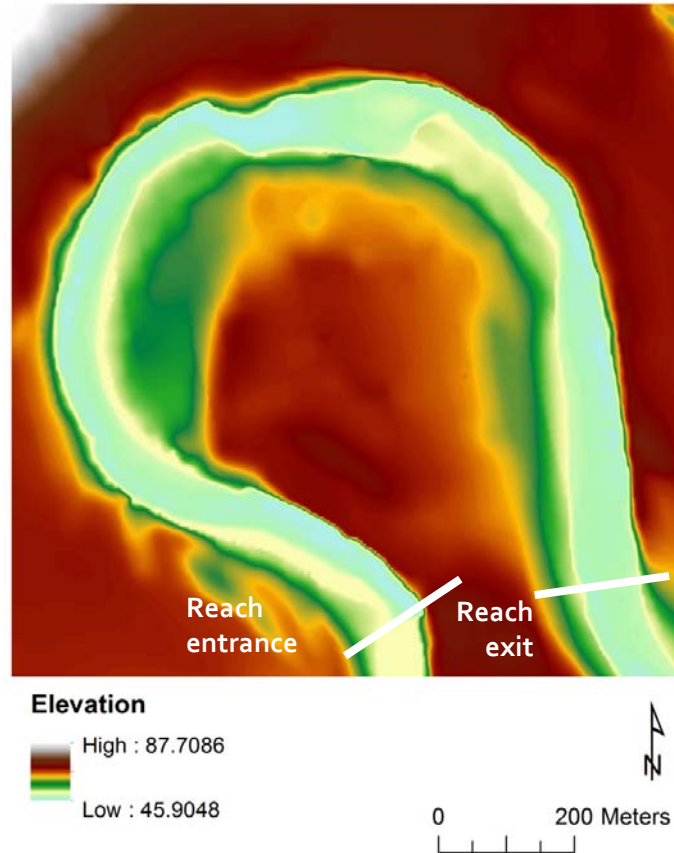


Figure 15. Point Kriging-interpolated Digital Terrain Model (DTM) of the study reach (cell size = 5 m) including the terrain information (from Intermap Technologies® NEXTMap® InSAR-derived DTM) and bathymetric information (from field survey)- visualized bilinear interpolation with a cell size of 1 m.

The cross validation of a gridded (interpolated) surface can be performed using numerous quantitative measures that can be used as a goodness-of-fit statistic for the semivariogram model. The literature suggests three particular statistics as the most consistently useful, including: 1) the *median absolute deviation* of the cross-validation residuals; 2) the *standard deviation* of the cross-validation residuals; and 3) the *rank correlation* between the measurements and the estimates (Isaaks and Srivastava, 1989; Kitanidis, 1997; Chiles and Delfiner, 1999; Olea, 1999). Specifically, median absolute deviation shows the median value of the sorted absolute deviations of the cross-validation residuals. It is calculated by: 1) computing the data's median value; 2) subtracting the median value from each data value; 3) taking the absolute value of the difference; 4) sorting the values; and 5) calculating the median of the values. Standard deviation of the cross-validation results gives the standard deviation of the cross-validation residuals. The Root Mean Square (RMS) data metric generates an output grid for which each nodal value is the root mean square of the cross-validation residuals.

We performed the cross validation using the three statistics, median absolute deviation, standard deviation, and rank correlation, discussed above to assess the spatial variation in the interpolation quality. The results show that the quality of the interpolation is satisfactory according to the values obtained for these three statistics (Table 4).

Table 4. Cross-validation results for the interpolated DTM point data using Kriging (Table 3).

Univariate Statistics		Univariate Cross-Validation Statistics			Rank Correlation
Min Z limit (m)	Max Z limit (m)	Median Absolute Deviation (m)	STD (m)	RMS (m)	Z – Estimated Z
46.130	52.811	0.027	0.082	0.084	0.992

The generated DTM of the study reach therefore characterizes both the channel morphology and overbank morphology. It should be noted that the radar-derived DTM has a spatial resolution of 5 meters and is based on the data acquired in 2005 (Figure 14). Because of the temporal difference between the radar-derived DTM and the in-situ data collected during 18–19 August 2010, the radar-derived DTM data cannot fully represent the temporally-concurrent morphology of the study reach above the EOW. However, the examination of the historical evolution of the study reach using historical aerial photographs showed that the migration of the study reach was limited. Thus, the use of 2005 radar-derived DTM did not significantly affect the results of our analysis.

5. CHARACTERIZATION OF CHANNEL MORPHOLOGY

Our first specific objective addresses the issue of identifying geomorphic units. To determine the spatial characteristics of the study reach including the geomorphic units, we employed a two-scheme approach: morphometric characterization based on (1) planform morphology and (2) terrain morphology.

5.1. Characterization of Planform Morphology

We performed a 2-Dimensional (2-D) characterization of our study reach by examining its morphometric properties including channel sinuosity, curvature, and channel width. Channel curvature spatial series characterizes the change in the direction angle along the channel planform over a unit meander arc-length, where the direction angle spatial series represents the direction of each point on the channel planform with respect to the down-valley direction (Güneralp and Rhoads, 2008).

We performed the analysis on planform morphology characterization using Geographic Information System (GIS) tools (ArcGIS v.10); the planform analysis tool (Lauer, 2006); a series of computer codes developed by the PI; and aerial photographs that temporally coincide with the time of field data acquisition. The computation of the channel width spatial series was performed by utilizing the planform analysis tool (Lauer, 2006). The tool inputs channel left bank and right bank of a river reach, and computes the channel centerline coordinates (X,Y) and corresponding channel width (W) with the specified spatial interval (Δs) based on these input data. The aforementioned computer codes were developed by the PI during a previous study in MATLAB® (Güneralp and Rhoads, 2008). The codes compute the curvature spatial series of a given channel planform centerline at a spatial interval defined by the user.

5.2. Characterization of Terrain Morphology

We examined the spatial characteristics of the study reach by analyzing its 2.5-D morphometric properties. These properties included elevation/bed morphology (variability), terrain slope, longitudinal and cross-sectional morphology. In the terrain morphology analysis, we used the digital terrain model (DTM) of the study reach (*see Section 4.3* for a detailed description of the DTM-generation procedure). We computed the morphometric variables using the capabilities of the ArcGIS® software package.

6. CHARACTERIZATION OF FLOW HYDRAULICS AT DIFFERENT FLOW CONDITIONS

In order to address *specific objectives 2–4* (*i.e.*, the spatial characteristics of flow hydraulics and the influence of channel morphology on the flow hydraulics), we examined the characteristics of flow hydraulics at different discharge conditions by modeling channel hydraulics.

We modeled the channel hydraulics for a set of discharges that are representative of *low*, *medium*, and *high* discharge conditions (Table 5). We informed our classification based on our findings from the planform and terrain morphometric analysis of the characteristics and spatial distribution of geomorphic units. The characteristics of our discharge classes are as follows:

- 1) *Low discharge (Q1)*. This discharge corresponds to the hydrologic condition during the field campaign conducted at August 18–19, 2010. For Q1, almost all of the major depositional units (*i.e.*, point bars, mid-channel bars) were emergent and the flow was concentrated around the thalweg. The discharge was calculated from the ADCP data as the average of multiple ADCP passes along a transect at the reach entrance.
- 2) *Medium discharge (Q2)*. Medium discharge corresponds to the hydrologic condition at which the mid-channel bar, which is a significant depositional geomorphic unit in the study reach, becomes submerged.
- 3) *High discharge (Q3)*. High discharge is defined as the hydrologic condition at which all of the significant depositional geomorphic units of the channel morphology, including mid-channel bar(s) and point bars, are submerged. It also characterizes the threshold of overbank flooding on the inner bank of the channel.

We determined the medium and high discharges by performing a series of exploratory analyses with a range of entrance discharges, and then examining the degree of submergence of the morphological units along the reach. The justification for such analyses is that the purpose of the study is to provide insights to fish habitat mapping, and thus, it is important to determine: (1) the thresholds of geomorphic units for water depths, or in other words, how the geomorphic units change with changing depths of water; and (2) the influence of the channel morphology on flow hydraulics which play a significant role in fish habitat.

Table 5. Select discharges and corresponding hydrologic conditions.

Discharge Class	Hydrological Condition	Entrance³ Discharge⁵ Q (m³/s)	Exit⁴ Stage WSE (m)
Low ¹	All depositional units ² are widely emergent, chute channel at Q1 (Figure 22) is submerged	24.592	52.47
Medium	Mid-channel bar at Q1 (Figure 22) is submerged, point bars are partially emergent	58.217	54.47
High	All depositional units (mid-channel bars and point bars) and chute channels are submerged	157.908	56.47

¹ Corresponds to the field-campaign discharge conditions.

² Point bars and mid-channel bars (see Figure 22).

³ Entrance denotes the location of the transect at the entrance of the reach (Figure 15).

⁴ Exit stage denotes the location of the transect at the exit of the channel (Figure 15).

⁵ In the set of average daily flow values at the USGS gage 08108700 Brazos Rv at SH 21 nr Bryan, TX, the Q₁, Q₂, and Q₃ flows correspond to the 32.5, 60.9, and 78.3 percentile flows, respectively.

6.1. Hydraulic Modeling

In this study, we performed the hydrodynamic modeling using FaSTMECH in order to identify and predict hydro-geomorphic features and flow hydraulics in a compound meander bend of the Brazos River at different levels of discharge.

FaSTMECH is an iterative quasi 3-D hydrodynamic and sediment transport solver for the Multi-Dimensional Surface Water Modeling System (MD_SWMS) that is developed and used by researchers at the USGS (Barton et al., 2005; McDonald et al., 2006; Kim et al., 2011). When modeling flow, this model has standard fluid dynamic assertions such as conservation of mass and momentum, fluid being incompressible, flow being steady, and conditions being hydrostatic. However, FaSTMECH also asserts that flow can be adequately simulated by relating the Reynold’s (turbulent) stresses to an isotropic eddy viscosity (Barton et al., 2005; Nelson, 2013). Hence, this approach assumes that the apparent viscosity of a flow caused by turbulent eddy separation can be simplified as being isotropic. Usage of this model involves calibration and validation for field conditions.

Most input parameters (*e.g.*, elevation, water depth, discharge, etc.) are field-informed. On the other hand, the others, such as roughness and lateral eddy viscosity, are given initial estimates and adjustments are made until the model outputs simulate field conditions and have greater iterative stability. In addition, an appropriate topographic model is one of the most important parameters to properly characterize flow patterns with a 2D depth averaged hydrodynamic model as flow is sensitive to perturbations in topography (Crowder and Diplas, 2000).

The elevation dataset input into this model consisted of field-inferred channel topography and an airborne radar-derived digital terrain model. This fused elevation dataset was then interpolated to a finer cell size of one meter to avoid introducing artificial roughness into model results. We obtained the field-informed flow parameters and channel topography as discussed in *Section 4, Data Collection and Processing*. Flow parameters consisted of channel discharge at the influent end (i.e., reach entrance) of the channel and WSE at the effluent end (i.e., reach exit) (Figure 15). We used ADCP-estimated WSE for the entire reach for validation of the model results, following methods from Barton et al. (2005). Three flow conditions, low (Q1), intermediate (Q2), and high (Q3) discharges, with effluent stages that begin at low flow with 52.47 meters and increment by 2 and 4 meters are simulated with Q1 being the field-acquired flow condition (Table 6).

Table 6. Details of model boundary conditions and calibration parameters for Q1, Q2, and Q3 flow discharge conditions.

	Q1	Q2	Q3
<i>Boundary Conditions</i>			
Effluent Stage, WSE (m)	52.47	54.47	56.47
Influent Discharge, Q (m^3/s)	24.592	58.217	157.908
Direction angle (degrees)	-18	-18	-18
<i>Calibration Parameters</i>			
C_D , initial (unitless)	0.030539	0.021773	0.018076
C_D , calibrated (unitless)	0.0001	0.029	0.024
Lateral Eddy Viscosity, initial (m^2/s)	0.003301	0.009608	0.020961
Lateral Eddy Viscosity, calibrated (m^2/s)	-0.15	0.009608	0.020961

With the model topography defined, we then created the model computational structure. The model structure for FaSTMECH is a curvilinear grid (Nelson, 2013). The curvilinear grid computational structure offers an advantage over other 2-D depth averaged models in that the coordinates of the model are composed of stream-wise direction and stream-normal direction. To facilitate this coordinate system/computational structure, we first traced a centerline that begins and ends in the same position as the flow within the model domain. The centerline is a generalized center-of-flow line fitted with two considerations, to depict center-of-channel flow and to accommodate all channel flow in different flow conditions. Once the centerline was defined by tracing from the influent to effluent end of the channel, the curvilinear grid was given width and number of streamwise and stream-normal grid cells to accommodate the model flow with a resolution of approximately 5 meters. It was necessary to increase the width of the

curvilinear grid for Q3, since wetted area in the model domain extended to (and presumably past) the edge of the grid. Parameters for entering curvilinear grids are featured in Table 7.

Table 7. Curvilinear grid parameters for Q1, Q2, and Q3 discharge conditions.

	Q1	Q2	Q3
Number of nodes at streamwise direction	445	445	445
Streamwise increment (m)	4.854	4.854	4.854
Number of nodes normal to streamwise direction	35	35	39
Cross-stream increment (m)	5.132	5.132	5.132
Width (m)	175	175	195
Centerline Tension	1	1	1

After the structure and domain of the model were defined, we input boundary conditions as defined above for the field-derived flow condition (Q1). One other consideration that must be made is the stability of the effluent boundary condition. Since FaSTMECH does not allow for recirculating flow on the effluent channel boundary, there is a risk of model instability should eddies appear. This is handled by forcing downstream velocity at the effluent end of the channel (McDonald, pers. comm.). Another concern that was noted in the simulation of Q1 was that of influent channel direction. This parameter does have some influence over WSE shape and trend. We conducted several experiments, and determined that the most appropriate direction that characterizes the model-observed WSE was 18 degrees toward the right bank of the channel (Table 6).

With field-acquired boundary-flow parameters defined for Q1, the initial estimates of calibration parameters (*i.e.*, C_D and lateral eddy viscosity) were informed with average depth and average channel velocity obtained from influent channel geometry and a modified approach provided by Ghani et al. (2007). C_D was held constant throughout the channel and was initially estimated based on Manning's n parameter (Ghani et al., 2007) and flow depth (Nelson, 2013). Lateral eddy viscosity is estimated as $0.01 * U_{avg} * d_{avg}$, where U_{avg} denotes the average river reach velocity in meters per second and d_{avg} denotes average river reach depth in meters (Conaway and Moran, 2004; Barton et al., 2005; Berenbrock and Tranmer, 2008). Based on field-acquired WSE slope versus model-calculated water surface slope, we calibrated the roughness by incrementing up or down. Then, we adjusted lateral eddy viscosity upward from the initial estimate to increase iterative stability of model to reasonable levels (Barton et al., 2005; Nelson, 2013). This adjustment was only necessary in the case of the Q1 low-discharge field condition.

Before 2–D estimates of hydrodynamic parameters can be obtained, an initial estimate of WSE must be made to determine wetted and non-wetted locations within the model domain. FaSTMECH can accomplish this by using a 1–D water surface elevation model. This model is informed by 2–D model boundary conditions and an estimate of roughness. We estimated the roughness a little higher than the 2–D model estimate (McDonald, pers. comm.). Hence, 1–D roughness is altered along with 2–D roughness during calibration as well.

With the approach of Ghani et al. (2007), along with influent channel geometry and sediment data, we generated a rating curve to inform boundary conditions of the medium- and high-flow conditions (i.e., Q2 and Q3, respectively). This approach derives a Manning’s n for a given stream with information regarding D_{50} and average flow depth. We determined the D_{50} value from the analysis of sediment grab samples as discussed in detail in *Section 4.2*, which is approximately 0.16 mm (fine sand) as the median grain size for the stream. We derived the flow depth from influent channel geometry. To calibrate Q2 and Q3 flows, we assumed WSE throughout the channel to have the same shape and just offset by the stage increment of 2 and 4 meters. Just as in Q1, we adjusted the roughness up or down depending on the relationship between observed and predicted water surface slope. Input values for both 1–D and 2–D model parameters for the three flow conditions are featured in Table 7.

Most of the 2–D hydrodynamic model parameters out of FaSTMECH are averaged at depth, which means that the entire water column from river bed to water surface is averaged. These 2–D parameters include several hydrodynamic variables of interests such as water surface elevation (WSE), shear stress magnitude and its streamwise and normal components, velocity and its streamwise and normal components, and the *Froude number*, which measures the kinetic versus inertial forces of a given flow (Dingman, 2009) as discussed in *Background, River Morphology, Hydrology, and Aquatic Habitat Interaction* (Table 8).

2–D computed parameters that are not averaged include depth and water surface elevation, and shear stress. Water surface elevation is initially estimated with a 1–D model based on downstream water surface elevation, lateral eddy viscosity, and roughness (McDonald, pers. comm.; Nelson, 2013). The 1–D water surface elevation is then further refined by the 2–D FaSTMECH hydrodynamic model. Depth is inferred as being the difference between water surface elevation and bed elevation.

To simulate 3–D flow, we implemented a quasi 3–D model within the FaSTMECH solver, which generates layer-averaged solutions that approximate a 3–D flow by specifying

depth-averaged layers. From these solutions helix strength can be derived. Helix strength is a quasi 3–D parameter that measures the angle difference between water flows close to the bed and water flows at the water surface. Helix strength is an indicator of helical flow that represents the angle difference between the top and bottom of the water column (Nelson, 2013).

Table 8. Hydrodynamic Model Output Parameters**.

Parameter Abbreviation	Definition (unit)
WSE	Computed Water Surface Elevation (meters)
Elev	Elevation above datum of river channel (meters).
Depth	Depth of flow (WSE – Bed elevation) (meters).
Vel	Depth-averaged velocity magnitude (meters/second).
SVel	Depth-averaged streamwise velocity magnitude (meters/second). Positive values indicate net velocity along flow; negative values indicate net velocity against flow.
NVel	Depth-averaged normal velocity (meters/second). The velocity of flow that is perpendicular to the streamwise velocity. Positive values correspond to the flow toward left bank; negative values correspond to the flow toward right bank
Shear	Shear stress magnitude near the river bed (kilograms.meters ⁻¹ second ⁻²).
SShear	Shear stress (kilograms.meters ⁻¹ second ⁻²) in the streamwise direction near the river bed. Positive values correspond to the shear stress in the streamwise direction; negative values correspond to that in the direction opposite to streamwise direction.
NShear	Normal shear stress perpendicular to SShear near the river bed (kilograms.meters ⁻¹ second ⁻²). Positive values correspond to the shear stress normal to streamwise direction toward the left bank; negative values correspond to that toward right bank.
Froude	Froude number to indicate the ratio of inertial to gravitational forces (unitless). For Froude number < 1, flow is subcritical; for Froude number = 1, the flow is critical, for Froude number > 1, then the flow is supercritical.
Helix	A quasi-3D model output that represents the difference in angle between surface flow and near-bed flow.

**These definitions are derived from Nelson (2013), FaSTMECH Model Notes. <http://i-ric.org>.

Fifty (50) vertical nodes per 2–D node were numerically solved to allow the model to output helix strength. Computationally, helix strength parameter is dependent on the number of 'vertical nodes' that one specifies when 3–D modeling. It has been observed that this and other quasi 3–D parameters are stabilized when the vertical nodes are specified as 50 or higher. With all necessary parameters, the models were run at 5000 iterations. Solutions were output with the curvilinear grid format.

Data processing of model outputs into a more common user-friendly format involved conversion of curvilinear grid to GeoTIFFs via Delaunay Triangulation and raster binning at one meter. We chose a binning size of one meter to reduce the chance of under-sampling and aliasing at bend apices—which have grid cells closer together than five meters. Channel boundaries for each image are defined and clipped in the ArcGIS Desktop® environment.

Model validation

We performed the model validation and calibration based on two criteria: 1) model stability as visualized through cross-sectional percent deviance from specific discharge and overall RMS cross-sectional discharge change; and 2) model efficacy as analyzed through observed and predicted WSE.

Following Conaway and Moran (2004), a model was considered to be suitably converged if the discharge deviance was within +/-3% at all cross-sections in the curvilinear grid. This threshold was relaxed slightly if the majority of the stream had cross-sectional values that were acceptable, and the net discharge was within threshold. For scenario Q1, the threshold for overall discharge deviance was ~0.74 m³/s (Table 9). There was a set of locations that were out of the 3% bound, and these locations are downstream of the mid-channel bar, which represents a macro-roughness feature (Figures 9, 16, and 22). Another consideration to note is the usage of ‘Force Downstream Velocity’ in these scenarios. FaSTMECH cannot process influent flow at the downstream boundary, which implies that certain features, such as eddies, can render the model unstable. An option to overcome this is ‘Force Downstream Velocity’, however locations immediately adjacent to the effluent boundary may not be as accurate otherwise (Nelson, 2013).

Table 9. FaSTMECH model error characteristics of each scenario.

	Q1	Q2	Q3
Convergent threshold at +/- 3% of discharge (m ³ s ⁻¹)	0.74	1.75	4.74
Overall RMS of discharge at 5000 th iteration (m ³ s ⁻¹)	0.78	0.69	0.38
Overall deviance % of discharge at 5000 th iteration (unitless)	3.16%	1.19%	0.23%
Highest cross-sectional deviance	+4.5%	~ -6.75%	+2.5%

We computed the water surface elevation for the low-discharge scenario, Q1, (Figure 17) and determined the differences between observed and modeled (predicted) water surface elevations (Figure 18). The location just upstream of the mid-channel bar is the very large ‘bump’, and the depression immediately after that corresponds to the two smaller channels on either side of the mid-channel bar.

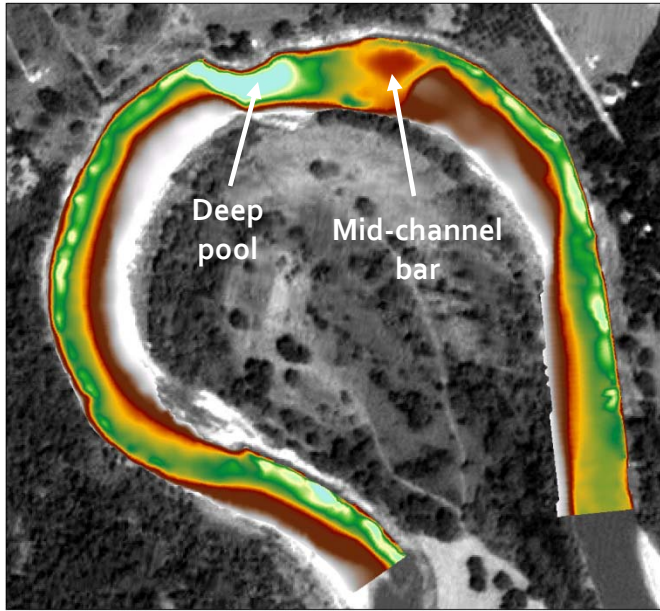


Figure 16. Elevation model representing the river channel clipped for the boundary defined by high discharge (Q3). Mid-channel bar represents a macro roughness structure (Figure 9a). Background aerial photo was acquired on August 17, 2010 (source: JAXA/Alaska Satellite Facility).

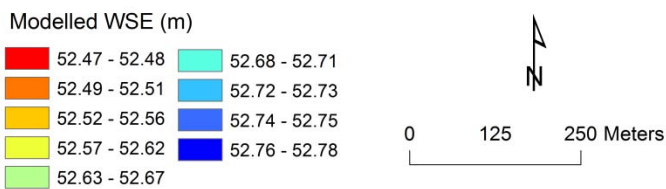
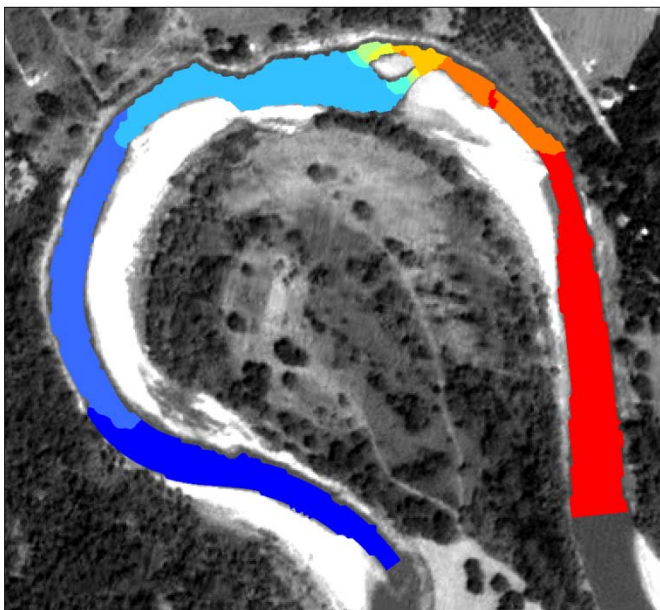


Figure 17. Water surface elevations predicted using the hydrodynamic model FaSTMECH and based on low-discharge scenario, Q1. Background aerial photo was acquired on August 17, 2010 (source: JAXA/Alaska Satellite Facility).

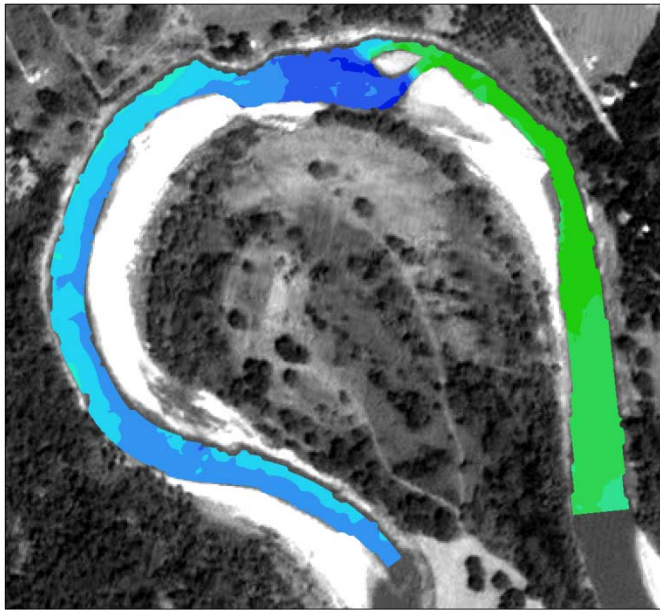
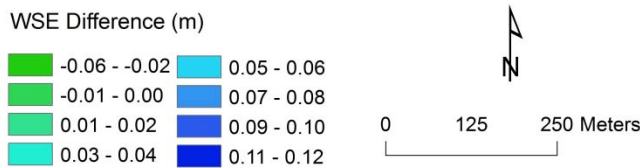


Figure 18. Difference between the measured and modeled water surface elevations. Background aerial photo was acquired on August 17, 2010 (source: JAXA/Alaska Satellite Facility).



Medium- and high-discharge scenarios, Q2 and Q3, had overall RMS values well below their respective thresholds (Table 9). However, the medium-discharge scenario (Q2) had a location (approximately 20 meters of river length) of relatively high percent deviance (-6%) that is situated close to the large pool element (Figure 17). For the high-discharge scenario, Q3, all cross-sections were within the prescribed threshold of +/-3% deviance (Table 9).

These more convergent and better predicted WSE values for Q2 and Q3 indicate the decreasing influence of the mid-channel bar structure as a macro-roughness element on flow dynamics. We conducted the model validation for the exploratory medium- and high-discharge scenarios (i.e., Q2 and Q3, respectively) with WSE acquired in the field plus 2 and 4 meters, respectively. The shape of observed and predicted WSEs match suitably well for the influent and effluent regions of the given reach in each scenario (e.g., Figure 18).

6.2. Delineation of the Physical Boundaries of Habitat Types

To delineate between habitat types, flow conditions relative to common morphology of habitats must be considered. In general, no general consensus on the depth for each habitat type

has been reached because habitat depth is dependent on the scale of the river, which is commonly why flow type is used for habitat distinction. For instance, Rabeni and Jacobson (1993) define pools as the depth range of 1–5 meters, whereas *Rhoads et al.* (2003) have depths with a range of 1–2 meters on the Embarrass River as being pools.

Clifford et al. (2006) uses detrended bathymetry data to distinguish between pools and riffles. By detrending the centerline bathymetry, Clifford et al. (2006) classify positive values as riffles and negative as pools. Detrending depth relates the hydraulic state to bathymetry and provides a way to quantitatively differentiate among topographic influences on flow in a river. Following Clifford et al. (2006), in this study, detrended depth data were used to delineate habitat types.

Detrending procedure

Starting with interpolated bed topography (Figure 16), in the form of a raster and following approach of Clifford et al. (2006), we classified wetted extents of the stream as being pools or sediment bars. This distinction is made from a negative (pool) or positive (sediment bar) residual from a detrended surface. We calculated the trended surface as a simple linear regression of bed topography at a centerline. The positional basis for this centerline is calculated on wetted extent. This detrending procedure involved data processing on three levels: 1) data processing for the centerline itself; 2) extension of the centerline-based data toward the left and right banks to create a surface; and 3) generation of the detrended surface.

Points used to generate the trended surface were also used to sample bed topography. Thus, these points contain point-sampled elevations of the detrended surface and bed. With a series of points representing a trended surface and sampled bed elevation, we generated the continuous surface via a Triangulated Irregular Network (TIN) and transformed the surfaces into raster formats, with a resolution of one meter. The detrended surface was calculated by subtracting the trended surface from the sampled bed elevation (Figure 16).

7. RESULTS

7.1. Morphometric Characteristics of the Study Reach

Planform Morphology

The reach has a very high sinuosity (~ 3.6). The results from the analysis of planform morphology indicate that the channel planform can be characterized as a compound meander loop where the spatial series of planform curvature consists of multiple curvature maxima and inflection points (Figures 19, 20).

The spatial series of curvature varies significantly along the channel, with values ranging from 0.09 to 0.43 m/m (Figure 20). This complex meander loop consists of a total of seven curvature maxima. The first inflection point marked as #1 on Figure 19 occurs at a transition zone from point bar to cutbank on the left bank and from cutbank to point bar on the right bank. The second and third inflection points (marked as #2 and #3) are located near the exit of the point bar and right before the mid-channel bar, respectively. These inflection points slightly downstream of the bend apex cause a shift in the direction of the channel. The other inflection points are at or after the exit of the meander loop (Figures 19–20).



Figure 19. Water surface centerline and the location of the inflection points (large green full circles) and the curvature maxima (small orange full circles). Background aerial photo was acquired on August 17, 2010 (source: JAXA/Alaska Satellite Facility).

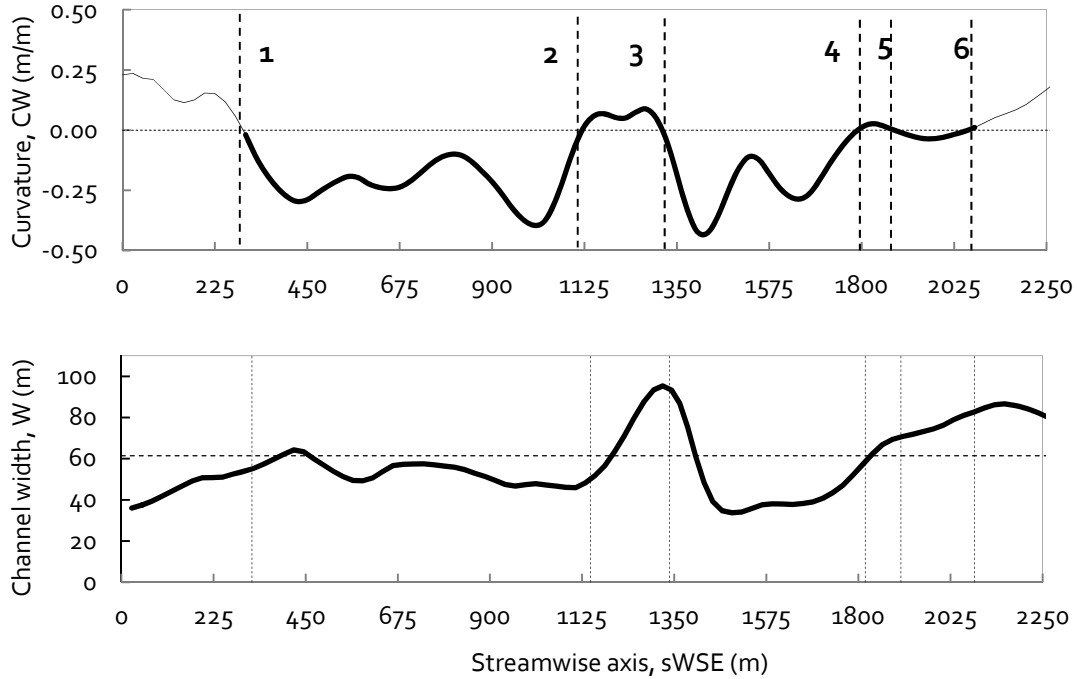


Figure 20. (a) Planform curvature spatial series along the water surface centerline obtained from the edge-of-water data collected during the field campaign of August 18–19, 2010. CW denotes the dimensionless curvature (i.e., curvature scaled with average channel width). The numbers 1–6 show the location of the inflection points (Figure 19). The curvature maxima marked as small dots (in the color orange) in Figure 19; (b) spatial variations in the channel width computed for the same WSE condition along the streamwise axis.

The channel width also varies spatially along the channel planform from 35.6 m to 86.7 meters. There is some variability in the reach section between the reach entrance and inflection point #2 (from ~37 to ~47 meters) over a length of ~1110 meters and the section between curvature maximum #6 and the reach exit (from ~34 to ~86 meters) over a length of ~765 meters. The highest variability in channel width is observed within the very short section starting at inflection point #2 and ending at the end of the mid-channel bar in the streamwise direction, which is located near the sixth curvature maximum (Figures 19– 20). Within this region, the channel width increases abruptly from ~54 meters and reaches to ~80 meters at the third inflection point, and it starts decreasing at this point to a lower value (~34 meters), compared to the width at the beginning of this section at the sixth curvature maximum.

Terrain Morphology

Terrain morphology reflects the characteristics of meandering channels that can also be observed from the elevation pattern of the reach. The slope distribution within the study area indicates that the cutbanks have the highest slopes (*i.e.*, 24– 52 degrees) whereas within the channel, the slope range is much lower, being between 0 and 10 degrees (Figure 21).

The slope range is also higher than that of the channel bed along the point bar edges and in a portion of the inner bend, being between 10 and 16 degrees (Figure 21). Along the right bank, between the point bars, where the direction change in the planform curvature occurs, the slope is considerably higher than that along the point bar edges (24–32 degrees). This high-slope range indicates the effect of hydraulics causing erosion on the right bank, leading to the development of a cutbank (Figure 21).

Based on the terrain morphology, we identified the following geomorphic units: point bar, pool, mid-channel bar, and chute channel. We also identified a bank-protection structure along the cutbank approximately at the same location as inflection point #2 (Figures 19–22).

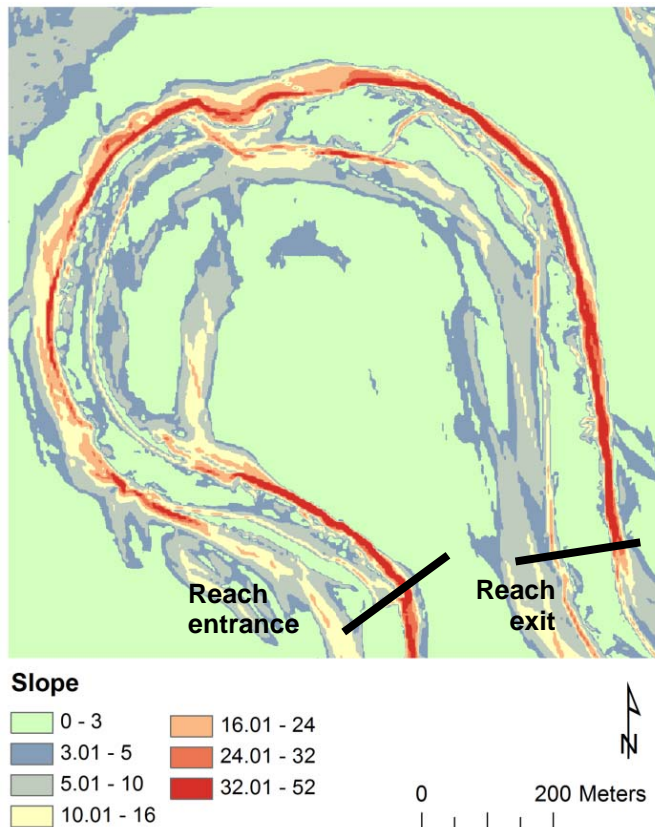


Figure 21. Terrain slope (in degrees) computed from the generated DTM of the study reach.

The mid-channel bars and the chute channels shift their location depending on the flow conditions. For example, the water flow is redirected from the chute channel #1 to chute channel #2 as the discharge changes from low (Q1) to medium (Q2). Similarly, although the mid-channel bar at low discharge (Q1) is located near the beginning of the second point bar, it shifts its position at medium discharge (Q2) to slightly downstream to where the point bar is located (Figure 19). For discharge conditions even lower than Q1, the mid-channel bar gets further exposed and connected to the point bar (Figure 23).



Figure 22. Morphological units along the study reach determined using terrain morphometrics and hydraulic modeling, which is discussed in detail below in *Section 7.1*. The purpose of the modeling was to determine the spatial characteristics of the flow hydraulics and the influence of channel morphology on the hydraulics.

The mid-channel bar and the bank-protection structure can be seen in Figure 23. Background aerial photo was acquired on August 17, 2010 (source: JAXA/Alaska Satellite Facility).

Morphological units

-  Bank Protection Structure
-  Chute cutoff at Q1
-  Chute cutoff at Q2
-  Pool
-  Mid-Channel Bar at Q1
-  Mid-Channel Bar at Q2
-  Point Bar



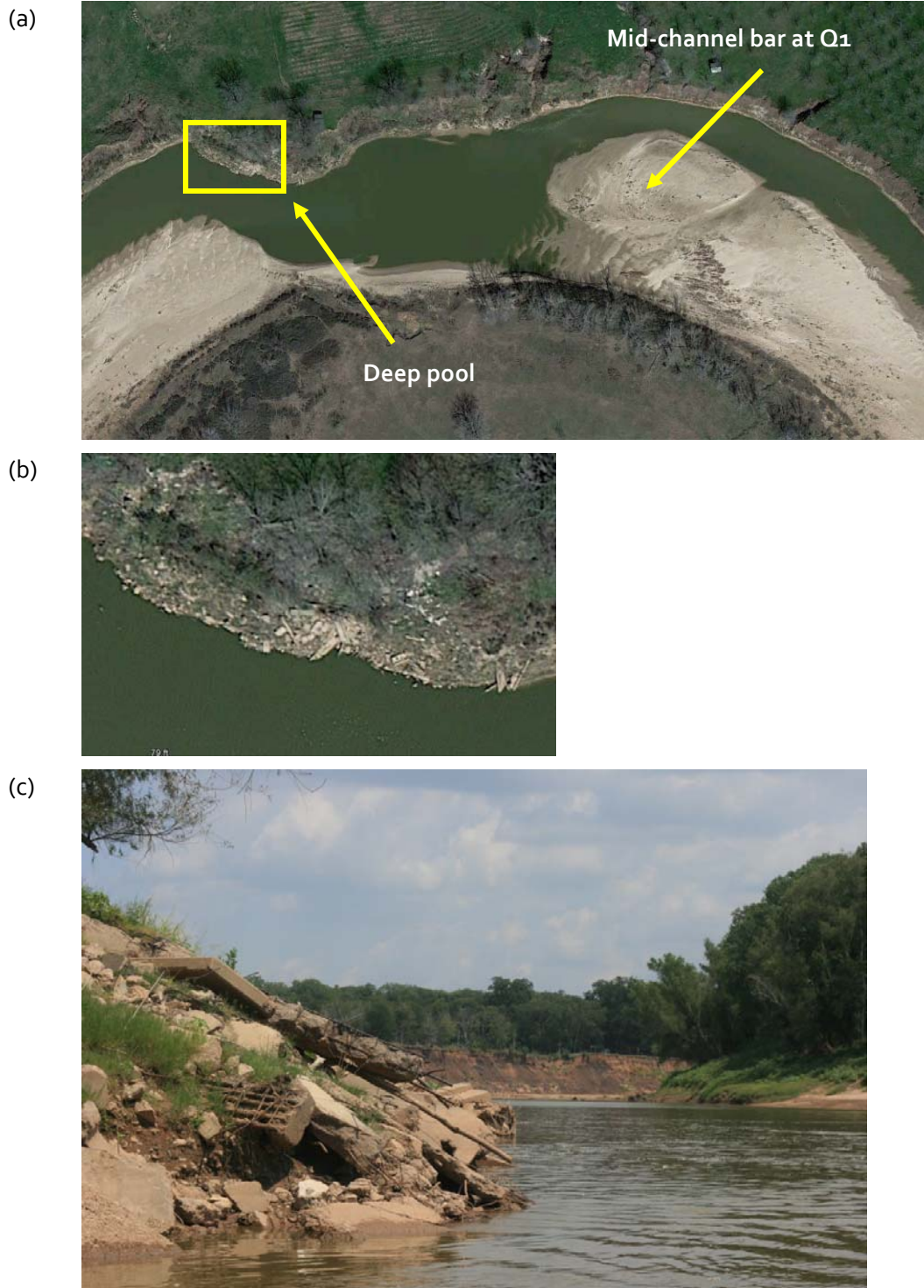


Figure 23. (a) Aerial photograph (acquired on February 26, 2013; true color, *source*: Google Earth) of the region containing the bank-protection structure, mid-channel bar, and the deep pool at a discharge lower than Q_1 (see Figure 22); (b) Enlarged aerial photograph subset of the bank-protection structure bounded by the box seen in (a); and (c) its ground-level photo (looking downstream) taken during the field campaign of August 18–19, 2010.

7.2. Physical Boundaries of Habitat Types

Topographic residuals

After detrending the elevation (Figure 24) following the procedure discussed in *Section 6.2*, we determined the topographic residual classes (Figure 25, Table 10). The residuals of the bed topography about the channel centerline level are defined as topographic highs characterizing bars (positive) and defined as topographic lows characterizing pools (negative). We also determine the 25th, 50th, 75th, 100th percentiles for both positive and negative residuals (*i.e.*, from -4 to 4 classes, where negative (positive) classes showing the topographic lows (highs) in Figure 25).

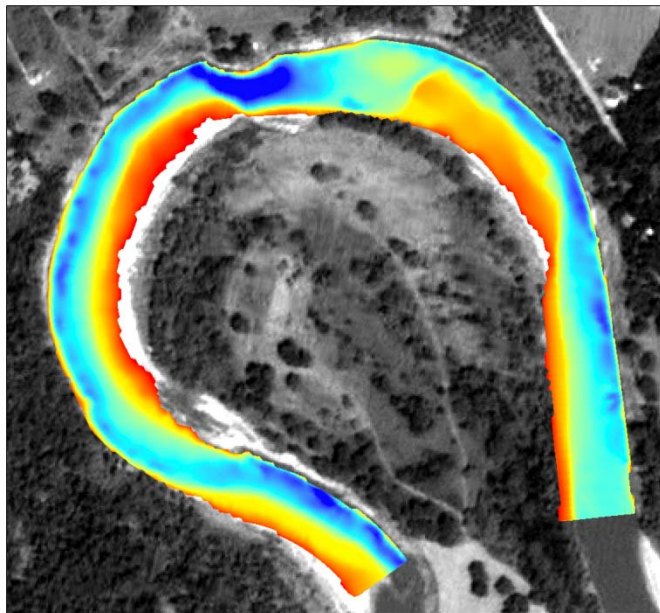


Figure 24. Detrended topographic surface of the terrain (Figure 25) characterizing the study reach. The positive residuals correspond to the topographic highs, and the negative residuals correspond to the topographic lows. Background aerial photo was acquired on August 17, 2010 (source: JAXA/Alaska Satellite Facility).

Topographic Residuals

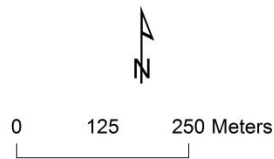
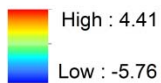


Table 10. Topographic residual classes determined using the detrended elevation data of the study reach.

Class	Description
-4 – -1:	Topographic residuals representing pools
1 – 4 :	Topographic residuals representing sediment bars
-4 :	Above 75th percentile of maximum pool depth
-3 :	Between 50 and 75th percentile of maximum pool depth
-2 :	Between 25 and 50th percentile of maximum pool depth
-1 :	Below 25th percentile of maximum pool depth
1 :	Below 25th percentile of maximum bar height
2 :	Between 25 and 50th percentile of maximum bar height
3 :	Between 50 and 75th percentile of maximum of bar height
4 :	Above 75th percentile of maximum of bar height

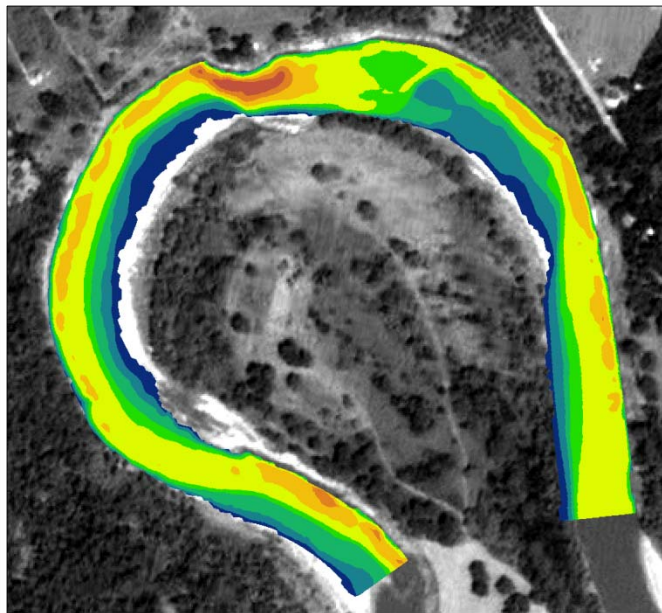


Figure 25. Topographic residual classes (presented in Table 10) obtained from the detrended elevations (Figure 24). Note that topography is defined as positive (sediment bars) and negative (pools) residuals of the bed topography about the channel centerline level. Background aerial photo was acquired on August 17, 2010 (source: JAXA/Alaska Satellite Facility).

The histogram of the detrended elevations (*i.e.*, topographic residuals) shows that the largest area, 36.62% of the residuals, within the channel boundary corresponds to the topographic lows characterized as those below the 25th percentile of the residuals (Figure 26). The second-largest area (*i.e.*, 10.91% of the residuals) corresponds to between 25 and 50th percentile of maximum pool depth. Only a minor percent amount corresponds to deep pools

(specifically, 1.44% and 0.84% for above 75th percentile and between 50 and 75th percentile of maximum pool depth, respectively).

In addition, the comparison of the percent amount of topographic residuals indicates almost the same amount, with 49.8% and 50.18%, corresponding to topographic lows and highs, respectively. However, the distribution of the topographic residuals representing sediment bars is more uniform among different percentiles (i.e., 13.82%, 13.55%, 14.00%, and 8.81% for 0-25th, 25-50th, 50-75th, and 75-100th percentiles, respectively) (Figure 26).

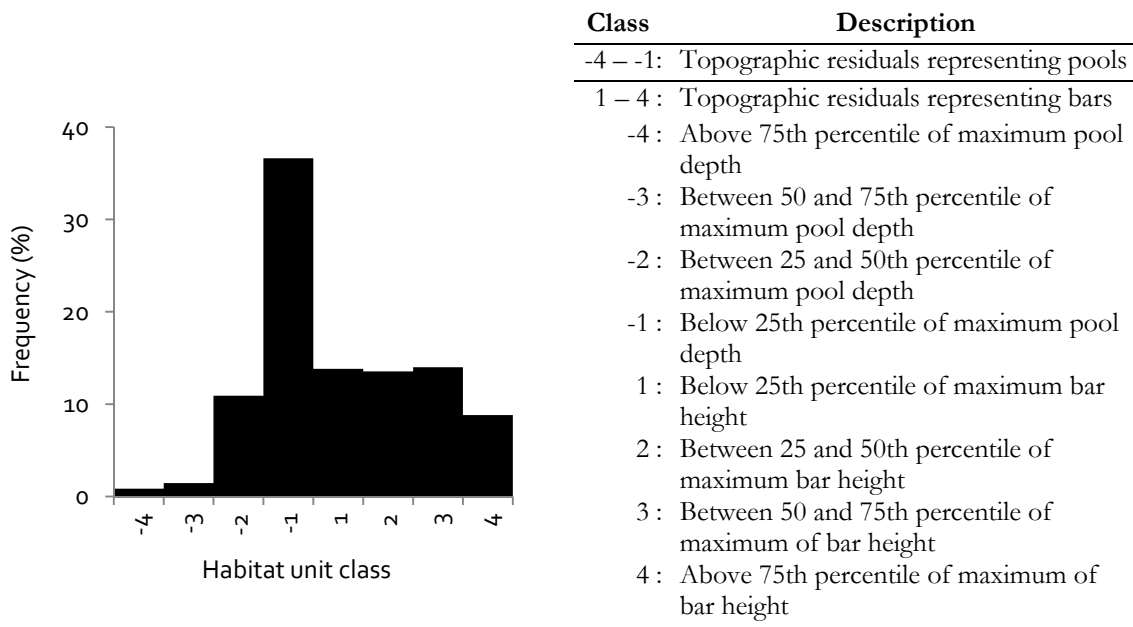


Figure 26. Histogram of habitat unit classes determined using the detrended elevation data (Figures 24–25).

7.3. Substrate Sediment Characteristics

The results show that bottom sediment largely consists of sediment less than 2 mm in diameter (i.e., sand, silt, and clay). Exceptions include the substrate sediment at transects T3 Right Bank (RB), T4 RB, and T5 RB, all of which contain more than 40% coarse grain (greater than 2 mm diameter) material (Figures 27–30, Table 11). Specifically, 85% percent of T5 RB consisted of coarse-grain sediments, with the second and third highest percentage of coarse material found in T4 RB and T3 RB (as 54.88% and 45.71%, respectively) of its total grain size greater than 2mm (Figures 27–30, Table 11).

Along the left bank (LB), the majority substrate material is sand; with all transects, except T5 and T6, containing around or above 50%. At transects T5 and T6 LB, the amount of sand is around 30% whereas the rest of the substrate material at these transects composed of silt and clay, both of which are also around 30% (Figures 27, 30).

In general, left-bank samples show a gradual increase regarding silt and clay content from transects T1 to T6, followed by a gradual decrease in silt and clay content from transects T6 to T8, then and again a slight increase from T8 to T10 (Figures 27, 30). The T3 LB, where the increase in silt and clay begins, is a transitional bank into a steep cutbank. The left banks of T4–9 are composed of cutbanks, with the peak in silt and clay content occurring at transect T5, which is near where the highest curvature of the meander bend occurs (Figures 19–20), and at T6, which is near the inflection point (marked as #2 in Figures 19–20). After the next inflection point located near T7 (marked as #3 in Figures 19–20), the silt and clay content start increasing again; however, it significantly decreases at T11, where the cutbank translates into a point bar (Figure 13).

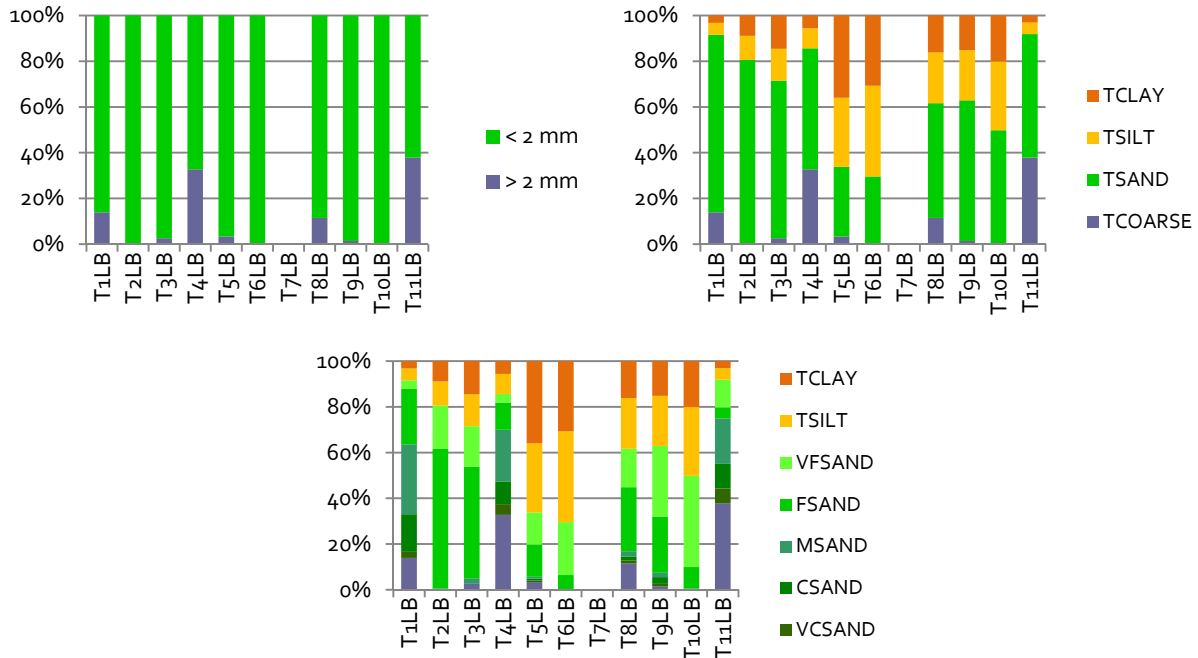


Figure 27. Sediment size distribution (%) along the study reach at the transects from T1–T 11 (Figure 13, Table 11), along the left bank (LB). Legend: TCOARSE: sediment >2 mm percent total; TFINE: sediment < 2 mm; TCLAY: clay percent total; TSILT: silt percent total; TSAND: sand percent total; VFSAND: very fine sand percent; FSAND: fine sand percent; MSAND: medium sand percent; CSAND: coarse sand percent; and VCSAND: very coarse sand percent.

In summary, along the left bank, the lowest silt and clay (or highest sand and coarser grain) content correspond to transects where there is either a point bar (*i.e.*, T1–T2), a low-sloped cutbank (T4), or a transition to point bar (T11) (Figure 13).

The channel centerline (C) samples consist of little coarse grain material, and only in T1 C and T2 C are the transects where any significant percentages of coarse material found, T1 C = 28.39%, T2 C = 10.15% (Figure 28, Table 11). The centerline substrate contains a majority of sand material, with only minor percentages of silt, clay, or coarse-grain material. The sand concentration is comprised of fine- and medium-size sands (Figures 28, 30). Transect T6 C shows a marked increase in the amount of coarse sand and a considerably minimal amount of fine sand that is not observed in any other centerline samples. No apparent trend within the sand size distributions is indicated in centerline samples.

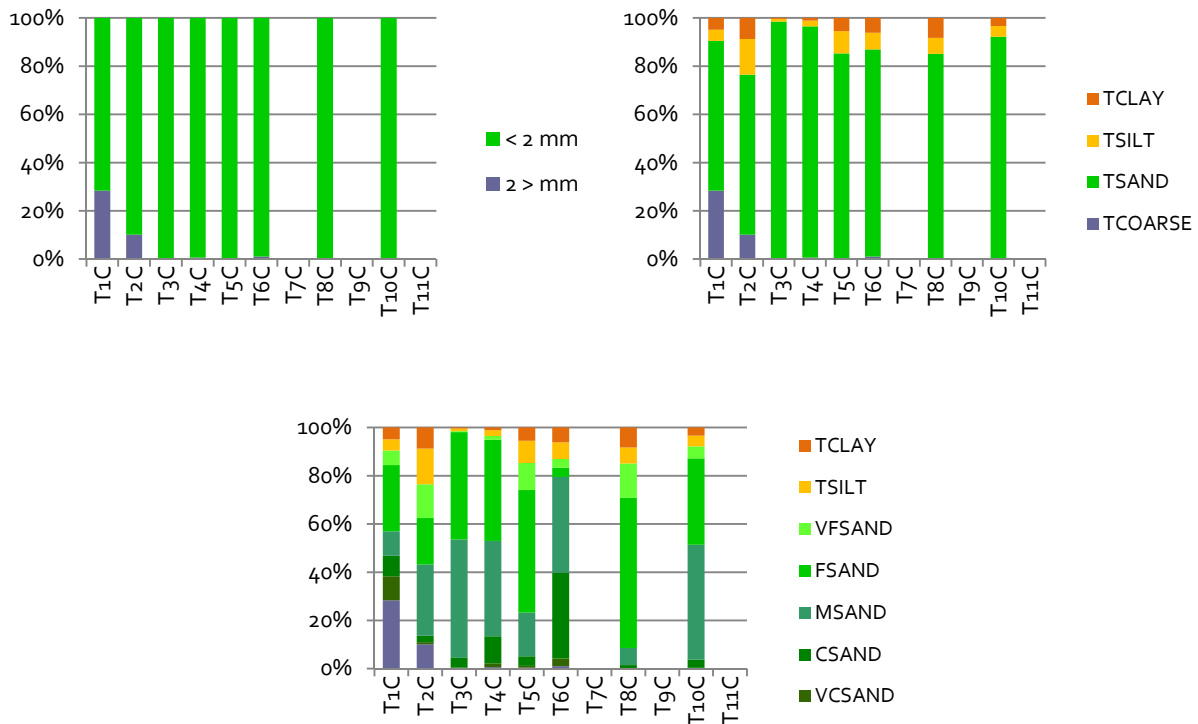


Figure 28. Sediment size distribution (%) along the study reach at the transects from T1–T 11 (Figure 13, Table 11), along the centerline (C). Legend: TCOARSE: sediment >2 mm percent total; TFINE: sediment < 2 mm; TCLAY: clay percent total; TSILT: silt percent total; TSAND: sand percent total; VFSAND: very fine sand percent; FSAND: fine sand percent; MSAND: medium sand percent; CSAND: coarse sand percent; and VCSAND: very coarse sand percent.

Right-bank (RB) samples indicate that the dominant substrate sediment is sand along transects T1–T2 RB, and T6–T11 RB (Figures 29–30). T1 RB and T2 RB each contain over 90% of grains less than 2mm (Figure 29). Within this distribution of sand, silt and clay material, T2 consists of 21% silt and 14% clay, with 62% sand (Table 11). However, there is an abrupt increase in coarse-grain substrate along transects T3–T5 RBs, followed by an abrupt decrease at transects T6–T11 (Figures 29–30). Transects T3–T5 RBs contain 45.71%, 54.88% and 85.13% coarse-grain material (> 2mm), respectively, and 45.33%, 14.71%, 13.53% sand, respectively. These high percentages are followed by a virtual absence of coarse-grain material along T6–11 RBs, with the highest percentage of coarse-grain material being 0.13% at transect T8 (Table 11). Transects T6–T11 RBs show a general increase in the percentage of sand, with the fine sand consisting of the largest portions of the samples (Figures 29–30). Right-bank samples taken along T1 RB and T2 RB correspond to cutbank and transition to cutbank units, respectively; T6–T9 RBs correspond to point bar units; and transects T10–T 11 RBs correspond to a transitional geomorphic zone from point bar to cutbank (Figure 13).

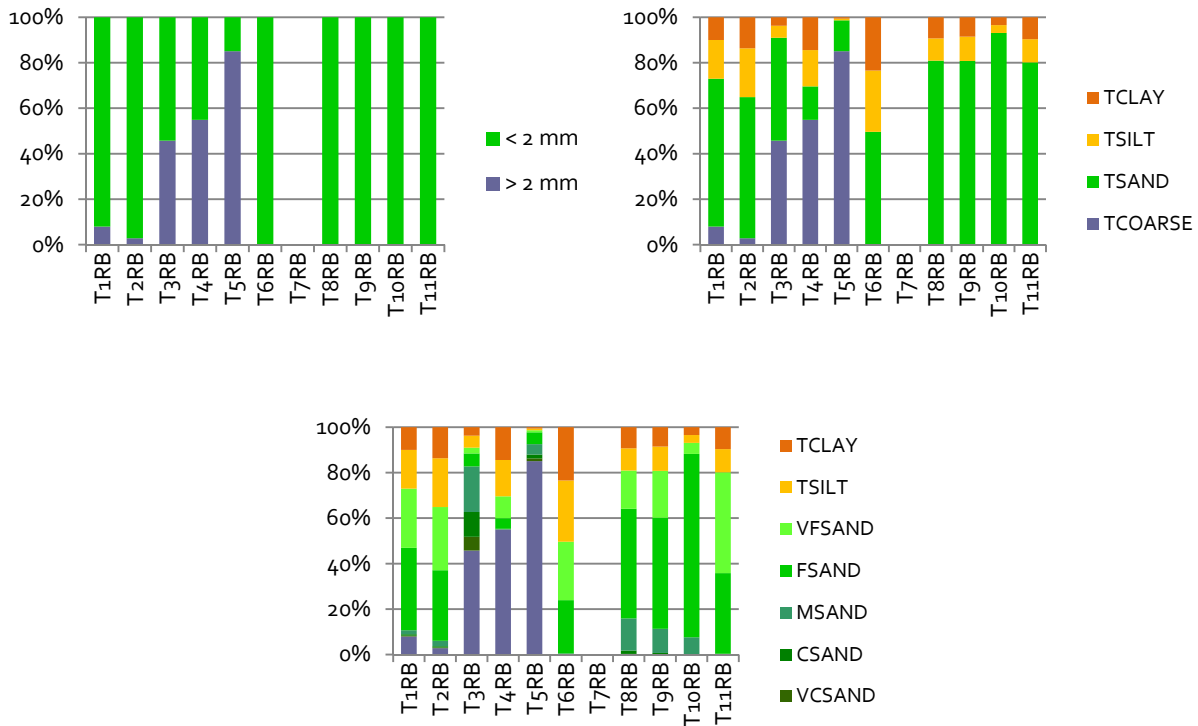


Figure 29. Sediment size distribution (%) along the study reach at transects from T1–T 11 (Figure 13, Table 11), along the right bank (RB). Legend: TCOARSE: sediment >2 mm percent total; TFINE: sediment < 2 mm; TCLAY: clay percent total; TSILT: silt percent total; TSAND: sand percent total; VFSAND: very fine sand percent; FSAND: fine sand percent; MSAND: medium sand percent; CSAND: coarse sand percent; and VCSAND: very coarse sand percent.

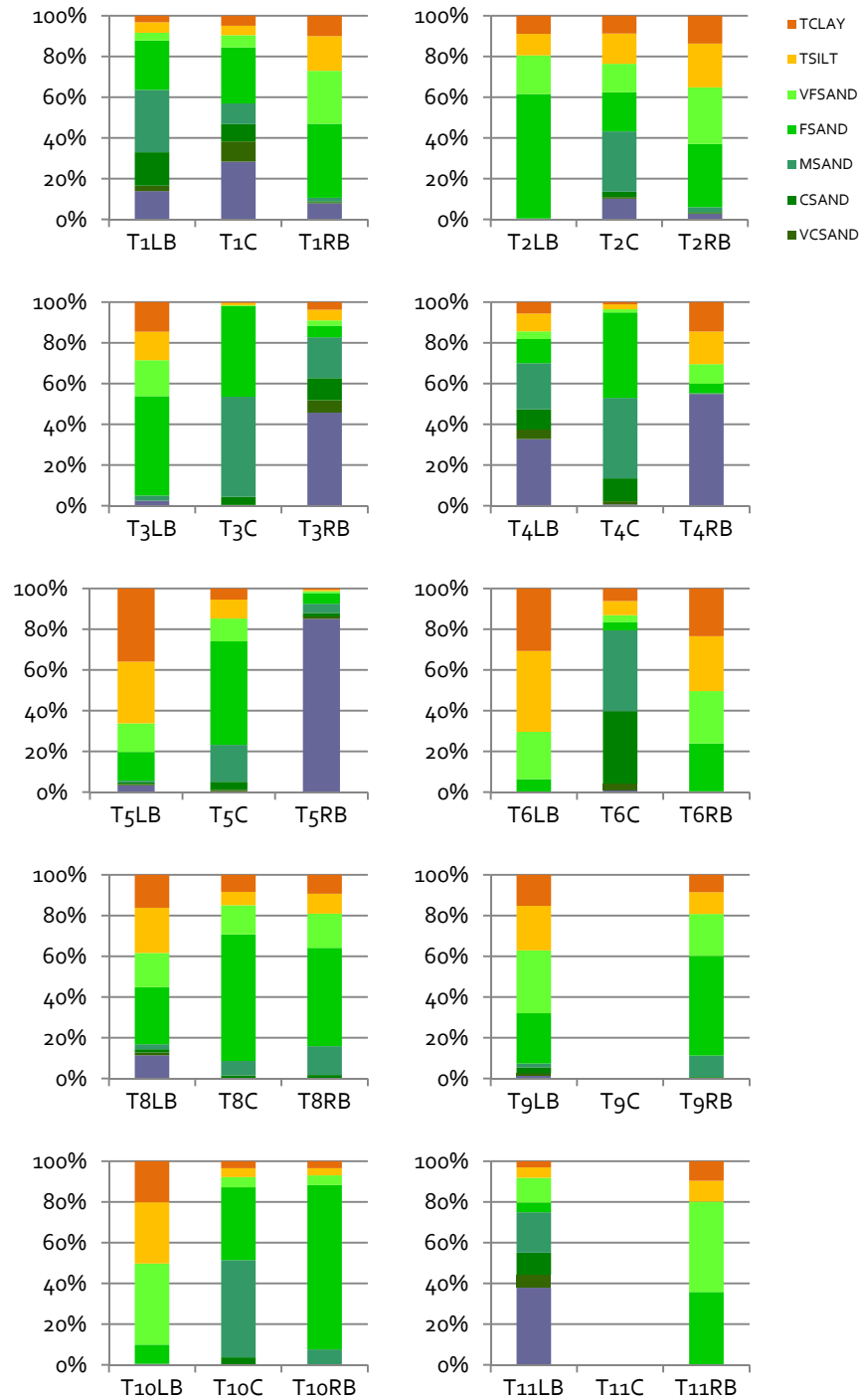


Figure 30. Sediment size distribution (%) along the study reach at each transect (T1–T 11) (Figure 13, Table 11) at the left bank (LB), right bank (RB), and centerline (C). Legend: TCLAY: clay percent total, TSILT: silt percent total, VFSAND: very fine sand percent, FSAND: fine sand percent, MSAND: medium sand percent, CSAND: coarse sand percent, VCSAND: very coarse sand percent, and TCOARSE: sediment >2 mm percent total.

Table 11. Sediment size distribution along the study reach at transects from T1–T 11 (Figure 13).

Transect	Water Depth (meter)	Total Coarse	Total Sand	Very coarse Sand	Coarse Sand	Medium Sand	Fine Sand	Very fine Sand	Total Silt	Total Clay
		>2 mm (%)	0.05–2.00 mm (%)	1.00–2.00 mm (%)	0.5–1.00 mm (%)	0.25–0.50 mm (%)	0.10–0.25 mm (%)	0.05–0.10 mm (%)	0.002–0.05 mm (%)	<0.002 mm (%)
T1 <i>Left bank</i> ¹	0.92	13.91	77.74	2.67	16.44	30.56	24.28	3.79	5.17	3.19
<i>Center</i>	3.03	28.39	62.08	9.95	8.45	10.17	27.50	6.02	4.65	4.87
<i>Right bank</i> ¹	1.43	7.90	65.11	0.37	0.64	1.75	36.29	26.06	17.04	9.95
T2 <i>Left bank</i>	0.92	0.23	80.31	0.00	0.00	0.30	61.06	18.96	10.58	8.88
<i>Center</i>	2.02	10.15	66.31	0.81	2.70	29.56	19.23	14.02	14.83	8.72
<i>Right bank</i>	2.57	2.75	62.14	0.29	0.58	2.43	31.02	27.81	21.49	13.61
T3 <i>Left bank</i>	1.18	2.57	68.98	0.00	0.00	2.44	48.81	17.73	13.93	14.52
<i>Center</i>	0.92	0.15	98.35	0.30	3.99	49.12	44.53	0.40	1.10	0.40
<i>Right bank</i>	0.11	45.71	45.33	6.08	10.91	20.09	5.70	2.55	5.27	3.69
T4 <i>Left bank</i>	2.12	32.73	52.94	4.71	9.96	22.60	11.91	3.77	8.74	5.58
<i>Center</i>	1.39	0.63	95.89	1.59	11.23	39.55	41.93	1.59	2.38	1.09
<i>Right bank</i>	0.33	54.88	14.71	0.05	0.09	0.32	4.60	9.66	16.02	14.39
T5 <i>Left bank</i>	0.97	3.36	30.44	0.68	0.77	0.87	14.01	14.11	30.25	35.95
<i>Center</i>	1.63	0.43	84.84	0.70	3.98	18.12	50.88	11.15	9.26	5.48
<i>Right bank</i>	0.34	85.13	13.53	1.15	1.71	4.55	5.25	0.88	0.77	0.57
T6 <i>Left bank</i>	2.33	0.00	29.60	0.00	0.10	0.20	6.10	23.20	39.70	30.70
<i>Center</i>	5.91	1.04	85.90	3.17	35.63	39.68	3.86	3.56	6.93	6.14
<i>Right bank</i>	0.42	0.04	49.58	0.00	0.10	0.30	23.49	25.69	26.99	23.39
T7 <i>Left bank</i>	–	–	–	–	–	–	–	–	–	–
<i>Center</i>	–	–	–	–	–	–	–	–	–	–
<i>Right bank</i>	–	–	–	–	–	–	–	–	–	–
T8 <i>Left bank</i>	2.00	11.45	50.21	1.33	1.59	2.48	27.98	16.82	22.23	16.12
<i>Center</i>	2.10	0.00	85.10	0.00	1.50	7.10	62.20	14.30	6.60	8.30
<i>Right bank</i>	1.16	0.13	80.79	0.10	1.50	14.18	48.24	16.78	9.79	9.29
T9 <i>Left bank</i>	1.47	1.36	61.55	1.18	2.96	1.87	24.66	30.88	21.90	15.19
<i>Center</i>	–	–	–	–	–	–	–	–	–	–
<i>Right bank</i>	0.31	0.00	80.80	0.00	0.70	10.60	48.90	20.60	10.70	8.50
T10 <i>Left bank</i>	2.10	0.04	49.78	0.00	0.10	0.40	9.40	39.88	30.09	20.09
<i>Center</i>	1.13	0.23	91.99	0.10	3.39	47.69	35.82	4.99	4.39	3.39
<i>Right bank</i>	0.10	0.00	93.10	0.00	0.10	7.50	80.70	4.80	3.50	3.40
T11 <i>Left bank</i>	0.57	37.88	54.04	6.40	10.81	19.88	4.78	12.18	5.03	3.04
<i>Center</i>	–	–	–	–	–	–	–	–	–	–
<i>Right bank</i>	0.31	0.01	80.19	0.00	0.10	0.20	35.50	44.39	10.20	9.60

¹ Left bank and the right bank correspond to the banks on the left and the right sides of the channel looking downstream (see Figure 13).

D₅₀ Distribution

The primary D_{50} size is sand along transects T1–T11 (Table 12). The results from the analysis of D_{50} distribution indicate a pattern reflecting the influence of geomorphic units in the substrate structure. Across each transect, there is a consistent substrate grain-size pattern; the grain size decreases from point bar side to cutbank side. For example, across transect T1 from point bar side (left bank) to cutbank side (right bank), the grain size changes from medium sand to very fine sand. Along the transect T2 from point bar (on the left bank) to the transition to point bar (right bank), the substrate grain size decreases from fine sand to very fine sand. Similarly, along T11 from transition from cutbank to point bar (left bank) to cutbank (right bank), the substrate grain size decreases from coarse sand to very fine sand (Table 12). Across transects T3–T10, where the cutbank and point bar are located along the left and the right banks, respectively, the grain size increases from fine to coarse. D_{50} increases from fine/medium sand to very coarse sand/fine granules at transects T3 and T4, whereas increases from silt to fine granules at transect T5 (Table 12). Across the transects T6–T10, the range of D_{50} is finer than that of T3–T5; specifically, D_{50} increases from silt to very fine sand at T6 and from very fine sand to fine sand at T7–T10.

Table 12. D_{50} (*i.e.*, sediment size characterizing the 50% finer sediment than the rest of the sediment) type, size, and corresponding geomorphic units and water depths along transects T1–T11 (Figure 13).

Transect	D₅₀, Sediment (Type)			Geomorphic Unit		D₅₀ Size, Diameter (mm)		
	<i>Left bank</i>	<i>Center</i>	<i>Right bank</i>	<i>Left bank</i>	<i>Right bank</i>	<i>Left bank</i>	<i>Center</i>	<i>Right bank</i>
T1	Medium sand	Medium sand	Very fine sand	Point bar	Cutbank	0.36	0.42	0.09
T2	Fine sand	Fine sand	Very fine sand	Point bar	T to point bar	0.13	0.20	0.08
T3	Fine sand	Medium sand	Very coarse sand	Cutbank	Point bar	0.11	0.27	1.29
T4	Medium sand	Medium sand	Very fine granules	Cutbank	Point bar	0.47	0.27	2.71
T5	Silt	Fine sand	Fine granules	Cutbank	Point bar	0.02	0.17	5.30
T6	Silt	Medium sand	Very fine sand	Cutbank	Point bar	0.03	0.44	0.05
T7	–	–	–	–	–	–	–	–
T8	Very fine sand	Fine sand	Fine sand	Cutbank	Point bar	0.08	0.15	0.14
T9	Very fine sand	–	Fine sand	Cutbank	Point bar	0.07	–	0.13
T10	Very fine sand	Medium sand	Fine sand	Cutbank	T to cutbank	0.05	0.26	0.17
T11	Coarse sand	–	Very fine sand	T to point bar	Cutbank	0.74	–	0.08

T to point bar: Transition to point bar; T to cutbank: Transition to cutbank

Table 12 (cont'd). D_{50} (*i.e.*, sediment size characterizing the 50% finer sediment than the rest of the sediment) type, size, and corresponding geomorphic units and water depths along transects T1–T11 (Figure 13).

Transect	D_{50} , Sediment (Type)			Geomorphic Unit		Water Depth (m)		
	<i>Left bank</i>	<i>Center</i>	<i>Right Bank</i>	<i>Left bank</i>	<i>Right bank</i>	<i>Left bank</i>	<i>Center</i>	<i>Right bank</i>
T1	Medium sand	Medium sand	Very fine sand	Point bar	Cutbank	0.92	3.03	1.43
T2	Fine sand	Fine sand	Very fine sand	Point bar	T to point bar	0.92	2.02	2.57
T3	Fine sand	Medium sand	Very coarse sand	Cutbank	Point bar	1.18	0.92	0.11
T4	Medium sand	Medium sand	Very fine granules	Cutbank	Point bar	2.12	1.39	0.33
T5	Silt	Fine sand	Fine granules	Cutbank	Point bar	0.97	1.63	0.34
T6	Silt	Medium sand	Very fine sand	Cutbank	Point bar	2.33	5.91	0.42
T7	–	–	–	–	–	–	–	–
T8	Very fine sand	Fine sand	Fine sand	Cutbank	Point bar	2.00	2.10	1.16
T9	Very fine sand	–	Fine sand	Cutbank	Point bar	1.47	1.65	0.31
T10	Very fine sand	Medium sand	Fine sand	Cutbank	T to cutbank	2.10	1.13	0.10
T11	Coarse sand	–	Very fine sand	T to point bar	Cutbank	0.57	0.90	0.31

T to point bar: Transition to point bar; T to cutbank: Transition to cutbank

7.4. Hydraulic Characteristics of the Study Reach

We performed the hydraulic modeling for field-based low discharge (Q1), and for two exploratory discharge scenarios, medium and high discharges (Q2 and Q3) as discussed in *Section 7*. The results for the model output parameters (e.g., water depth, velocity, Froude number) are presented in Table 13 and Figures 31–36. These results (as well as the results of the analysis based on the detrended surfaces as discussed in *Section 7.2*) were shared with the Fish Group led by Dr. F.I. Gelwick, Department of Wildlife and Fisheries Sciences, Texas A&M University, to be used in the analysis and assessment of aquatic habitats. Specifically, we provided the following:

1. Maps of depth and velocity at stage Q1 coupled with catch per unit effort (CPUE) measurements for Gill Netting, Seine, Electroshocking, and DIDSON observations,
2. Model output parameters at discrete fish field-sample locations (or were extracted within a distance of 15 m from a given sample point).

Table 13. The model output parameters and their values for the field-based low flow (Q1), and exploratory medium (Q2), and exploratory high flow (Q3) discharge conditions. For the definition of these parameters, refer to Table 8.

Parameter*	Unit	Value Range (min – max)		
		Low-discharge (field based) (Q1)	Medium-discharge scenario (Q2)	High-discharge scenario (Q3)
WSE	meters	52.47 – 52.78	54.47 – 54.75	56.47 – 56.76
Elev	meters	46.34 – 52.70	46.34 – 54.66	46.34 – 56.62
Depth	meters	0.003 – 6.39	0.015 – 8.26	0.029 – 10.25
Vel	meters/second	0.00 – 1.56	0.00 – 0.75	0.00 – 1.00
SVel	meters/second	-0.13 – 1.55	-0.057 – 0.75	-0.074 – 1.00
NVel	meters/second	-0.49 – 0.86	-0.15 – 0.34	-0.18 – 0.15
Froude	unitless	0.00 – 0.75	0.00 – 0.54	0.00 – 0.27
Helix	unitless	-23.13 – 21.42	-14.13 – 10.34	-297.6 – 14.89

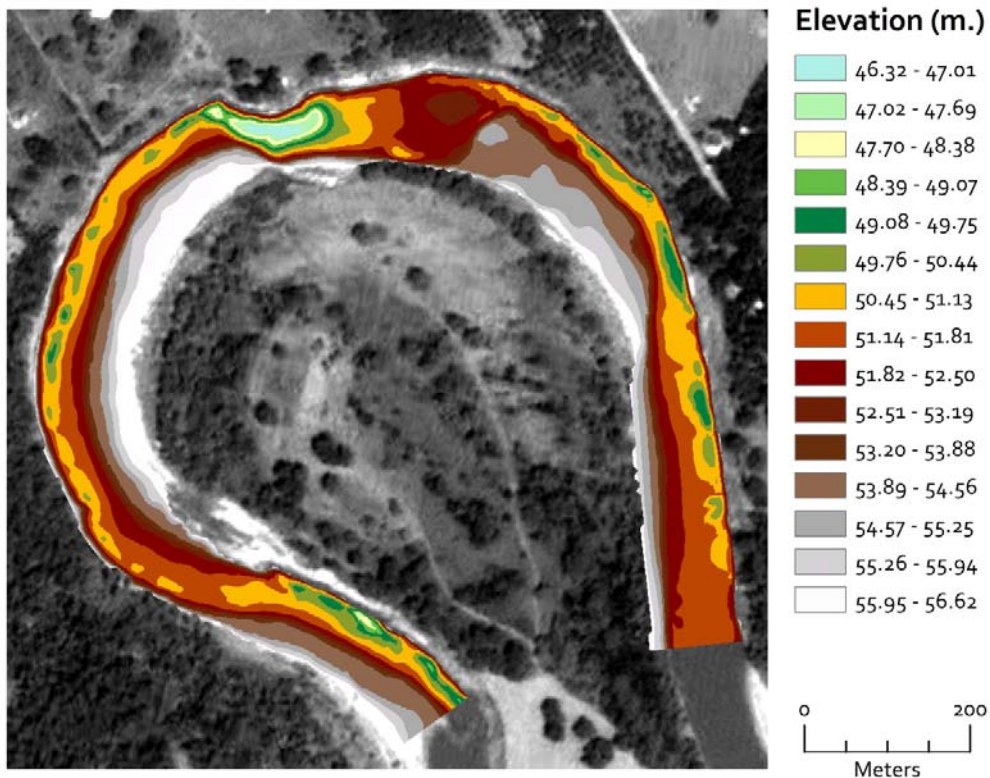


Figure 31. Elevation distribution above datum of river channel.

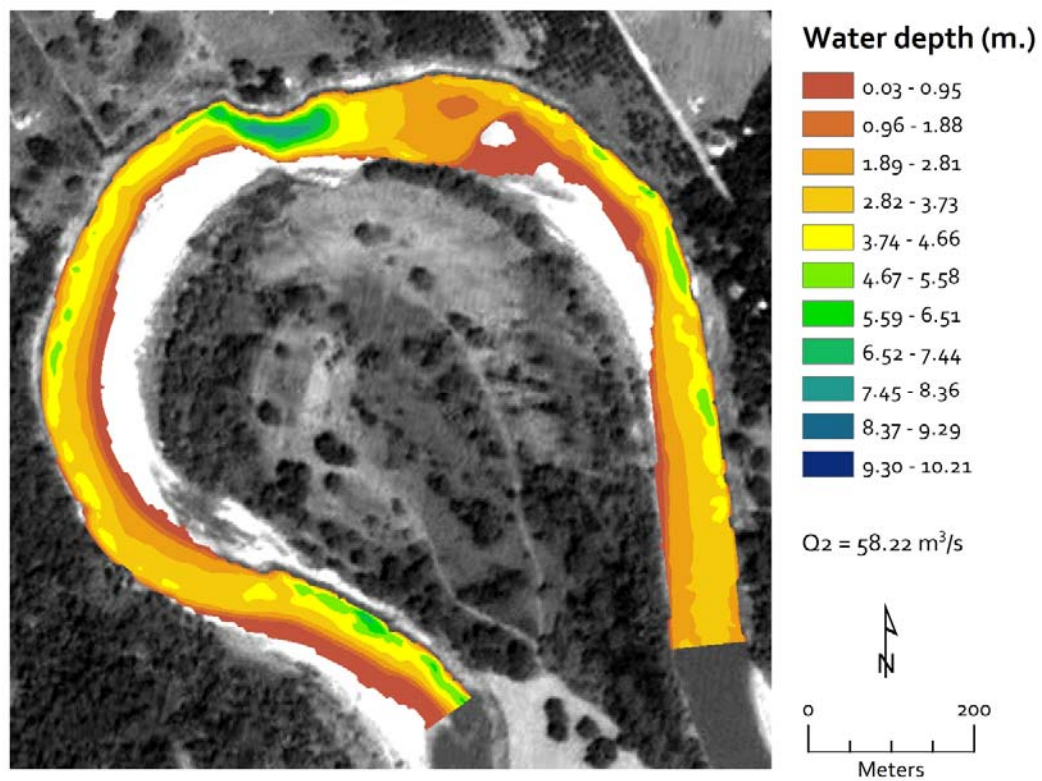
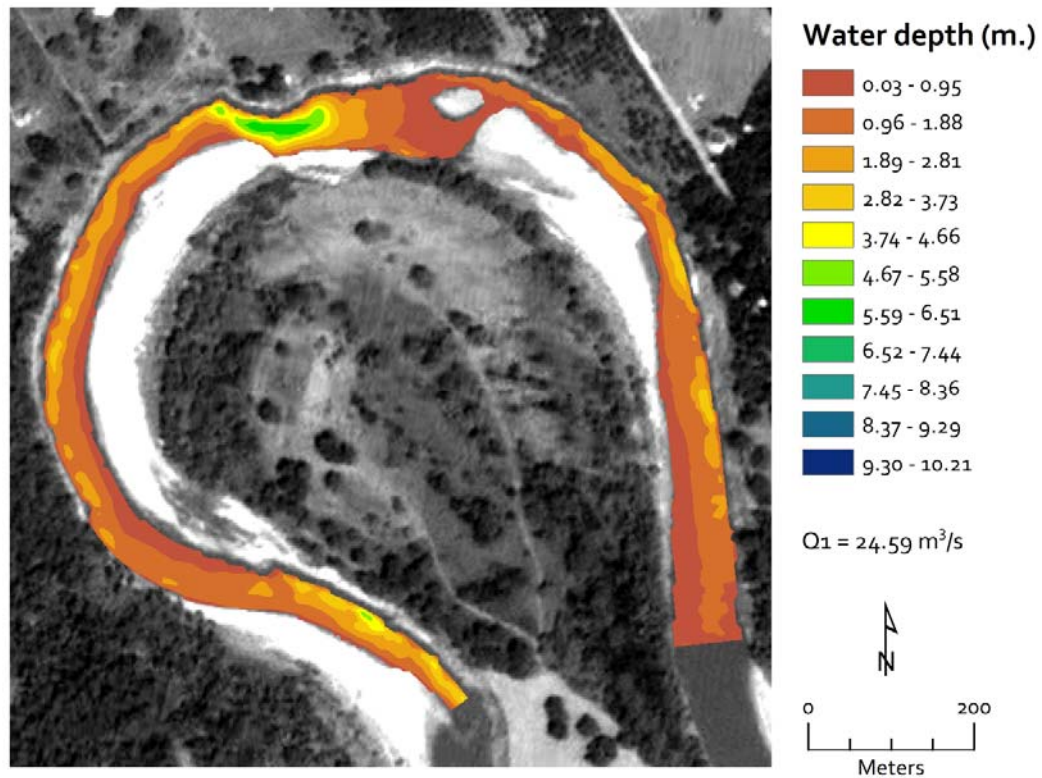


Figure 32. Water depth distribution along the reach.

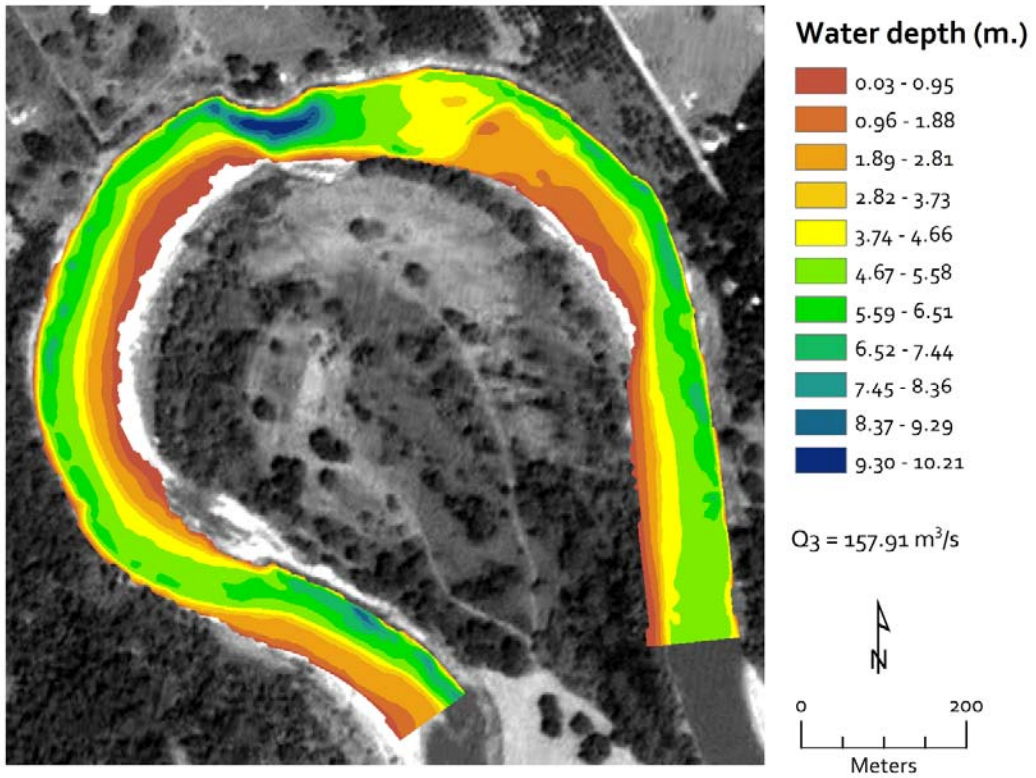


Figure 32 (cont'd). Water depth distribution along the reach.

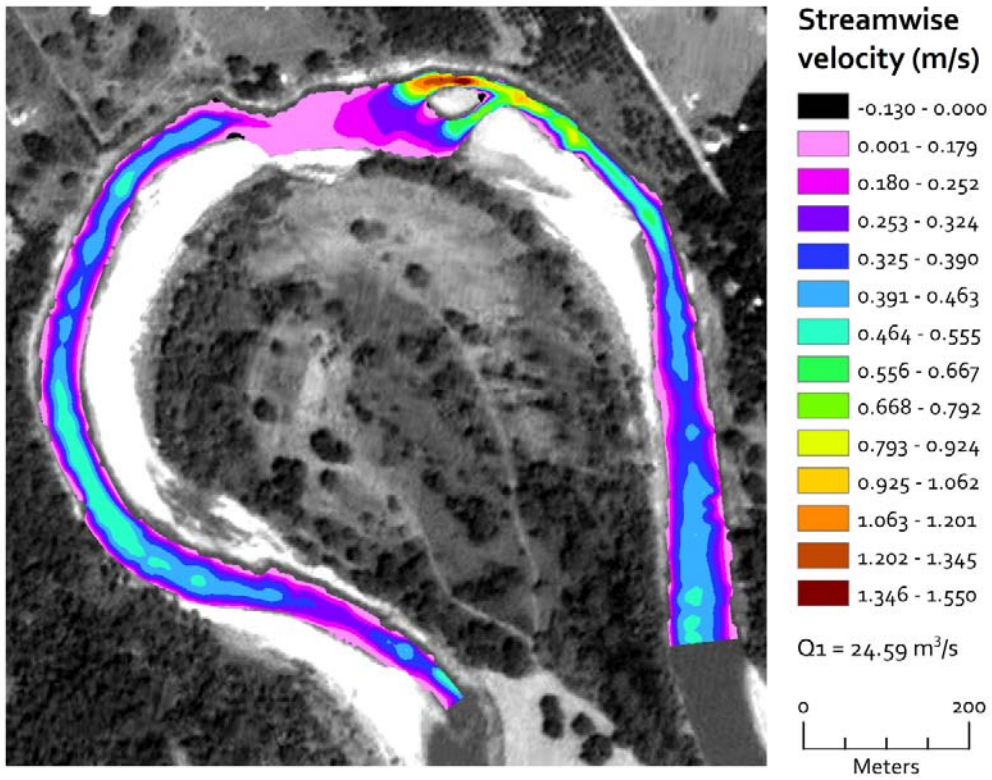


Figure 33. Streamwise velocity distribution along the reach.

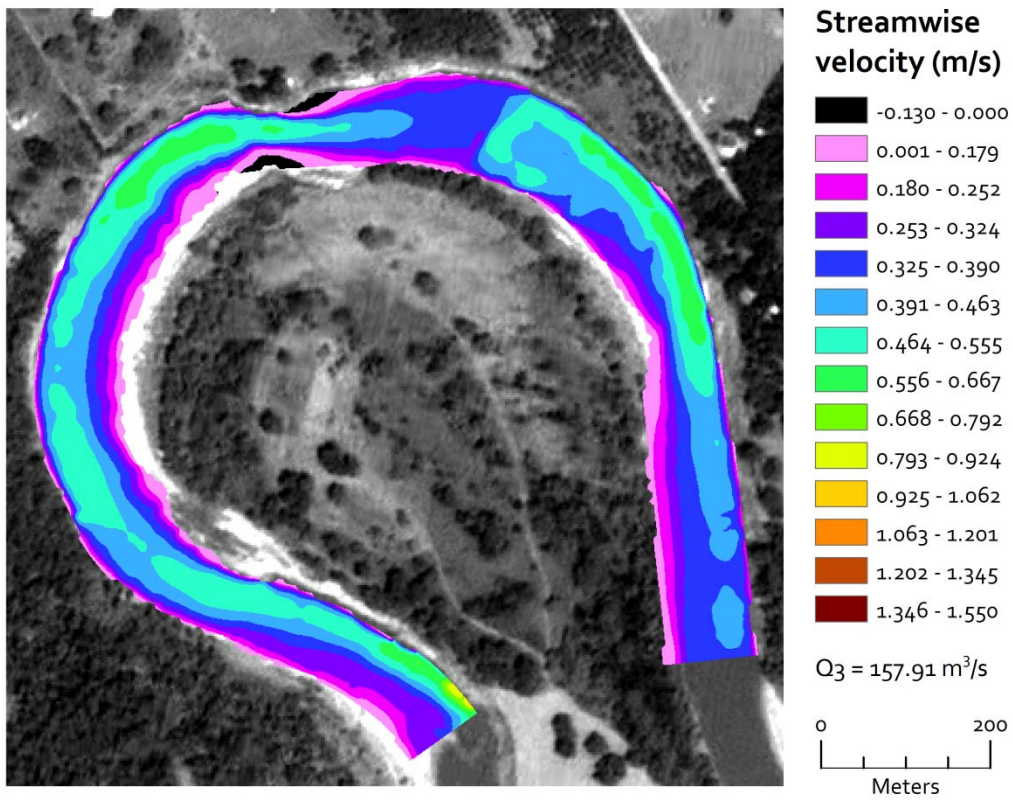
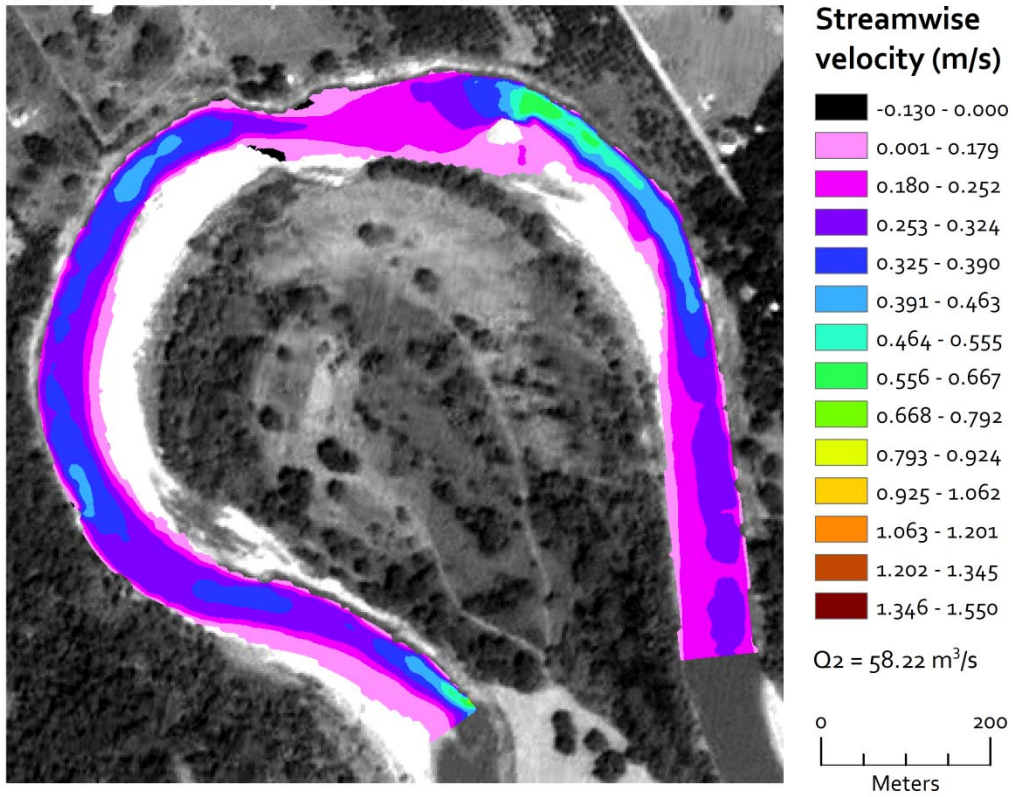


Figure 33 (cont'd). Streamwise velocity distribution along the reach.

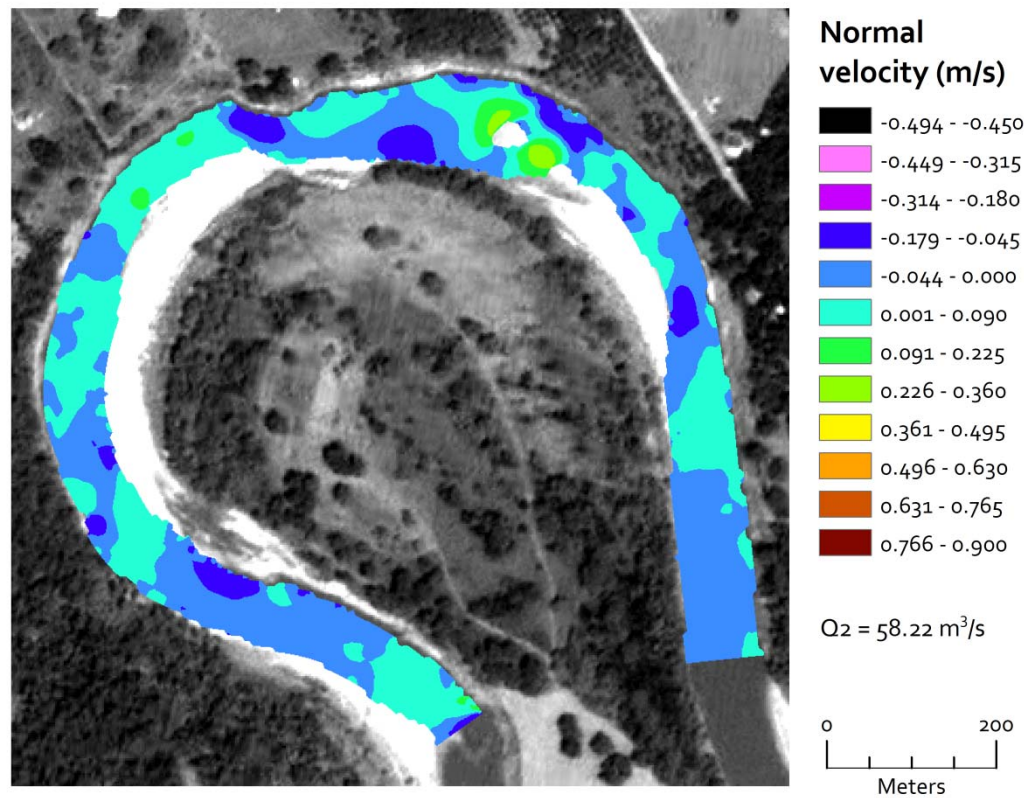
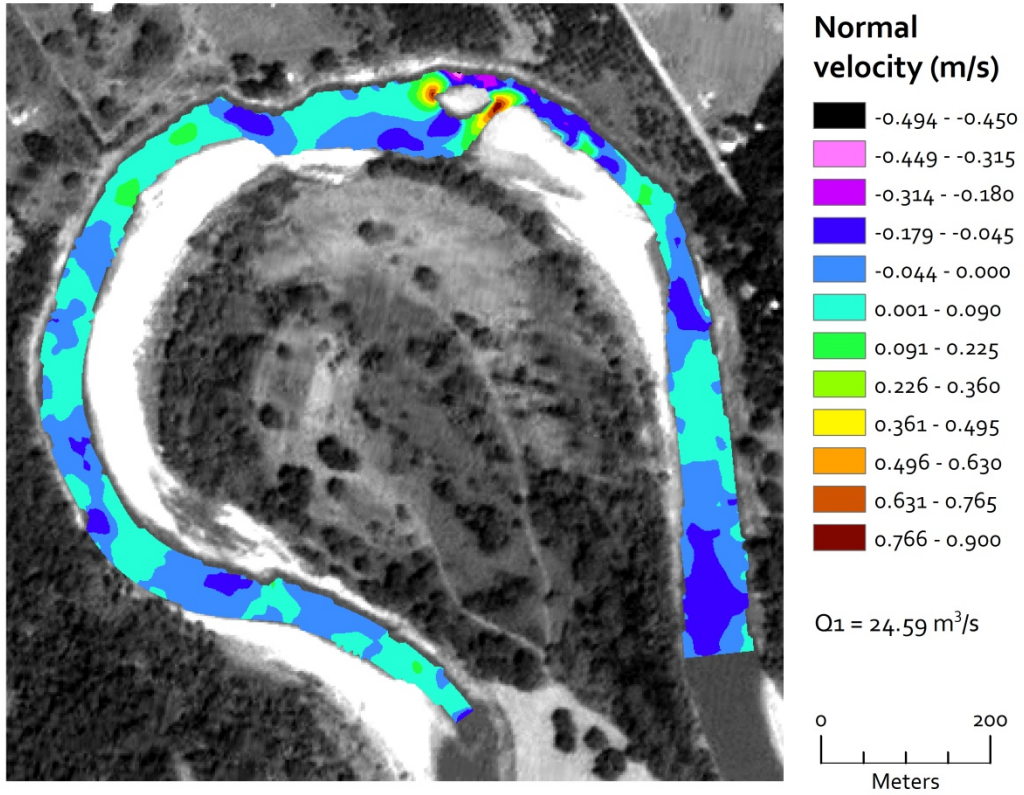


Figure 34. Normal velocity distribution along the reach.

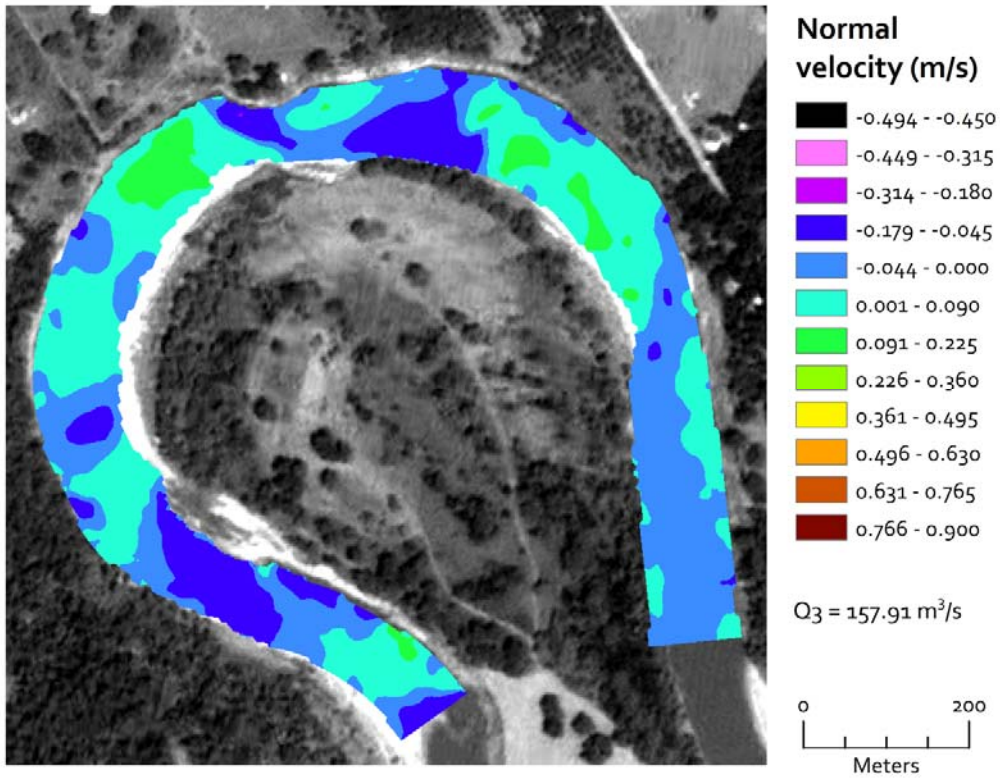


Figure 34 (cont'd). Normal velocity distribution along the reach.

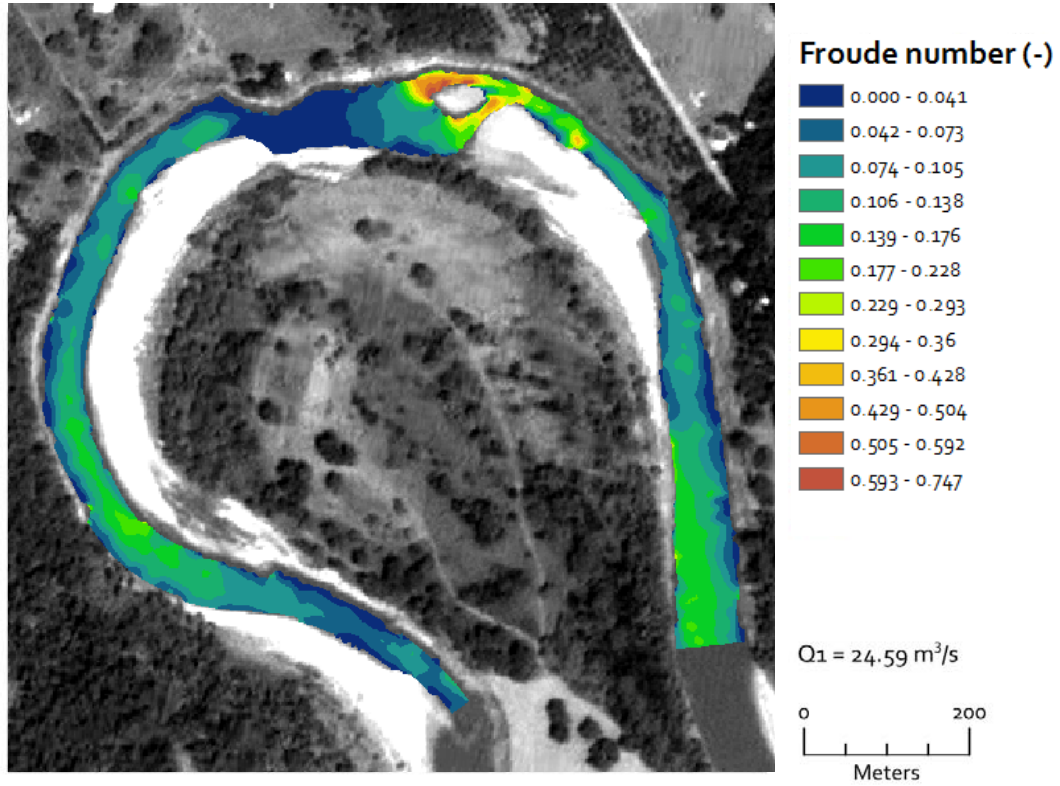


Figure 35. Froude number distribution along the reach.

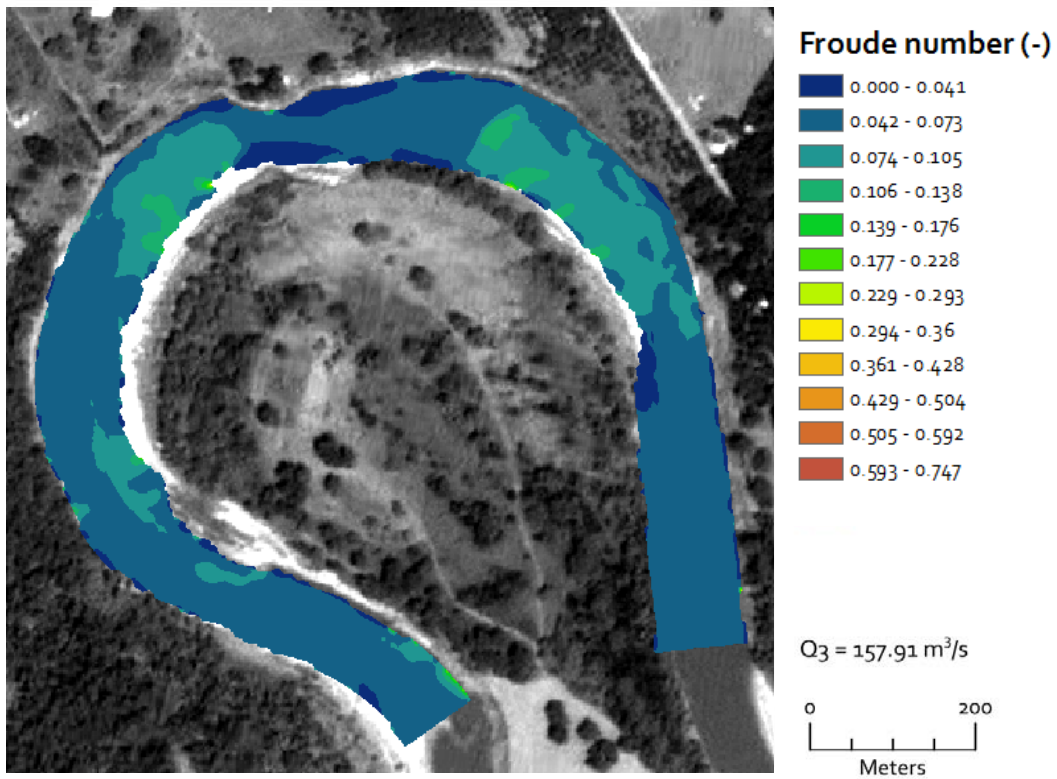
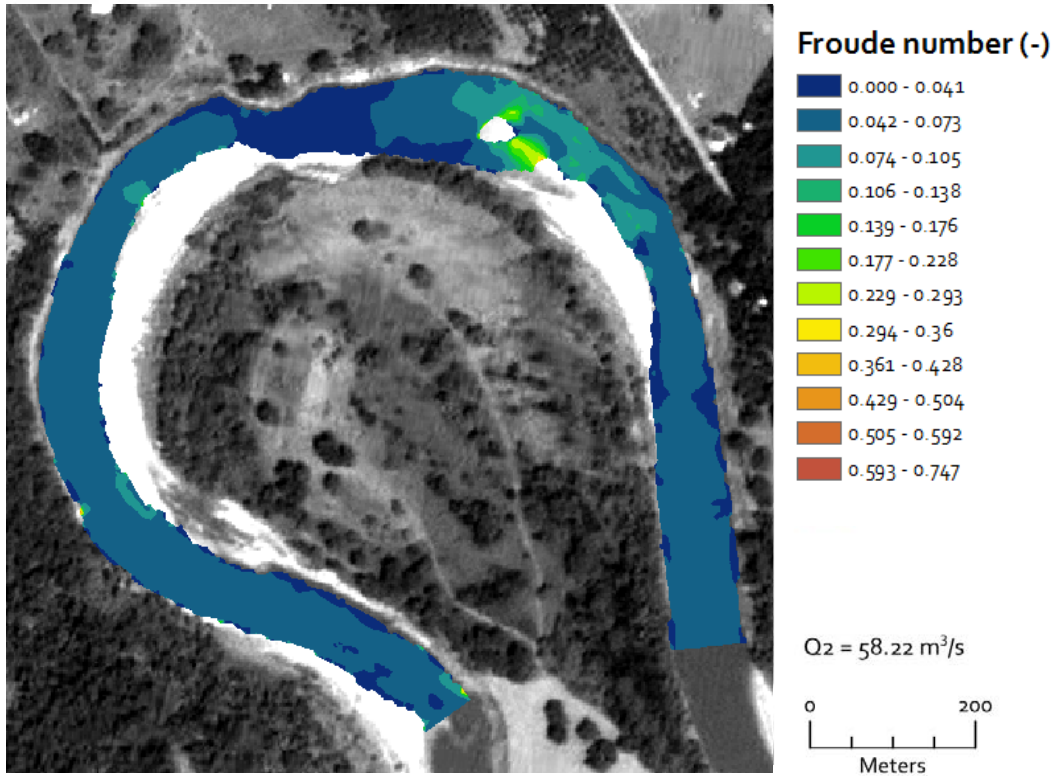


Figure 35 (cont'd). Froude number distribution along the reach.

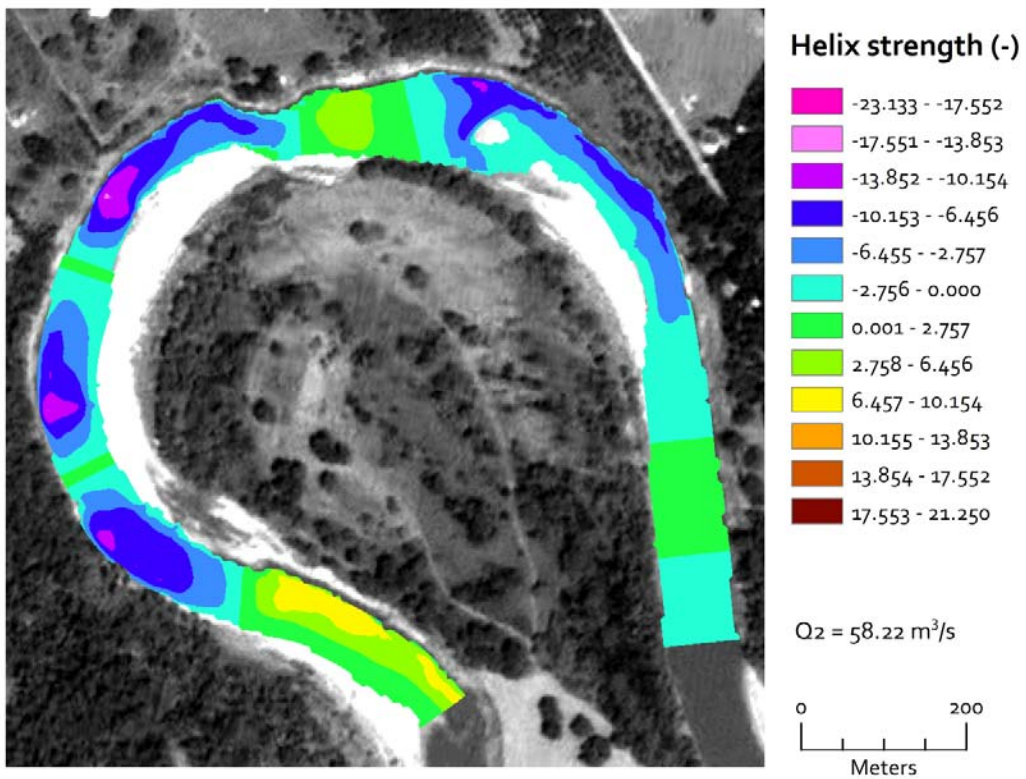
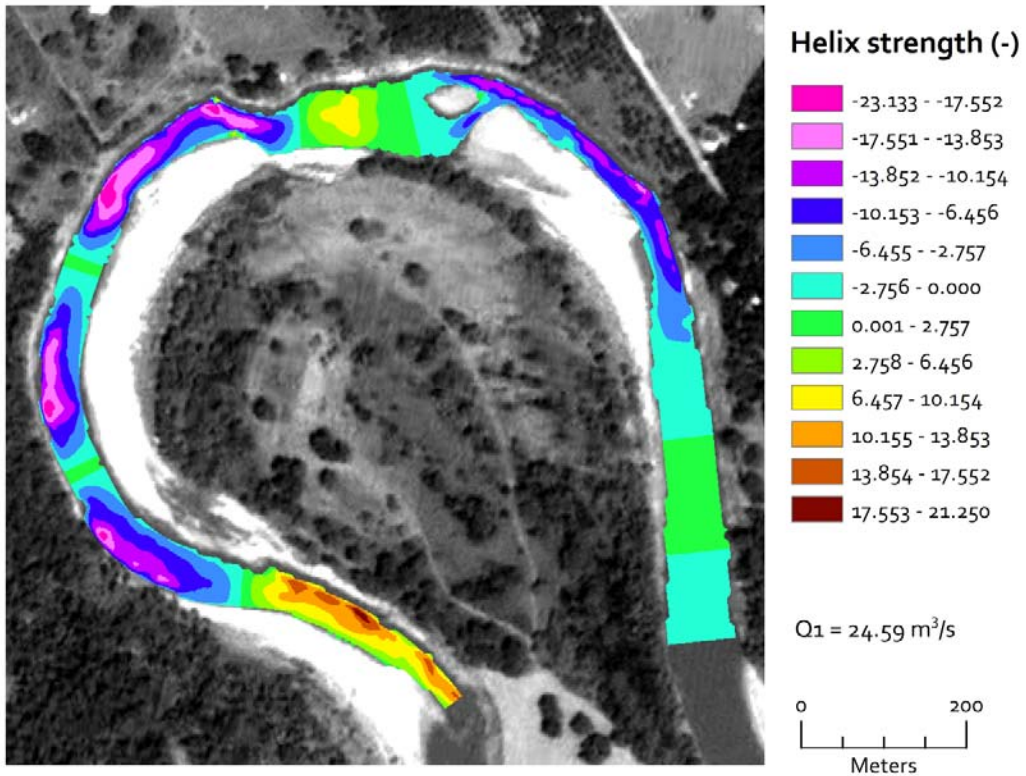


Figure 36. Helix strength distribution along the reach.

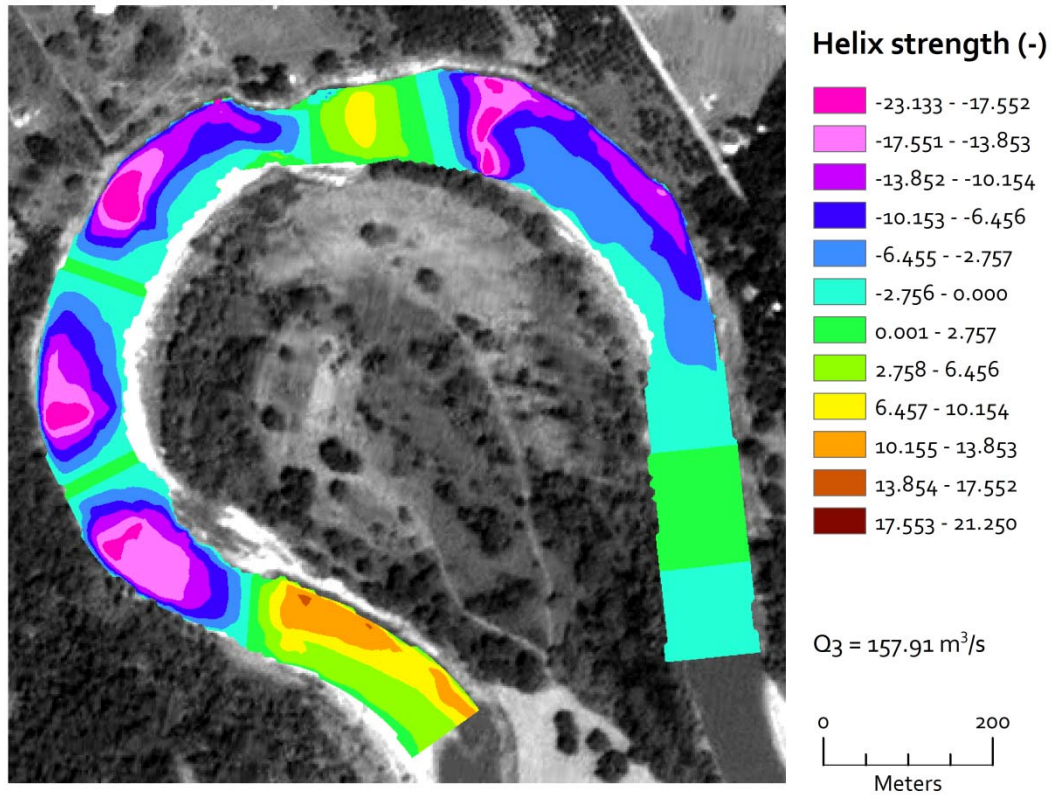


Figure 36 (cont'd). Helix strength distribution along the reach.

7.5. Distribution of Hydraulic Characteristics of Study Reach In Relation to the Physical Boundaries of Habitat Types

We examined the frequency and spatial distribution of the model output parameters including water depth, streamwise velocity, normal velocity, Froude number, and helix strength (Table 8, Figures 37–41). The distributions of these parameter values indicate unique influence of channel morphology on flow structure.

The water depth histograms become bimodal with increasing discharge from Q1 to Q3 (Figure 37a–c). This distribution indicates the increasing variability in channel morphology as the sand bars (including point bars and mid-channel bars) become more and more inundated (Figure 37a–c). The dominant mode shifts positively (toward to higher depths) because of the increase in stage. Although the water depth with the highest frequency is 1.03 m during Q1, the dominant frequencies correspond to 0.62 and 2.68 meters during Q2, representing the influence of topographic highs and topographic lows, respectively, identified by the detrended elevations

(Figures 24–25). During Q3, these highest frequencies correspond to 2.47 and 4.74 meters, respectively (Figure 37c).

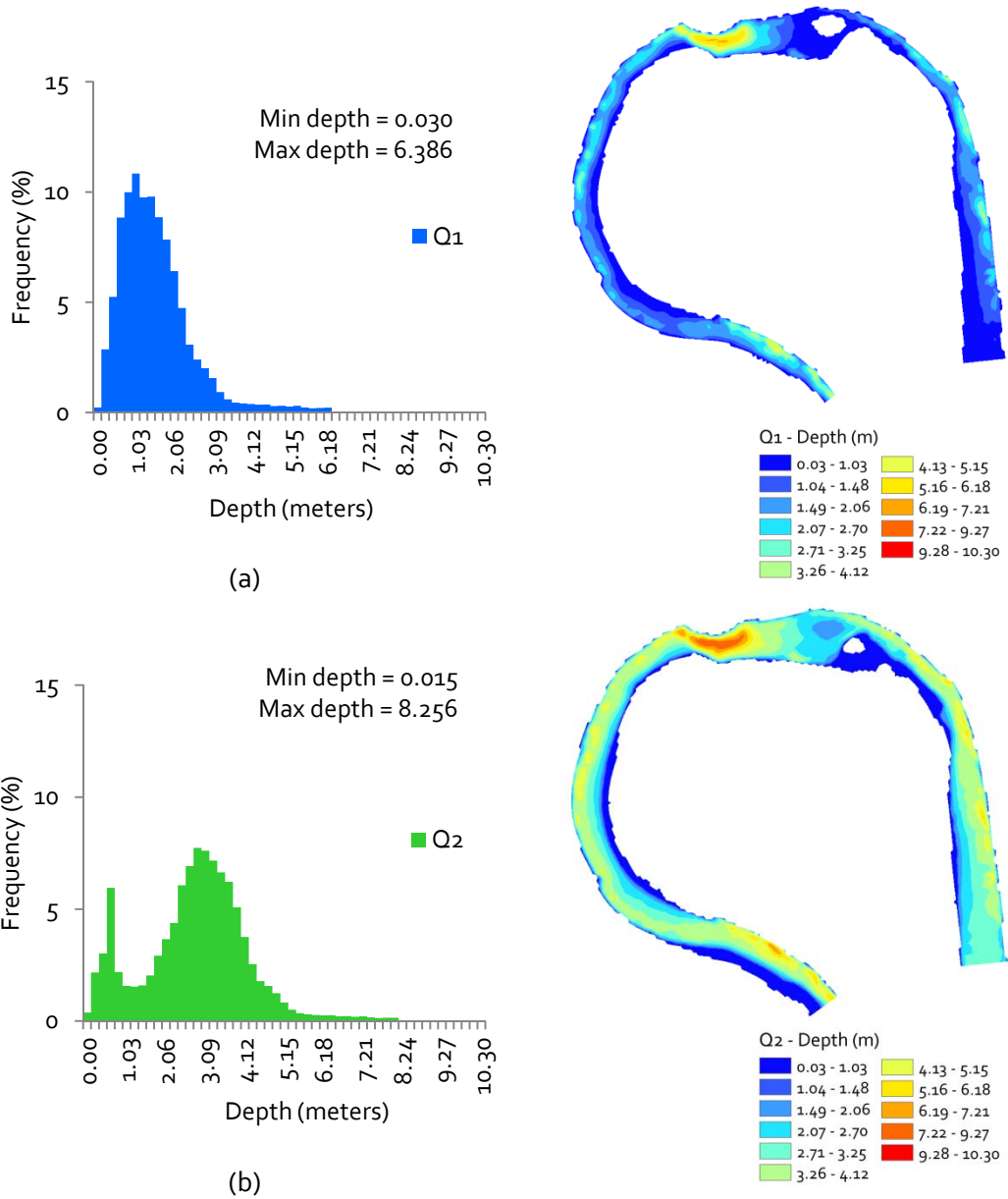


Figure 37. Histograms of water depth values at (a) low (Q1), (b) medium (Q2), and (c) high (Q3) discharge conditions. Min depth and Max depth denote the minimum and maximum values of water depths associated with given discharge conditions. The classes used in the spatial distribution directly correspond to the classes used in the histogram.

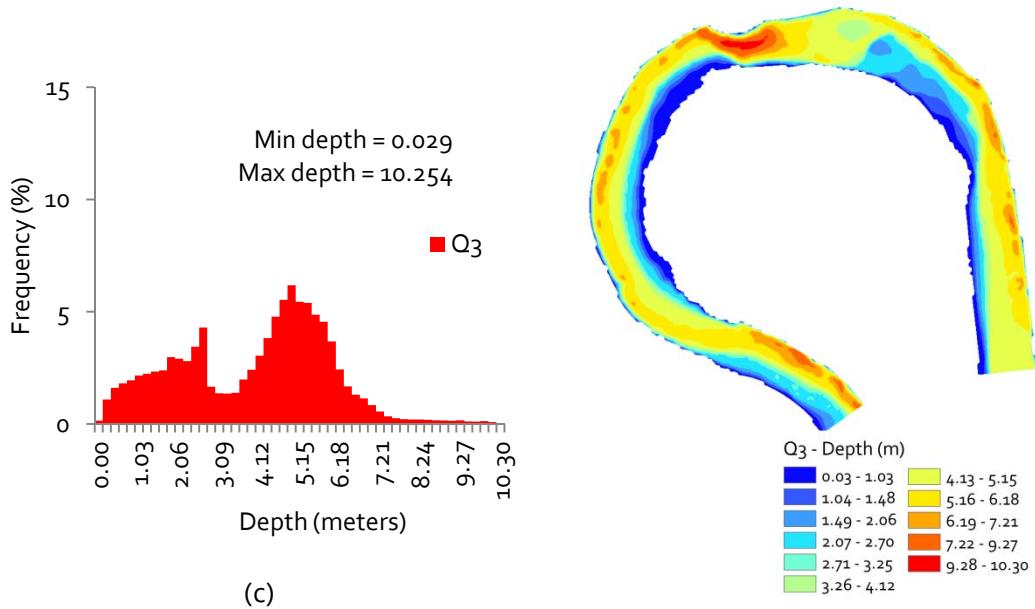
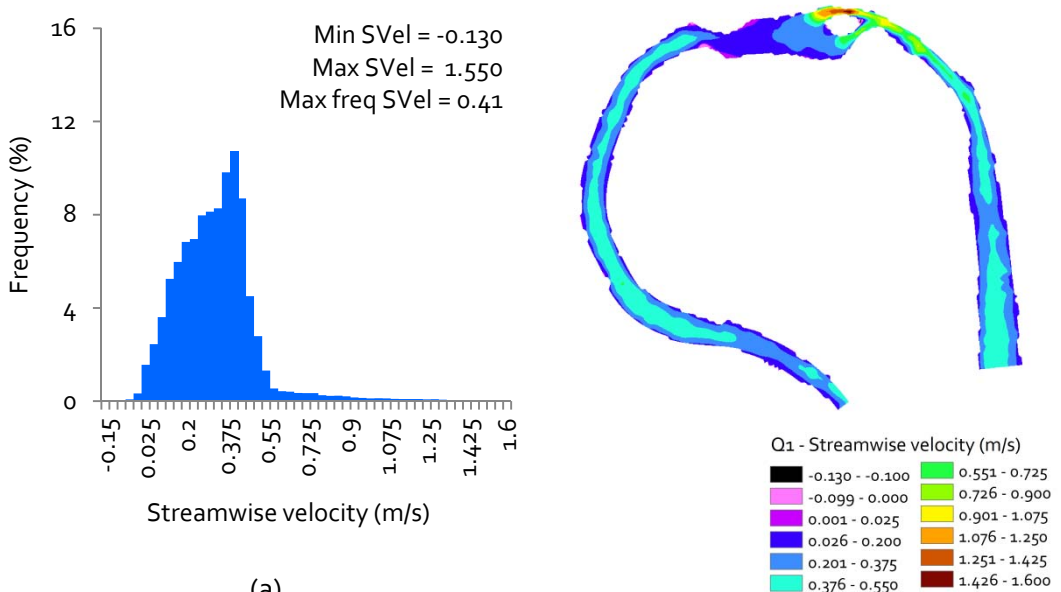


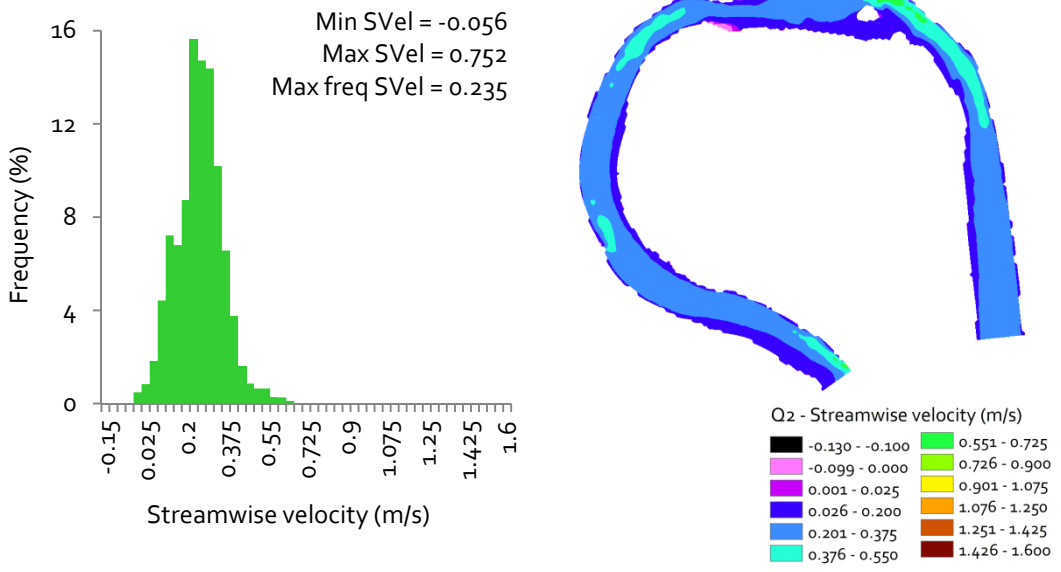
Figure 37 (con'td). Histograms of water depth at (a) low (Q1), (b) medium (Q2), and (c) high (Q3) discharge conditions. Min depth and Max depth denote the minimum and maximum values of water depths associated with given discharge conditions. The classes used in the spatial distribution directly correspond to the classes used in the histogram.

The comparison of the velocity distribution results among different discharge conditions shows that much of the variation in streamwise velocity for stages Q1, Q2, and Q3 have to do with the flow dynamics, which reflects the influence of channel morphology on the flow pattern (Figure 38). Streamwise velocity distribution for the low discharge, Q1, follows a Gaussian distribution with negative skewness, although a very thin and long tail is on the positive end of the distribution (Figure 38a).

The convex increase on the negative side of the distribution is most likely attributed to overall channel shape—as depth appears to have a dominant control on velocity for stage Q1. The long, thin positive tail of the distribution implies a small number of very high-velocity locations, and these are attributed to the portion of the stream where the mid-channel bar constricts flow by dividing the wide channel into two very narrow channels (Figures 9, 22, 25, 38a). According to continuity of flow, this geometry would imply very high velocities to take place at these locations. Velocity decreases once the channel returns to the pre-pool width (Figure 38a). Upstream of the deep pool and downstream of the mid-channel bar (Figures 16, 22, 25), the flow with higher velocities is concentrated in the deeper portions of the channel following the spatial pattern of the thalweg (Figure 38a).



(a)



(b)

Figure 38. Histograms of streamwise velocity at (a) low (Q1), (b) medium (Q2), and (c) high (Q3) discharge conditions. Min SVel and Max SVel denote the minimum and maximum values of velocities associated with given discharge conditions. The classes used in the spatial distribution directly correspond to the classes used in the histogram. For the definition of streamwise velocity, refer to Table 8.

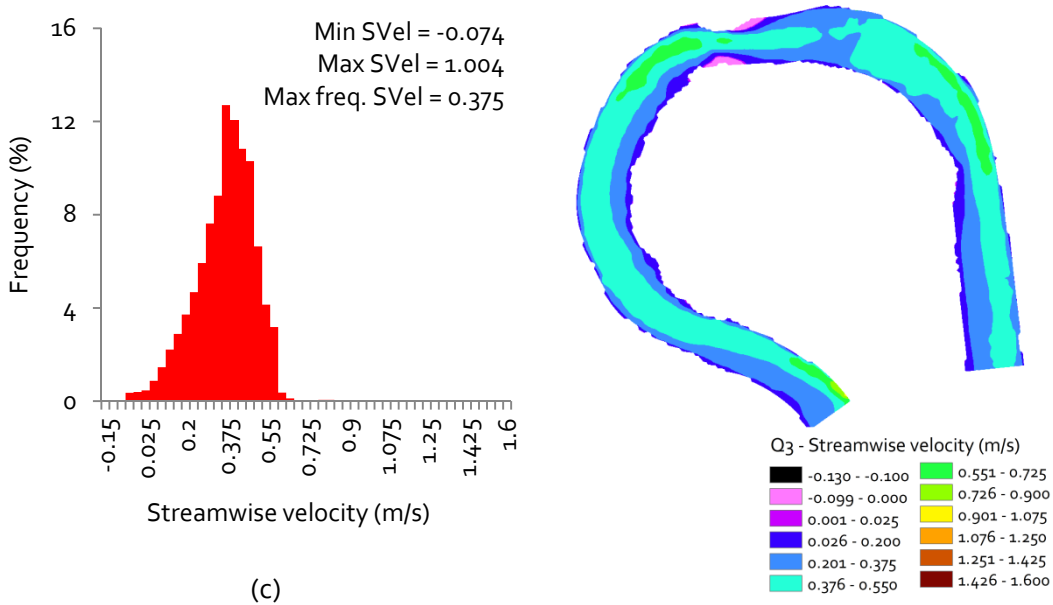


Figure 38 (cont'd). Histograms of streamwise velocity at (a) low (Q1), (b) medium (Q2), and (c) high (Q3) discharge conditions. Min Vel and Max Vel denote the minimum and maximum values of velocities associated with given discharge conditions. The classes used in the spatial distribution directly correspond to the classes used in the histogram. For the definition of the streamwise velocity, refer to Table 8.

Another special sub-class of stream velocity is negative stream velocities, also known as associated with backwaters. Model outputs suggest that backwaters occur at areas coincident with eddies. Eddies form at areas of flow separation, or locations where there are sharp changes in geometry (Munson et al., 2009). In the case of the study reach, eddies are observed at margins where there is a sharp change in channel geometry.

For the low-discharge condition Q1, at which the mid-channel bar is exposed (Figures 9, 22, 24), the streamwise velocity with the highest frequency (i.e., 10.72%) is 0.41 m/s (Figure 38a). In addition, the majority of the streamwise velocities (about 67%) are lower than the velocity corresponding to the highest frequency. Only 4.7% of the velocities have a velocity value of 0.585 m/s or higher, with the highest velocity being ~1.56 m/s. These velocities (> 0.585 m/s) are localized around and immediately downstream of the mid-channel bar region (Figure 38a). For Q1, backwaters are located immediately upstream of inflection point 2, where the very dramatic change in channel geometry occurs immediately upstream of a bank protection structure (Figure 23). A backwater region also occurs at the confluent end of the mid channel bar. Eddies are noted to occur at the confluent zone because of complicated turbulent interactions in flow.

Kurtosis and skewness in the histogram of the streamwise velocity of discharge Q2 are more leptokurtic and less skewed because of the changed influence of the channel morphology on the flow pattern with the increased stage (Figure 38b). The flow velocity is concentrated between 0.026 m/s and 0.550 m/s, with the highest magnitude and lowest frequency velocities being within the range of 0.551–0.725 m/s. These highest velocities correspond to the lower end of the mid-channel bar structure and indicate the influence of the mid-channel bar on the flow patterns. With the increasing stage, the divergence and convergence of flow around the mid-channel bar Q1 (Figure 19) is not present anymore; however, a new mid-channel bar emerges (i.e., mid-channel bar Q2) at the location previously classified as point bar (Figures 22, 38b). As expected, the flow is shifted toward the cutbank on the left side of the channel along this newly-emerged bar. For Q2, backwater regions grow near inflection point 2 and immediately downstream of the bank protection structure. These locations would correspond to locations of flow separation.

During high-discharge condition, Q3, mid-channel bars for Q1 and the one emerged during Q2 are submerged, as well as all the point bars (Figures 22, 38c). The concave monotonic increase on the negative side of the histogram (the regions with the velocities below 0.375 m/s), again, characterizes the influence of the channel morphology under this new high-stage condition and typically corresponds to the higher elevations in the reach. The most dominant velocity range of 0.375–0.550 m/s is higher than the dominant velocity range for Q2. Thus, this velocity range also has more spatial continuity, compared to the spatial distribution of the same range in Q2 conditions (Figures 38b–c). Very low frequencies representing high velocities (i.e., 0.551–0.750 m/s) indicate the localized strong flow structure (Figure 38c). The spatial distribution of the streamwise flow is influenced by the abrupt widening of the channel near the submerged mid-channel bar, and narrowing of the channel immediately downstream of the mid-channel bar, with a decrease and then an increase again in the velocities, respectively. Thus, even though the mid-channel bar structures do not divide the channel and significantly deflect it to the outer bank, the influence of the complex morphology in this region is clearly observable (Figures 22, 38). For Q3, backwater regions occur in the same locations as intermediate flow stage (Q2), but grow in area. This pattern is likely due to increase in velocity from Q1 to Q3 and flow reattachment zones (end of backwater regions) occurring further downstream.

Although Q2 is slightly more leptokurtic than Q1 and Q3, the histograms of normal velocity are quite similar for all three discharge stages (Figure 39a–c). The histograms for Q1 and Q2 have longer tails than the histogram for Q3. These long tails correspond to low frequency, or in other words, localized, very high/low normal velocities (Figures 39a–b *vs.* Figure 39c).

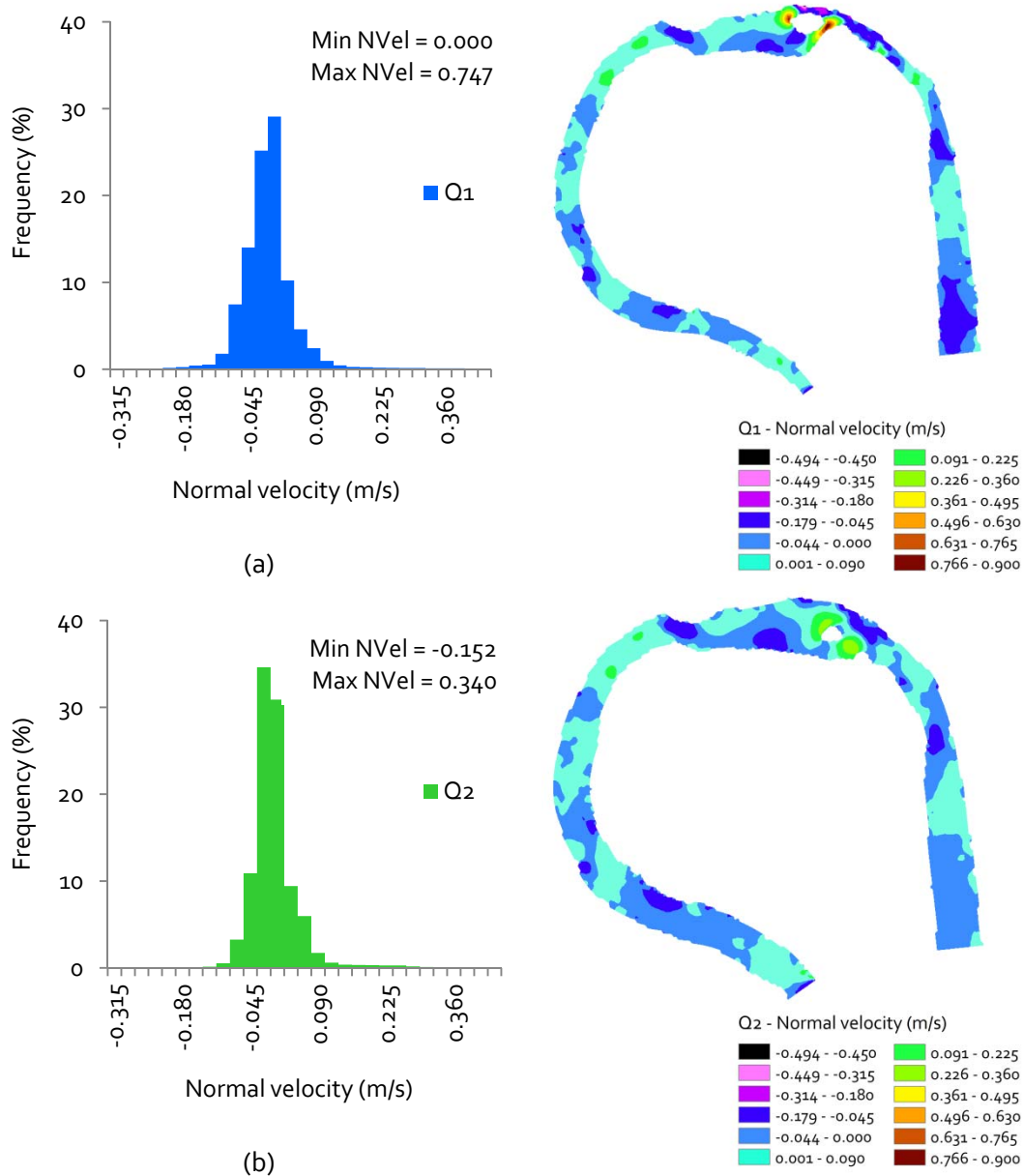


Figure 39. Histograms of normal velocity at (a) low (Q1), (b) medium (Q2), and (c) high (Q3) discharge conditions. Min Vel and Max Vel denote the minimum and maximum values of velocities associated with given discharge conditions. The classes used in the spatial distribution directly correspond to the classes used in the histogram. For the definition of normal velocity, refer to Table 8.

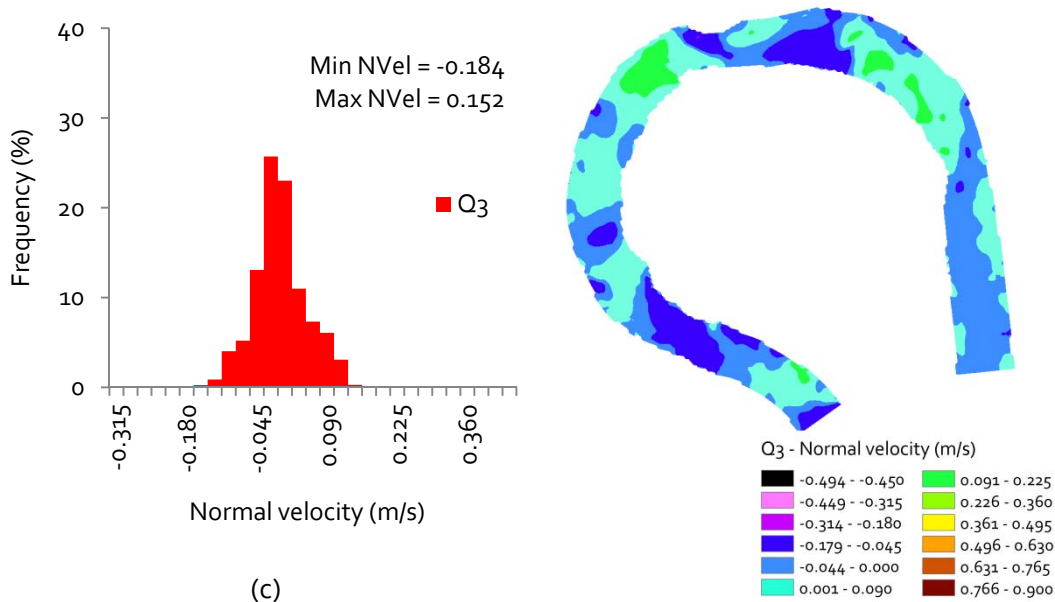


Figure 39 (cont'd). Histograms of normal velocity at (a) low (Q1), (b) medium (Q2), and (c) high (Q3) discharge conditions. Min Vel and Max Vel denote the minimum and maximum values of velocities associated with given discharge conditions. The classes used in the spatial distribution directly correspond to the classes used in the histogram. For the definition of normal velocity, refer to Table 8.

Overall, the spatial distributions of the normal velocities are also similar for difference discharge conditions. These distributions, compared to the spatial patterns of the streamwise velocity, indicate much more variability characterized by shifts from negative patterns to positives. The spatial distributions of the regions characterized by positive and negative normal velocities are quite stable (Figure 39). The most significant change in the patterns occurs in the regions containing the mid-channel bar downstream of the deep pool (Figures 22, 24, 39).

During the low discharge, Q1, conditions, because of the more prominent influence of the mid-channel bar structure causing divergence/convergence of the flow, the normal velocities are very high and positive at the entrance and the exit of the mid-channel bar (Figure 39a) and high and negative along the channel on the cutbank side. With increasing discharge, the normal velocities in these hot spots slightly decrease and shift their location toward the point bar where the mid-channel bar Q2 forms. With further increase in the discharge from Q2 to Q3, all bars are submerged and the high velocities shift their location slightly toward the edge of the point bar and downstream reflecting the effect of the topographic highs on the flow distribution (Figures 39a–c).

The Froude number distribution on the study reaches varies systematically with increasing flow, becoming narrow in range and more leptokurtic (Figures 40a–c). This implies that Froude number has a higher variability for the low flow condition, Q1, than the two higher flow conditions and that, at the higher flow rates; the values of Froude number are concentrated within a smaller range of values (Figure 40a).

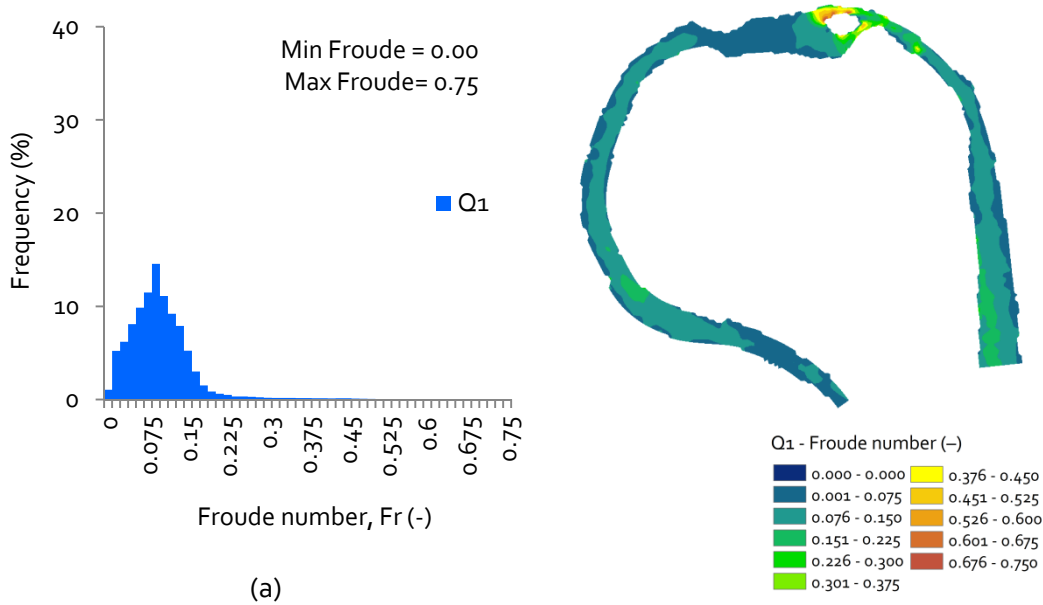


Figure 40. Histograms of Froude number at (a) low (Q1), (b) medium (Q2), and (c) high (Q3) discharge conditions. Min Froude and Max Froude denote the minimum and maximum values of Froude number associated with given discharge conditions. The classes used in the spatial distribution directly correspond to the classes used in the histogram. For the definition of Froude number, refer to Table 8.

This is mainly because of the flow being restricted in narrow channels, and thus, giving rise to large velocities at low depth, resulting in high Froude numbers (*Dingman, 2009*) (Figure 40a). Froude number distribution for stages Q2 and Q3 are similar and leptokurtic, because flow gets less and less restricted as the discharge, and thus, stage increases. This implies that there is greater depth and lower average velocity, resulting in lower Froude numbers (Figures 40b–c).

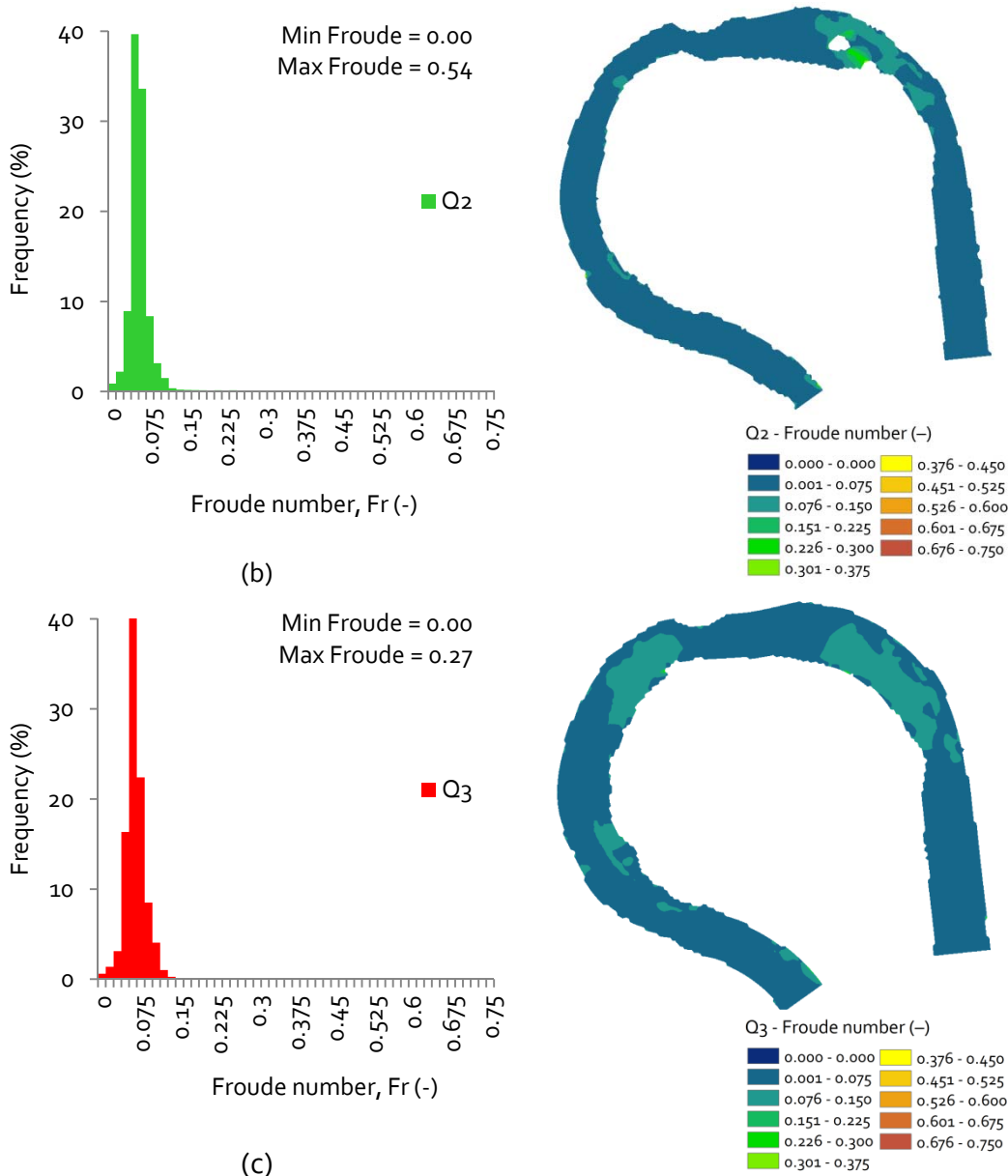


Figure 40 (cont'd). Spatial distribution and histogram of Froude number at (a) low (Q1), (b) medium (Q2), and (c) high (Q3) discharge conditions. Min Froude and Max Froude denote the minimum and maximum values of Froude number associated with given discharge conditions. The classes used in the spatial distribution directly correspond to the classes used in the histogram. For the definition of Froude number, refer to Table 8.

Nevertheless, the topographic highs or shallower geomorphic units, such as mid-channel bars and point bars, have an apparent effect on the Froude number distribution. Although the Froude number values are significantly lower for Q2, over the region of mid-channel bar and downstream, the values are higher than the other regions of the study reach. As the sand bars get

inundated with increasing discharge, they become shallow and rough structures, causing increased Froude numbers over them (Figure 40c).

The overall shape of the distribution for Helix strength is similar for all stages (Figure 41). The spatial distribution of the helix strength represents the combined influence of channel and planform morphology, with the highest values of the helix strength being associated with the regions characterized by high curvature values (Figures 16–17 vs. Figure 41). The kurtosis for helix strength in Q2 is more platikurtic, however. This implies that there is less deviance in angle between the water flowing near the surface and water flowing near the bed for stage Q2 than stage Q1 and Q3 (Figures 41a–c).

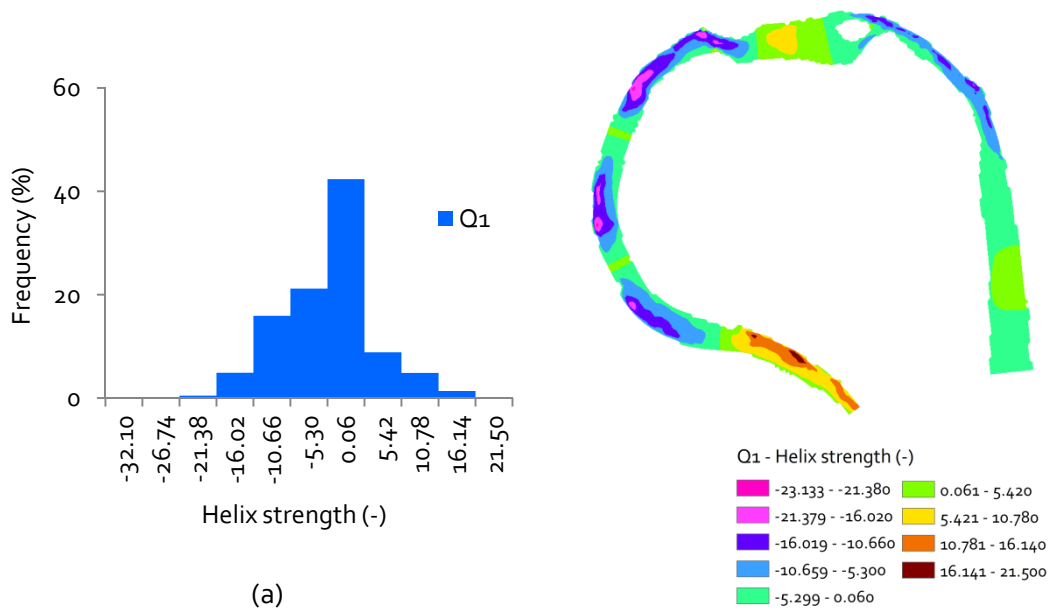


Figure 41. Spatial distribution and histogram of helix strength at (a) low (Q1), (b) medium (Q2), and (c) high (Q3) discharge conditions. The classes used in the spatial distribution directly correspond to the classes used in the histogram. For the definition of the helix strength, refer to Table 8.

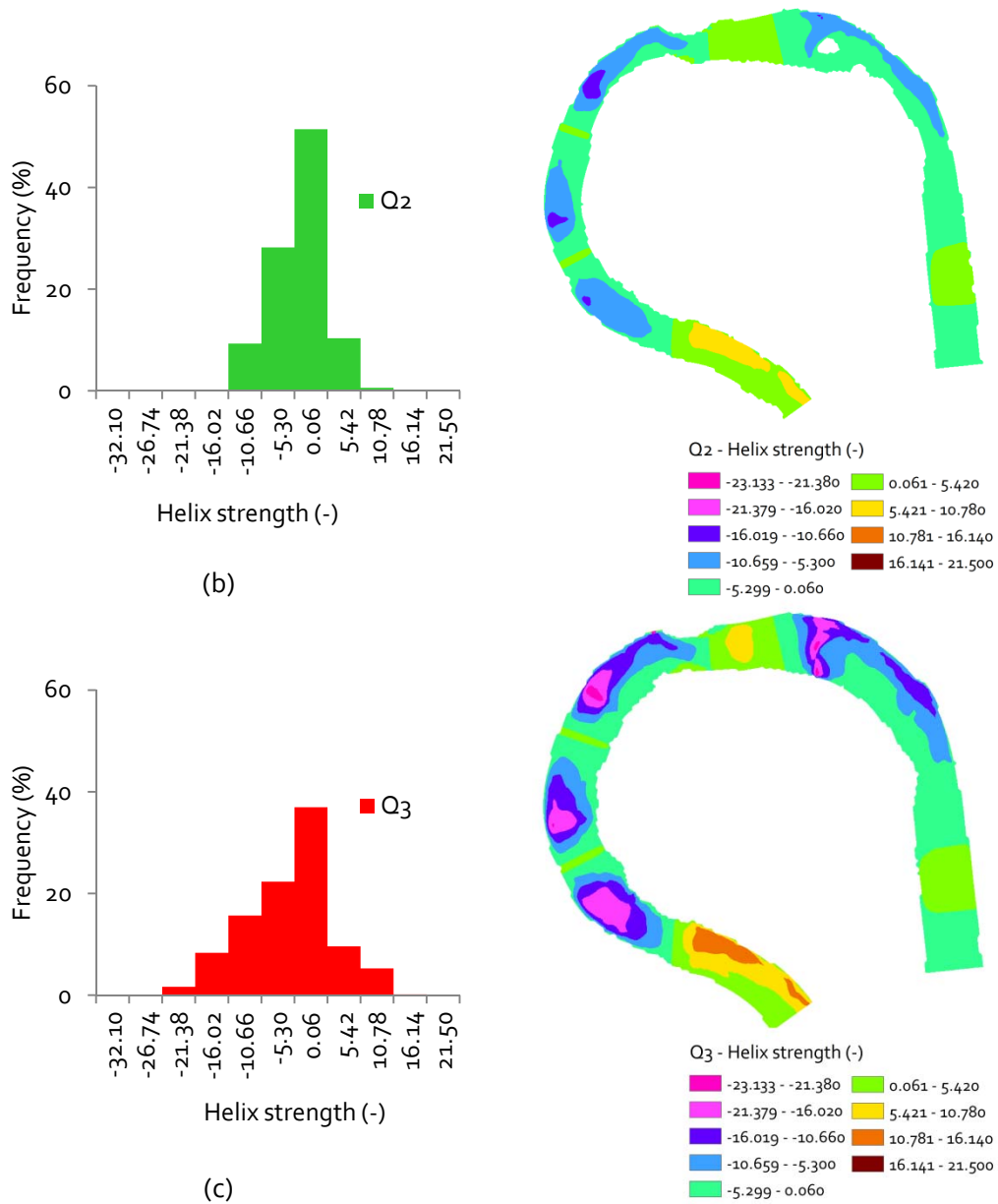


Figure 41 (cont'd). Spatial distribution and histogram of helix strength at (a) low (Q1), (b) medium (Q2), and (c) high (Q3) discharge conditions. The classes used in the spatial distribution directly correspond to the classes used in the histogram. For the definition of the helix strength, refer to Table 8.

7.6. Relations between Channel Morphology and Flow Hydraulics

Following the purpose of this study, which is to characterize the channel morphology and flow hydraulics of a select river reach on the lower Brazos River, Texas, we discussed our findings in relation to the four specific questions that were posed.

1. *What are the spatial characteristics of the channel morphology (i.e., geomorphic units)?*

Channel morphology is discussed in terms of geomorphic units. These geomorphic units are defined in this work as topographic highs (sediment bars) and lows (pools) (Figures 24–25). For most of the reach, topographic lows are situated near cutbanks and topographic highs are coincident with point bars. The channel is characterized by steep cutbanks. In addition to the point bars, there is also a mid-channel bar in the middle of this reach, between inflection points #2 and #3 in Figure 19. Upstream of this location, there is a deep pool at over 4 meters in depth (after detrending), and 200 meters downstream of this deep pool is a topographic high that represents a mid-channel bar at its apex (and a topographic residual class 1 sediment bar otherwise (Figures 24–26). Channel dimensions are nearly twice as wide as the part of the reach that is upstream of this location and nearly quadruple the channel width at the location upstream that is bounded by curvature maxima between inflection points #3 and #4 (Figures 19–20). The channel width returns to pre-pool and mid-channel bar width downstream of the second curvature maxima between inflection points marked as #3 and #4 (Figures 19–20).

2. *What are the spatial characteristics of flow hydraulics at different discharge conditions (i.e., low, medium, and high discharges)?*

Flow hydraulics are described in terms of water surface elevation, depth, streamwise and normal depth-averaged flow velocities, and Froude number. These parameters are all collinear or related to one another. Froude number is a function of velocity (Nelson, 2013; Dingman, 2009). Streamwise velocity distribution within the reach has three distinct regimes of faster speeds near the center of the channel—common throughout most of the reach; slower flow regime throughout the channel—over the large pool at inflection point #2; and high speed throughout constricted channels between inflection point #3 to the second location of high curvature (Figures 19, 38).

These three regimes represent a control on velocity distribution by the pool and mid-channel bar. As flow increases to Q2, velocity distribution becomes more homogenous with areas of local high velocity near locations of high curvature in the stream, and areas of low

velocity at margins coincident with sand bars (Figures 37, 38b). There is a flow constriction present in roughly the same location as for Q1. However, this flow-constricted area appears to have accelerated flow preferential to that channel north of the dislocated mid-channel bar—perhaps as a control of the sand bar or low depth at the south constricted channel (Figure 38a). At Q3, there is no flow constriction and flow is more homogenous, with overall greatest velocity and local acceleration still coincident with locations of high curvature (Figures 19, 38c). The pool and mid-channel bar appear to have the least influence in Q3.

For normal velocity, magnitude is greatest at Q1 between inflection point #3 and before the first location of high curvature (Figures 19, 39a). Spatial heterogeneity is greatest at Q1, with alternations happening less as stage is increased (Figure 39). Relative magnitude of velocity changes depends on the focus of the study location (whether we are looking at the reach section upstream of inflection point #3 or downstream). Upstream of inflection point #3, overall magnitude of normal velocity increases as stage increases. However, this overall magnitude decreases downstream as stage increases (Figures 19, 39).

3. *How does the channel morphology influence the spatial characteristics of flow hydraulics within the study meander bend?*

Channel morphology influences hydraulics in the compound meander bend via curvature, depth, cross-sectional area, and unique geometries such as the bank-protection structure near inflection point #2 (Figures 19, 22–23). Much of this discussion focuses on locations featured in Figure 22. Curvature is observed to have an influence on streamwise velocity, where high curvature produces regions in the reach of high core velocity. Areas with inflection points tend to dampen core velocity, such as the location between inflection point #4 and #6 (Figures 19, 38). The location between inflection points #2 and #3 do not adhere to this observation, but the controlling factor here is depth. At the large pool, flow continuity bodes that velocity should be slower to conserve for deeper areas or greater cross-sectional channel area. This is true until inflection point #3 at the mid-channel bar. Continuity also bodes that areas of lower cross-sectional area have higher velocities, and this is true for this part of the reach. Without constriction, areas of low depth feature lower velocities (Figure 38). Normal velocity is strongly influenced by curvature and depth as well. One other feature to influence normal velocity is the bank-protection structure near inflection point #2 (Figure 19). This structure has a weak deflection associated with it. Deflection is defined in this work as negative

normal velocity that occurs upstream and positive normal velocity that occurs immediately downstream of the feature (Figure 39).

4. *How does this morphological influence on the spatial characteristics of flow hydraulics change with changing discharge?*

Increasing discharge influences streamwise velocity distribution by making core velocity more prominent and decreasing in range and variability, especially between inflection points at 2 and 4. The results suggest that the reason for this is that obstruction of flow decreases as discharge increases. As for normal velocity, increasing discharge has a variable effect based on whether the location within the reach is upstream or downstream of inflection point 3 (Figures 16, 39). If the location in question is upstream of the inflection point #3, then magnitude of normal velocity change increases. However, magnitude decreases past inflection point #3. Inflection point #3 is coincident with the mid-channel bar, and this implies that the mid-channel bar and perhaps the pool have a control on the behavior of normal velocity as discharge increases. For all discharge conditions, locations of high positive normal velocity are clustered near point bar apices. As stage increases, this velocity increases. A likely cause of this increase is the decreased effects of the pool and mid-channel bar with the increased overall velocity and the increased sandbar influence as stage increases. The weak deflection associated with the bank-protection structure appears to increase in magnitude and period as discharge increases.

7.7. Limitations of the study

There is a need for a thorough sensitivity analysis of the hydraulic model that we developed. Throughout calibration and validation of this model, it was found that certain locations exhibited divergences and oscillations to some degree between observed and predicted, particularly at the low-flow (Q1) condition. In particular, this manifests as a larger separation of water surface elevation upstream of the second high-curvature point after inflection point #3 (Figure 22). One approach to test this sensitivity is to create variable roughness throughout the model, in particular near the area immediately downstream and upstream of the mid-channel bar. Without field-measured roughness elements, it would be necessary to use variable roughness as a calibration measure.

Furthermore, it should also be noted that the only field-based morphological and hydrological data available for this study come from the flow conditions that we defined as low

flow (Q1). We were able to perform a detailed model calibration and validation only for Q1 model. Therefore, the models that we developed and used in the analysis of medium- and high-flow scenarios (Q2 and Q3) should be considered as exploratory as we were not able to perform a detailed, field data-based validation of these models. The results obtained from Q2 and Q3 models provide insights on geomorphology and flow hydraulics relationship although the findings should not be used for drawing predictive conclusions.

8. SUMMARY AND CONCLUSIONS

In this study, we characterized the channel morphology and flow hydraulics of a select river reach on the lower Brazos River, Texas, to inform fish habitat mapping and assessment. The study reach is a large sand-bed meandering reach located in an incised section of the lower Brazos River near Bryan, Texas and presents morphological characteristics of high-amplitude meandering rivers.

For this study, we utilized both field-based morphological and hydraulics data and capabilities of the hydraulic-modeling tool FaSTMECH (Barton et al., 2005; McDonald et al., 2006; Kim et al., 2011; Nelson, 2013). In order to be able to determine the distinct regions within the reach with unique geomorphic and hydraulic properties, we organized our analysis around four major questions and determined: (1) the spatial characteristics of the channel morphology (geomorphic units); (2) the spatial characteristics of flow hydraulics at a discharge condition corresponding to low flow (Q1) and at which the fish data collection was performed, as well as at other exploratory discharge conditions, corresponding to medium (Q2) and high (Q3) flows; (3) the influence of channel morphology on the spatial characteristics of flow hydraulics within this meander bend; and (4) how the influence of channel morphology on the spatial characteristics of flow hydraulics changes with changing discharge conditions.

The findings of the study indicate that the unique geomorphology represented by this highly sinuous compound meandering bend reach strongly influences the flow hydraulics. The findings also point out that the morphological control on the flow dynamics changes with changing discharge conditions. In many locations along the reach, the inflection points, where the channel curvature is zero and changes its direction (thus affecting the flow direction), play an important role in the hydraulic phenomena. The results show that the channel planform morphology (i.e., locations of inflection points and high-curvature regions) has a strong influence on the spatial structure of the hydraulic parameters, including streamwise velocity.

The results also indicate that the influence of local bed morphological structures decreases with increasing discharge. For example, as water stage increases, the impact of local bed morphology decreases in favor of the effects of the channel planform morphology. This can be observed at locations with very sharp curvature zones, such as near the bank-protection structure. Near the bank-protection structure, there is a small patch of negative normal velocity, and this patch becomes larger with a twin on the other side of this structure (deflection) as stage increases. In addition, the decrease in velocity caused by the pool is very apparent in the low-flow (Q1) stage, but hardly noticeable in the high-flow (Q3) stage. The decreasing influence of local bed morphology versus channel planform morphology on the flow hydraulics at increasing discharges is also true for the constriction of flow caused by the mid-channel bar –representing a macro roughness structure– and the lack of constriction apparent in streamwise velocity for the high-flow (Q3) scenario.

Another important property of flow hydraulics present in the study reach is the difference in the two constricted channels for the intermediate-flow scenario (Q2). In this flow, one of the channels (north of the mid-channel bar) had very high streamwise velocity, but the other channel had very low streamwise velocity. This discrepancy in velocity is very likely attributable to the large discrepancy in cross-sectional area between the two channels –one being deep and narrow, and formed near the cutbank, and the other one simply being a component of the large point bar, which functions as a macro roughness structure at intermediate-flow scenario (Q2), similar to the mid-channel bar in the low-flow (Q1) scenario.

Finally, it should be noted that the specific findings obtained from this study may only apply to this particular study reach. However, the general findings of how flow and channel morphology relate to hydraulic characteristics are informative for other reaches on the Brazos River, and elsewhere, with similar morphological, hydrological, and environmental properties.

REFERENCES

- TPWD et al., 2008 Alford, J.J., and Holmes, J.C., 1985. Meander scars as evidence of major climate change in southwest Louisiana. *Annals - Association of American Geographers* 75(3), 395-403.
- Amsler, M.L., Blettler, M.C.M., and Ezcurra De Drago, I., 2009. Influence of hydraulic conditions over dunes on the distribution of the benthic macroinvertebrates in a large sand bed river. *Water Resources Research* 45(6).
- Baras, E., Philippart, J.C., and Nindaba, J., 1996. Importance of gravel bars as spawning grounds and nurseries for European running water cyprinids. . In: M. Leclerc, H. Capra, S. Valentin, A. Boudreault and Y. Côté (Editors), *Ecohydraulics 2000. Proceedings of the 2nd International Symposium on Habitat Hydraulics*. INRS-Eau, Québec City, Canada, pp. 367-378.
- Barton, G.J., McDonald, R., Nelson, J.M., and Dinehart, R.L., 2005. Simulation of flow and sediment mobility using a multidimensional flow model for the white sturgeon critical-habitat reach, Kootenai River near Bonners Ferry, Idaho. USGS Scientific Investigations Report 2005-5230, 64 pp.
- Berenbrock, C., and Tranmer, A.W., 2008. Simulation of Flow, Sediment Transport, and Sediment Mobility of the Lower Coeur d'Alene River, Idaho. USGS Open-File Report 2008-5093, 164 pp.
- Blum, M.D., Morton, R.A., and Durbin, J.M., 1995. Deweyville terraces and deposits of the Texas Gulf coastal plain. *Gulf Coast Association of Geological Societies Transactions* 45, 53-60.
- Braaten, P.J., and Berry Jr, C.R., 1997. Fish associations with four habitat types in a South Dakota prairie stream. *Journal of Freshwater Ecology* 12(3), 477-489.
- Brierley, G.J., and Fryirs, K., 2000. River styles, a geomorphic approach to catchment characterization: Implications for river rehabilitation in Bega catchment, New South Wales, Australia. *Environmental Management* 25(6), 661-679.
- Brierley, G.J., and Fryirs, K.A., 2005. *Geomorphology and river management: applications of the River Styles framework*. Blackwell, Oxford, UK.
- Brooks, A.J., Haeusler, T., Reinfelds, I., and Williams, S., 2005. Hydraulic microhabitats and the distribution of macroinvertebrate assemblages in riffles. *Freshwater Biology* 50(2), 331-344.
- Brown, A.V., and Brussock, P.P., 1991. Comparisons of benthic invertebrates between riffles and pools. *Hydrobiologia* 220(2), 99-108.
- Caratti, J.F., Nesser, J.A., and Maynard, C.L., 2004. Watershed classification using canonical correspondence analysis and clustering techniques: A cautionary note. *Journal of the American Water Resources Association* 40(5), 1257-1268.
- Chiles, J.P., and Delfiner, P., 1999. *Geostatistics: Modeling Spatial Uncertainty*. John Wiley and Sons, New York, 695 pp.

- Clifford, N.J.,Harmar, O.P.,Harvey, G., and Petts, G.E., 2006. Physical habitat, eco-hydraulics and river design: A review and re-evaluation of some popular concepts and methods. *Aquatic Conservation: Marine and Freshwater Ecosystems* 16(4), 389-408.
- Coffman, D.K.,Malstaff, G., and Heitmuller, F.T., 2011. Characterization of geomorphic units in the alluvial valleys and channels of Gulf Coastal Plain rivers in Texas. SIR 2011-5067. US Geological Survey, 31. pp, <http://pubs.usgs.gov/sir/2011/5067/pdf/sir2011-5067.pdf>
- Conaway, J.S., and Moran, E.H., 2004. Development and Calibration of a Two-Dimensional Hydrodynamic Model of the Tanana River near Tok, Alaska. USGS Open-File Report 2004-1225, 22 pp.
- Crowder, D.W., and Diplas, P., 2000. Using two-dimensional hydrodynamic models at scales of ecological importance. *Journal of Hydrology* 230, 172-191.
- Davis, J.A., and Barmuta, L.A., 1989. An ecologically useful classification of mean and near-bed flows in streams and rivers. *Freshwater Biology* 21(2), 271-282.
- Dent, C.L.,Grimm, N.B., and Fisher, S.G., 2001. Multiscale effects of surface-subsurface exchange on stream water nutrient concentrations. *Journal of the North American Benthological Society* 20(2), 162-181.
- Dingman, S.L., 2009. *Fluvial Hydraulics*. Oxford University Press, New York, 559 pp.
- Fischer, H.,Sukhodolov, A.,Wilczek, S., and Engelhardt, C., 2003. Effects of flow dynamics and sediment movement on microbial activity in a lowland River. *River Research and Applications* 19(5-6), 473-482.
- Frissell, C.A.,Liss, W.J.,Warren, C.E., and Hurley, M.D., 1986. A hierarchical framework for stream habitat classification: Viewing streams in a watershed context. *Environmental Management* 10(2), 199-214.
- Frothingham, K.M.,Rhoads, B.L., and Herricks, E.E., 2001. Stream Geomorphology and Fish Community Structure in Channelized and Meandering Reaches of an Agricultural Stream, *Geomorphic Processes and Riverine Habitat*. American Geophysical Union, pp. 105-117.
- Frothingham, K.M.,Rhoads, B.L., and Herricks, E.E., 2002. A multiscale conceptual framework for integrated ecogeomorphological research to support stream naturalization in the Agricultural Midwest. *Environmental Management* 29(1), 16-33.
- Ghani, A.A.,Zakaria, N.A.,Kiat, C.C.,Ariffin, J.,Hasan, Z.A., and Ghaffar, A.B.A., 2007. Revised equations for Manning's coefficient for sand-bed rivers. *International Journal of River Basin Management* 5(4), 329-346.
- Gorecki, V.I.,Fryirs, K.A., and Brierley, G.J., 2006. The relationship between geomorphic river structure and coarse particulate organic matter (CPOM) storage along the Kangaroo River, New South Wales, Australia. *Australian Geographer* 37(3), 285-311.
- Goovaerts, P., 1997. *Geostatistics for Natural Resource Evaluation*. Applied Geostatistics. Oxford University Press, New York, NY.

- Gregory, S.V., Swanson, F.J., McKee, W.A., and Cummins, K.W., 1991. An Ecosystem Perspective of Riparian Zones. *BioScience* 41(8), 540-551.
- Güneralp, İ., and Rhoads, B.L., 2008. Continuous characterization of the planform geometry and curvature of meandering rivers. *Geographical Analysis* 40(1), 1-25.
- Hart, D.D., and Finelli, C.M., 1999. Physical-biological coupling in streams: The pervasive effects of flow on benthic organisms. *Annual Review of Ecology and Systematics* 30, 363-395.
- Hesse, R., Allee, W.C., and Schmidt, K.P., 1937. Ecological animal geography; an authorized, rewritten edition based on *Tiergeographie auf oekologischer Grundlage* / by Richard Hesse, prepared by W. C. Allee and Karl P. Schmidt. J. Wiley & Sons, Inc., New York, <http://www.biodiversitylibrary.org/item/27612>
- Huet, M., 1949. Aperçu des relations entre la pente et les populations piscicoles des eaux courantes. *Schweizerische Zeitschrift für Hydrologie* 11(3-4), 332-351.
- Isaaks, E.H., and Srivastava, R.M., 1989. *Applied Geostatistics*. Oxford University Press, Inc., New York, 561 pp.
- Kemp, J.L., Harper, D.M., and Crosa, G.A., 1999. Use of 'functional habitats' to link ecology with morphology and hydrology in river rehabilitation. *Aquatic Conservation: Marine and Freshwater Ecosystems* 9(1), 159-178.
- Kim, M.H., Morlock, S.E., Arihood, L.D., and Keisler, J.L., 2011. Observed and forecast flood-inundation mapping application: A pilot study of an eleven-mile reach of the White River, Indianapolis, Indiana. USGS Scientific Investigations Report 2011-5138.
- Kitanidis, P.K., 1997. *Introduction to Geostatistics: Applications in Hydrogeology*. Cambridge University Press, Cambridge, 249 pp.
- Kondolf, G.M., Montgomery, D.R., Piégay, H., and Schmitt, L., 2003. Geomorphic classification of rivers and streams. In: G.M. Kondolf and H. Piégay (Editors), *Tools in Fluvial Geomorphology*. John Wiley & Sons, New York, pp. 171-204.
- Lake, P.S., 2000. Disturbance, patchiness, and diversity in streams. *Journal of the North American Benthological Society* 19(4), 573-592.
- Lancaster, J., and Hildrew, A.G., 1993. Flow refugia and the microdistribution of lotic macroinvertebrates. *Journal of the North American Benthological Society* 12(4), 385-393.
- Lauer, J.W., 2006. *NCED Stream Restoration Toolbox. Channel Planform Statistics*. National Center for Earth-Surface Dynamics, February 14, 2006.
- Linam, G.W., Kleinsasser, L.J., and Mayes, K.B., 2002. Regionalization of the Index of Biotic Integrity for Texas Streams. *River Studies Report No. 17*. Texas Parks and Wildlife Department, Resource Protection Division, Austin, Texas, 140 pp.

- Marchese, M.R., Wantzen, K.M., and Ezcurra de Drago, I., 2005. Benthic invertebrate assemblages and species diversity patterns of the upper Paraguay River. *River Research and Applications* 21(5), 485-499.
- McDonald, R., 2013. Personal Communication, Issues with FaSTMECH, B. Hales, Feb 21, 2013.
- McDonald, R., Barton, G., Nelson, J., and Paragamian, V., 2006. Modeling hydraulic and sediment transport processes in white sturgeon spawning habitat on the Kootenai River, Idaho. Proceedings of the Eighth Federal Interagency Sedimentation Conference, Reno, Nevada, April 2-6.
- Miller, J.R., and Ritter, J.B., 1996. An examination of the Rosgen classification of natural rivers. *Catena* 27(3-4), 295-299.
- Moir, H.J., Gibbins, C.N., Soulsby, C., and Webb, J., 2004. Linking channel geomorphic characteristics to spatial patterns of spawning activity and discharge use by Atlantic salmon (*Salmo salar* L.). *Geomorphology* 60(1-2), 21-35.
- Moir, H.J., and Pasternack, G.B., 2008. Relationships between mesoscale morphological units, stream hydraulics and Chinook salmon (*Oncorhynchus tshawytscha*) spawning habitat on the Lower Yuba River, California. *Geomorphology* 100(3-4), 527-548.
- Morton, R.A.B., M. D., and White, W.A., 1996. Characteristics of incised valley fills, coastal plain rivers of southeastern Texas. *Transactions Gulf Coast Association of Geological Societies* 46, 321-331.
- Munson, B.R., Young, D.F., Okiishi, T.H., and Huebsch, W.W., 2009. *Fundamentals of Fluid Mechanics*. John Wiley & Sons, Hoboken, NJ.
- Naiman, R.J., 1998. Biotic stream classification. In: R.J. Naiman and R.E. Bilby (Editors), *River Ecology and Management: Lessons from the Pacific Coastal Ecoregion*. Springer-Verlag, New York, pp. 97-119.
- Nelson, J.M., 2013. FaSTMECH Model Notes. Available Online, <http://i-ric.org>
- Niezgoda, S.L., and Johnson, P.A., 2005. Improving the urban stream restoration effort: Identifying critical form and processes relationships. *Environmental Management* 35(5), 579-592.
- NRC (National Research Council), 2005. *The science of instream flows, a review of the Texas Instream Flow Program*. The National Academies Press, 149 pp.
- Olea, R., 1999. *Geostatistics for Engineers and Earth Scientists*. Kluwer Academic Publishers, Boston,, 303 pp.
- Phillips, J.D., 2006. *Geomorphic Context, Constraints, and Change in the Lower Brazos and Navasota Rivers, Texas*. Texas Water Development Board Report, 81 pp, http://www.twdb.texas.gov/publications/reports/contracted_reports/doc/2005483564_Phillips.pdf

- Phillips, J.D., 2007a. Field data collection in support of geomorphic classification of the lower Brazos and Navasota Rivers. Texas Water Development Board, 100 pp, http://www.twdb.texas.gov/publications/reports/contracted_reports/doc/0604830639_BrazosY2rept.pdf
- Phillips, J.D., 2007b. Geomorphic processes, controls, and transition zones in the lower Sabine River. Texas Water Development Board, 56 pp, http://www.twdb.texas.gov/publications/reports/contracted_reports/doc/0600010595_Sabine.pdf
- Phillips, J.D., 2008a. Geomorphic processes, controls, and transition zones in the middle and lower Trinity River. Texas Water Development Board, 63 pp, http://www.twdb.texas.gov/publications/reports/contracted_reports/doc/0704830781_TrinityZones08.pdf
- Phillips, J.D., 2008b. Geomorphic units of the lower Sabine River. Texas Water Development Board, 64 pp, http://www.twdb.texas.gov/publications/reports/contracted_reports/doc/0704830782_SabineGeomorphic.pdf
- Phillips, J.D., 2011. Geomorphic processes, controls, and transition zones in the Guadalupe River. Texas Water Development Board, 78 pp, http://www.twdb.texas.gov/publications/reports/contracted_reports/doc/0904831034_Guadalupe.pdf
- Rabeni, C.F., and Jacobson, R.B., 1993. The importance of fluvial hydraulics to fish-habitat restoration in low-gradient alluvial streams. *Freshwater Biology* 29(2), 211-220.
- Rhoads, B.L., Schwartz, J.S., and Porter, S., 2003. Stream geomorphology, bank vegetation, and three-dimensional habitat hydraulics for fish in midwestern agricultural streams. *Water Resources Research* 39(8), ESG21-ESG213.
- Richter, B.D., Mathews, R., Harrison, D.L., and Wigington, R., 2003. Ecologically sustainable water management: Managing river flows for ecological integrity. *Ecological Applications* 13(1), 206-224.
- Rivers-Moore, N.A., and Jewitt, G.P.W., 2007. Adaptive management and water temperature variability within a South African river system: What are the management options? *Journal of Environmental Management* 82(1), 39-50.
- Rosgen, D.L., 1994. A classification of natural rivers. *Catena* 22(3), 169-199.
- Rosgen, D.L., 1996. Applied river morphology. Wildland hydrology, Pagosa Springs, Colorado, 390 pp.
- Saffel, P.D., and Scarnecchia, D.L., 1995. Habitat use by juvenile bull trout in belt-series geology watersheds of northern Idaho. *Northwest Science* 69(4), 304-317.
- Schmitt, L., Lafont, M., Trémolières, M., Jezequel, C., Vivier, A., Breil, P., Namour, P., Valin, K., and Valette, L., 2011. Using hydro-geomorphological typologies in functional ecology:

- Preliminary results in contrasted hydrosystems. *Physics and Chemistry of the Earth* 36(12), 539-548.
- Schneider, K.N., and Winemiller, K.O., 2008. Structural complexity of woody debris patches influences fish and macroinvertebrate species richness in a temperate floodplain-river system. *Hydrobiologia* 610(1), 235-244.
- Schwartz, J.S., 2002. Stream Habitat Characterized by Stage-Specific Flows and Three-Dimensional Geomorphological Complexity: Development of Ecological Criteria for Stream Restoration Design. PhD Thesis, University of Illinois at Urbana-Champaign, Urbana-Champaign, Urbana-Champaign, IL.
- Schwartz, J.S., and Herricks, E.E., 2005. Fish use of stage-specific fluvial habitats as refuge patches during a flood in a low-gradient Illinois stream. *Canadian Journal of Fisheries and Aquatic Sciences* 62(7), 1540-1552.
- SonTek, 2011. RiverSurveyor S5/M9 System Manual Firmware Version 2.00. SonTek, a Division of YSI Inc., San Diego, CA, 156 pp, <http://www.sontek.com/riversurveyor-s5-m9.php>
- Statzner, B., Gore, J.A., and Resh, V.H., 1988. Hydraulic Stream Ecology: Observed Patterns and Potential Applications. *Journal of the North American Benthological Society* 7(4), 307-360.
- Statzner, B., and Higler, B., 1986. Stream hydraulics as a major determinant of benthic invertebrate zonation patterns. *Freshwater Biology* 16(1), 127-139.
- Surfer, 2012. Quick Start Guide, Contouring and 3D Surface Mapping for Scientists and Engineers. Golden Software, Inc, <http://www.goldensoftware.com/products/surfer>
- Thomson, J.R., Taylor, M.P., and Brierley, G.J., 2004. Are River Styles ecologically meaningful? A test of the ecological significance of a geomorphic river characterization scheme. *Aquatic Conservation: Marine and Freshwater Ecosystems* 14(1), 25-48.
- Thomson, J.R., Taylor, M.P., Fryirs, K.A., and Brierley, G.J., 2001. A geomorphological framework for river characterization and habitat assessment. *Aquatic Conservation: Marine and Freshwater Ecosystems* 11(5), 373-389.
- TPWD, TCEQ, and TWDB (Texas Parks and Wildlife Department, Texas Commission on Environmental Quality, Texas Water Development Board), 2008. Texas Instream Flow Studies: Technical Overview. Texas Water Development Board Report 369, Austin, Texas, http://www.twdb.texas.gov/surfacewater/flows/instream/doc/R369_InstreamFlows.pdf
- Vannote, R.L., Minshall, G.W., Cummins, K.W., Sedell, J.R., and Cushing, C.E., 1980. The river continuum concept. *Canadian Journal of Fisheries and Aquatic Sciences* 37(1), 130-137.
- Wadson, R.A., and Rowntree, K.M., 1998. Application of the hydraulic biotope concept to the classification of instream habitats. *Aquatic Ecosystem Health and Management* 1(2), 143-157.

Waters, M.R., and Nordt, L.C., 1995. Late Quaternary Floodplain History of the Brazos River in East-Central Texas. *Quaternary Research* 43(3), 311-319.